

# Testing Relativistic Gravity with Radio Pulsars

Norbert Wex

Max-Planck-Institut für Radioastronomie  
Auf dem Hügel 69, D-53121, Bonn, Germany

August 28, 2013

## Abstract

Before the 1970s, precision tests for gravity theories were constrained to the weak gravitational fields of the Solar system. Hence, only the weak-field slow-motion aspects of relativistic celestial mechanics could be investigated. Testing gravity beyond the first post-Newtonian contributions was for a long time out of reach.

The discovery of the first binary pulsar by Russell Hulse and Joseph Taylor in the summer of 1974 initiated a completely new field for testing the relativistic dynamics of gravitationally interacting bodies. For the first time the back reaction of gravitational wave emission on the binary motion could be studied. Furthermore, the Hulse-Taylor pulsar provided the first test bed for the orbital dynamics of strongly self-gravitating bodies.

To date there are a number of pulsars known, which can be utilized for precision test of gravity. Depending on their orbital properties and their companion, these pulsars provide tests for various different aspects of relativistic dynamics. Besides tests of specific gravity theories, like general relativity or scalar-tensor gravity, there are pulsars that allow for generic constraints on potential deviations of gravity from general relativity in the quasi-stationary strong-field and the radiative regime.

This article presents a brief overview of this modern field of relativistic celestial mechanics, reviews some of the highlights of gravity tests with radio pulsars, and discusses their implications for gravitational physics and astronomy, including the upcoming gravitational wave astronomy.

# Contents

<b>1</b>	<b>Introduction</b>	<b>3</b>
1.1	Radio pulsars and pulsar timing . . . . .	5
1.2	Binary pulsar motion in gravity theories . . . . .	6
1.3	Gravitational spin effects in binary pulsars . . . . .	10
1.4	Phenomenological approach to relativistic effects in binary pulsar observations . . . . .	12
<b>2</b>	<b>Gravitational wave damping</b>	<b>17</b>
2.1	The Hulse-Taylor pulsar . . . . .	17
2.2	The Double Pulsar — The best test for Einstein’s quadrupole formula, and more . . . . .	20
2.3	PSR J1738+0333 — The best test for scalar-tensor gravity . . . . .	25
2.4	PSR J0348+0432 — A massive pulsar in a relativistic orbit . . . . .	29
2.5	Implications for gravitational wave astronomy . . . . .	35
<b>3</b>	<b>Geodetic precession</b>	<b>38</b>
3.1	PSR B1534+12 . . . . .	38
3.2	The Double Pulsar . . . . .	39
<b>4</b>	<b>The strong equivalence principle</b>	<b>43</b>
4.1	The Damour-Schäfer test . . . . .	45
4.2	Direct tests . . . . .	47
<b>5</b>	<b>Local Lorentz invariance of gravity</b>	<b>48</b>
5.1	Constraints on $\hat{\alpha}_1$ from binary pulsars . . . . .	48
5.2	Constraints on $\hat{\alpha}_2$ from binary and solitary pulsars . . . . .	50
5.3	Constraints on $\hat{\alpha}_3$ from binary pulsars . . . . .	53
<b>6</b>	<b>Local position invariance of gravity</b>	<b>54</b>
<b>7</b>	<b>A varying gravitational constant</b>	<b>55</b>
<b>8</b>	<b>Summary and Outlook</b>	<b>61</b>

# 1 Introduction

In about two years from now we will be celebrating the centenary of Einstein's general theory of relativity. On November 25th 1915 Einstein presented his field equations of gravitation (without cosmological term) to the Prussian Academy of Science [1]. With this publication, general relativity (GR) was finally completed as a logically consistent physical theory (*“Damit ist endlich die allgemeine Relativitätstheorie als logisches Gebäude abgeschlossen.”*). Already one week before, based on the vacuum form of his field equations, Einstein was able to show that his theory of gravitation naturally explains the anomalous perihelion advance of the planet Mercury [2]. While in hindsight this can be seen as the first experimental test for GR, back in 1915 astronomers were still searching for a Newtonian explanation [3]. In his 1916 comprehensive summary of GR [4], Einstein proposed three experimental tests:

- Gravitational redshift (Einstein suggested to look for red-shift in the spectral lines of stars).
- Light deflection (Einstein explicitly calculated the values for the Sun and Jupiter).
- Perihelion precession of planetary orbits (Einstein emphasized the agreement of GR, with the observed perihelion precession of Mercury with a reference to his calculations in [2]).

Gravitational redshift, a consequence of the equivalence principle, is common to all metric theories of gravity, and therefore in some respect its measurement has less discriminating power than the other two tests [5]. The first verification of gravitational light bending during the total eclipse on May 29th 1919 was far from being a high precision test, but clearly decided in favor of GR, against the Newtonian prediction, which is only half the GR value [6]. In the meantime this test has been greatly improved, in the optical with the astrometric satellite HIPPARCOS [7], and in the radio with very long baseline interferometry [8, 9, 10]. The deflection predicted by GR has been verified with a precision of  $1.5 \times 10^{-4}$ . An even better test for the curvature of spacetime in the vicinity of the Sun is based on the Shapiro delay, the so-called “fourth test of GR” [11]. A measurement of the frequency shift of radio signals exchanged with the Cassini spacecraft lead to a  $10^{-5}$  confirmation of GR [12]. Apart from the four “classical” tests, GR has passed many other tests in the Solar system with flying colors: Lunar Laser Ranging tests for the strong equivalence principle and the de-Sitter precession of the Moon's orbit [13], the Gravity Probe B experiment for the relativistic spin precession of a gyroscope (geodetic and frame

dragging) [14], and the Lense-Thirring effect in satellite orbits [15], just to name a few.

GR, being a theory where fields travel with finite speed, predicts the existence of gravitational waves that propagate with the speed of light [16] and extract energy from (non-axisymmetric) material systems with accelerated masses [17]. This is also true for a self-gravitating system, where the acceleration of the masses is driven by gravity itself, a question which was settled in a fully satisfactory manner only several decades after Einstein's pioneering papers (see [18] for an excellent review). This fundamental property of GR could not be tested in the slow-motion environment of the Solar system, and the verification of the existence of gravitational waves had to wait until the discovery of the first binary pulsar in 1974 [19]. Also, all the experiments in the Solar system can only test the weak-field aspects of gravity. The spacetime of the Solar system is close to Minkowski space everywhere: To first order (in standard coordinates) the spatial components of the spacetime metric can be written as  $g_{ij} = (1 - 2\Phi/c^2)\delta_{ij}$ , where  $\Phi$  denotes the Newtonian gravitational potential. At the surface of the Sun one finds  $\Phi/c^2 \sim -2 \times 10^{-6}$ , while at the surface of a neutron star  $\Phi/c^2 \sim -0.2$ . Consequently, gravity experiments with binary pulsars, not only yielded the first tests of the radiative properties of gravity, they also took our gravity tests into a new regime of gravity.

To categorize gravity tests with pulsars and to put them into context with other gravity tests it is useful to introduce the following four gravity regimes:

- G1** *Quasi-stationary weak-field regime:* The motion of the masses is slow compared to the speed of light ( $v \ll c$ ) and spacetime is only very weakly curved, i.e. close to Minkowski spacetime everywhere. This is, for instance, the case in the Solar system.
- G2** *Quasi-stationary strong-field regime:* The motion of the masses is slow compared to the speed of light ( $v \ll c$ ), but one or more bodies of the system are strongly self-gravitating, i.e. spacetime in their vicinity deviates significantly from Minkowski space. Prime examples here are binary pulsars, consisting of two well-separated neutron stars.
- G3** *Highly-dynamical strong-field regime:* Masses move at a significant fraction of the speed of light ( $v \sim c$ ) and spacetime is strongly curved and highly dynamical in the vicinity of the masses. This is the regime of merging neutron stars and black holes.
- GW** *Radiation regime:* Synonym for the collection of the radiative properties of gravity, most notably the generation of gravitational waves by material sources, the propagation speed of gravitational waves, and their polarization properties.

Figure 1 illustrates the different regimes. Gravity regime G1 is well tested in the Solar system. Binary pulsar experiments are presently our only precision experiments for gravity regime G2, and the best tests for the radiative properties of gravity (regime GW)<sup>1</sup>. In the near future, gravitational wave detectors will allow a direct detection of gravitational waves (regime GW) and probe the strong and highly dynamical spacetime of merging compact objects (regime G3). As we will discuss at the end of this review, pulsar timing arrays soon should give us direct access to the nano-Hz gravitational wave band and probe the properties of these ultra-low-frequency gravitational waves (regime GW).

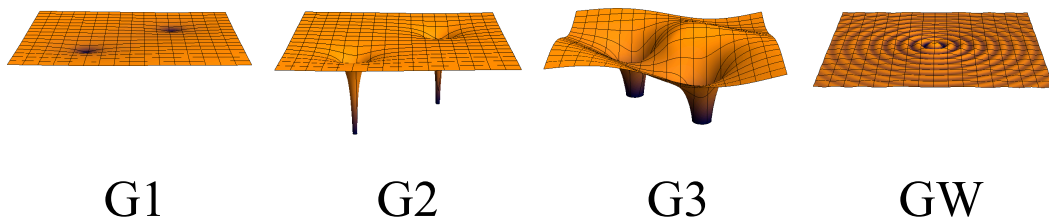


Figure 1: Illustration of the different gravity regimes used in this review.

## 1.1 Radio pulsars and pulsar timing

Radio pulsars, i.e. rotating neutron stars with coherent radio emission along their magnetic poles, were discovered in 1967 by Jocelyn Bell and Antony Hewish [21]. Seven years later, Russell Hulse and Joseph Taylor discovered the first binary pulsar, a pulsar in orbit with a companion star [19]. This discovery marked the beginning of gravity tests with radio pulsars. Presently, more than 2000 radio pulsars are known, out of which about 10% reside in binary systems [22]. The population of radio pulsars can be nicely presented in a diagram that gives the two main characteristics of a pulsar: the rotational period  $P$  and its temporal change  $\dot{P}$  due to the loss of rotational energy (see figure 2). Fast rotating pulsars with small  $\dot{P}$  (millisecond pulsars) appear to be particularly stable in their rotation. On long time-scales, some of them rival the best atomic clocks in terms of stability [23, 24]. This property makes them ideal tools for precision astrometry, and hence (most) gravity tests with pulsars are simply clock comparison experiments to probe the spacetime of the binary pulsar, where the “pulsar clock” is read off by counting the pulses in the pulsar signal (see figure 3). As a result, a wide range of relativistic effects related to orbital binary dynamics, time dilation and delays in the signal propagation

<sup>1</sup> Gravitational wave damping has also been observed in a double white-dwarf system, which has an orbital period of just 13 minutes [20]. This experiment combines gravity regimes G1 (note,  $v/c \sim 3 \times 10^{-3}$ ) and GW of figure 1.

can be tested. The technique used is the so-called *pulsar timing*, which basically consists of measuring the exact arrival time of pulses at the radio telescope on Earth, and fitting an appropriate *timing model* to these arrival times, to obtain a phase-connected solution. In the phase-connected approach lies the true strength of pulsar timing: the timing model has to account for every (observed) pulse over a time scale of several years, in some cases even several decades. This makes pulsar timing extremely sensitive to even tiny deviations in the model parameters, and therefore vastly superior to a simple measurement of Doppler-shifts in the pulse period. Table 1 illustrates the current precision capabilities of pulsar timing for various experiments, like mass determination, astrometry and gravity tests. We will not go into the details of pulsar observations and pulsar timing here, since there are numerous excellent reviews on these topics, for instance [25, 26], just to mention two. In this review we focus on the relativistic effects that play a role in pulsar timing observations, and how pulsar timing can be used to test gravitational phenomena in generic as well as theory-based frameworks.

Table 1: Examples of precision measurements using pulsar timing. A number in bracket indicates the (one-sigma) uncertainty in the last digit of each value. The symbol  $M_{\odot}$  stands for the Solar mass. (cf. table 1 in [28]).

Rotational period:	5.757451924362137(2) ms	[29]
Orbital period:	0.102251562479(8) d	(Kramer et al., in prep.)
Small eccentricity:	$(3.5 \pm 1.1) \times 10^{-7}$	[30]
Distance:	157(1) pc	[29]
Proper motion:	140.915(1) mas yr <sup>-1</sup>	[29]
Masses of neutron stars:	$m_p = 1.4398(2) M_{\odot}$	[31]
	$m_c = 1.3886(2) M_{\odot}$	[31]
Mass of millisecond pulsar:	1.667(7) $M_{\odot}$	[32]
Mass of white-dwarf companion:	0.207(2) $M_{\odot}$	[33]
Mass of Jupiter and moons:	$9.547921(2) \times 10^{-4} M_{\odot}$	[34]
Relativistic periastron advance:	4.226598(5) deg yr <sup>-1</sup>	[31]
Gravitational wave damping:	0.504(3) pico-Hz yr <sup>-1</sup>	(Kramer et al., in prep.)
GR validity (observed/GR):	1.0000(5)	(Kramer et al., in prep.)

## 1.2 Binary pulsar motion in gravity theories

While in Newtonian gravity there is an exact solution to the equations of motion of two point masses that interact gravitationally, no such exact analytic solution is known in GR. In GR, the two-body problem has to be solved numerically or on the basis of approximation methods. A particularly well established and successful approximation scheme, to tackle the problem of motion of a system of well-separated

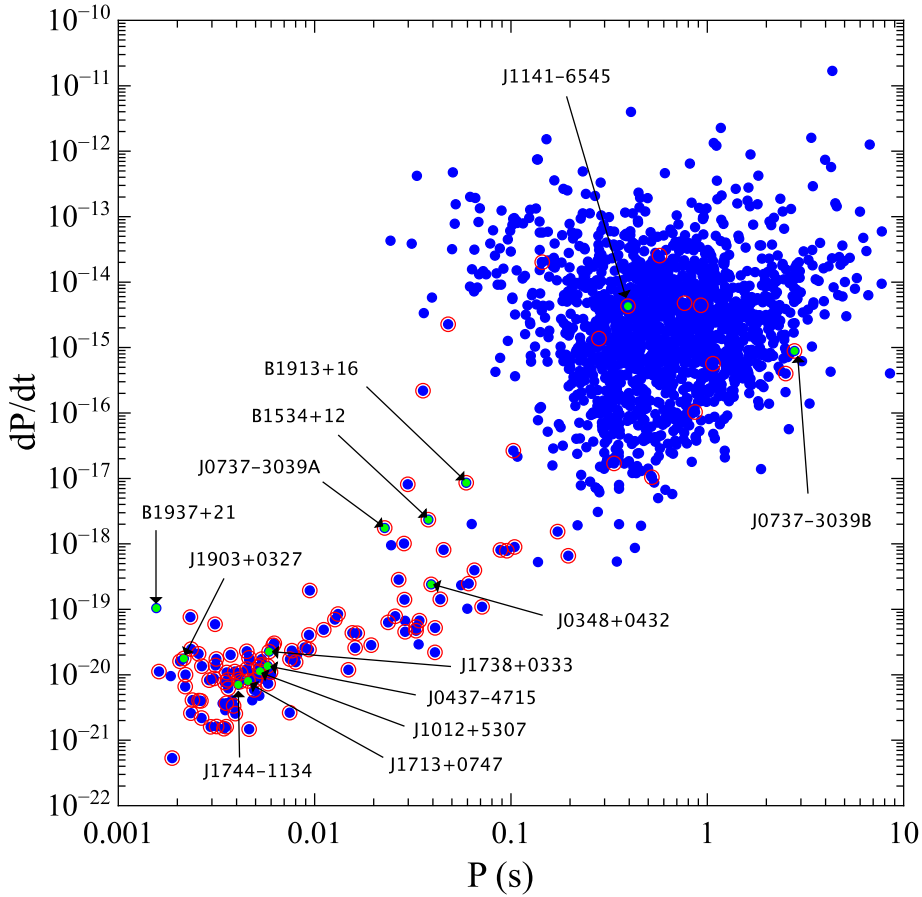


Figure 2: The  $P-\dot{P}$  diagram for radio pulsars. Binary pulsars are indicated by a red circle. Pulsars that play a particular role in this review are marked with a green dot and have their name as a label. The data are taken from the *ATNF Pulsar Catalogue* [22].

bodies, is the *post-Newtonian approximation*, which is based on the weak-field slow-motion assumption. However, to describe the motion and gravitational wave emission of binary pulsars, there are two main limitations of the post-Newtonian approximation that have to be overcome (cf. [35]):

- A) Near and inside the pulsar (and its companion, if it is also a neutron star) the gravitational field is strong and the weak-field assumption no longer holds.
- B) When it comes to generation of gravitational waves (of wavelength  $\lambda_{\text{GW}}$ ) and

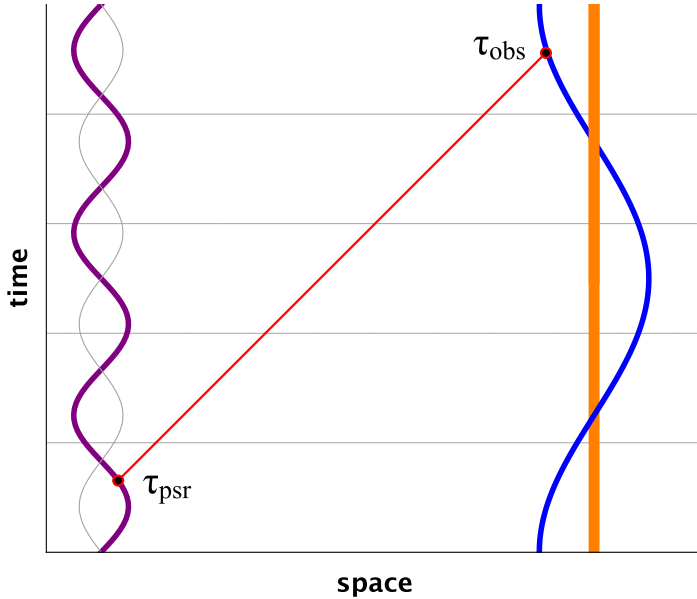


Figure 3: Spacetime diagram illustration of pulsar timing. Pulsar timing connects the proper time of emission  $\tau_{\text{psr}}$ , defined by the pulsar’s intrinsic rotation, and the proper time of the observer on Earth  $\tau_{\text{obs}}$ , measured by the atomic clock at the location of the radio telescope. The timing model, which expresses  $\tau_{\text{obs}}$  as a function of  $\tau_{\text{psr}}$ , accounts for various “relativistic effects” associated with the metric properties of the spacetime, i.e. the world line of the pulsar and the null-geodesic of the radio signal. In addition, it contains a number of terms related to the Earth motion and relativistic corrections in the Solar system, like time dilation and signal propagation delays (see [27] for details).

their back-reaction on the orbit (of size  $r$  and period  $P_b$ ), the post-Newtonian approximation is only valid in the near zone ( $r \ll \lambda_{\text{GW}} = cP_b/2$ ), and breaks down in the radiation zone ( $r > \lambda_{\text{GW}}$ ) where gravitational waves propagate and boundary conditions are defined, like the ‘no incoming radiation’ condition.

The discovery of the Hulse-Taylor pulsar was a particularly strong stimulus for the development of consistent approaches to compute the equations of motion for a binary system with strongly self-gravitating bodies (gravity regime G2). As a result, by now there are fully self-consistent derivations for the gravitational wave emission and the damping of the orbit due to gravitational wave back-reaction for such systems. In fact, in GR, there are several independent approaches that lead to the same result, giving equations of motion for a binary system with non-rotating



components that include terms up to 3.5 post-Newtonian order ( $v^7/c^7$ ) [36, 37]. For the relative acceleration in the center-of-mass frame one finds the general form

$$\ddot{\mathbf{r}} = -\frac{GM}{r^2} \left[ (1 + A_2 + A_4 + A_5 + A_6 + A_7) \frac{\mathbf{r}}{r} + (B_2 + B_4 + B_5 + B_6 + B_7) \dot{\mathbf{r}} \right], \quad (1)$$

where the coefficients  $A_k$  and  $B_k$  are of order  $c^{-k}$ , and are functions of  $r \equiv |\mathbf{r}|$ ,  $\dot{r} \equiv |\dot{\mathbf{r}}|$ , and the masses (see [36] for explicit expressions). The quantity  $M$  denotes the total mass of the system. At this level of approximation, these equations of motion are also applicable to binaries containing strongly self-gravitating bodies, like neutron stars and black holes. This is a consequence of a remarkable property of Einstein’s theory of gravity, the *effacement of the internal structure* [38, 35]: In GR, strong-field contributions are absorbed into the definition of the body’s mass.

In GR’s post-Newtonian approximation scheme, gravitational wave damping enters for the first time at the 2.5 post-Newtonian level (order  $v^5/c^5$ ), as a term in the equations of motion that is not invariant against time-reversal. The corresponding loss of orbital energy is given by the *quadrupole formula*, derived for the first time by Einstein within the linear approximation, for a material system where the gravitational interaction between the masses can be neglected [17]. As it turns out, the quadrupole formula is also applicable for gravity regime G2 of figure 1, and therefore valid for binary pulsars as well (cf. [35]).

In alternative gravity theories, the gravitational wave back-reaction, generally, already enters at the 1.5 post-Newtonian level (order  $v^3/c^3$ ). This is the result of the emission of dipolar gravitational waves, and adds terms  $A_3$  and  $B_3$  to equation (1) [5, 39]. Furthermore, one does no longer have an effacement of the internal structure of a compact body, meaning that the orbital dynamics, in addition to the mass, depends on the “sensitivity” of the body, a quantity that depends on its structure/compactness. Such modifications already enter at the “Newtonian” level, where the usual Newtonian gravitational constant  $G$  is replaced by a (body-dependent) effective gravitational constant  $\mathcal{G}$ . For alternative gravity theories, it therefore generally makes an important difference whether the pulsar companion is a compact neutron star or a much less compact white dwarf. In sum, alternative theories of gravity generally predict deviations from GR in both the quasi-stationary and the radiative properties of binary pulsars [40, 41].

At the first post-Newtonian level, for fully conservative gravity theories without preferred location effects, one can construct a generic *modified Einstein-Infeld-Hoffmann Lagrangian* for a system of two gravitationally interacting masses  $m_p$  (pulsar) and  $m_c$  (companion) at relative (coordinate) separation  $r \equiv |\mathbf{x}_p - \mathbf{x}_c|$  and

velocities  $\mathbf{v}_p = \dot{\mathbf{x}}_p$  and  $\mathbf{v}_c = \dot{\mathbf{x}}_c$ :

$$\begin{aligned}
L_O = & -m_p c^2 \left( 1 - \frac{\mathbf{v}_p^2}{2c^2} - \frac{\mathbf{v}_p^4}{8c^4} \right) - m_c c^2 \left( 1 - \frac{\mathbf{v}_c^2}{2c^2} - \frac{\mathbf{v}_c^4}{8c^4} \right) \\
& + \frac{\mathcal{G} m_p m_c}{r} \left[ 1 - \frac{\mathbf{v}_p \cdot \mathbf{v}_c}{2c^2} - \frac{(\mathbf{r} \cdot \mathbf{v}_p)(\mathbf{r} \cdot \mathbf{v}_c)}{2c^2 r^2} + \varepsilon \frac{(\mathbf{v}_p - \mathbf{v}_c)^2}{2c^2} \right] \\
& - \xi \frac{\mathcal{G}^2 M m_p m_c}{2c^2 r^2}, \tag{2}
\end{aligned}$$

where  $M \equiv m_p + m_c$ . The body-dependent quantities  $\mathcal{G}$ ,  $\varepsilon$  and  $\xi$  account for deviations from GR associated with the self-energy of the individual masses [5, 40]. In GR one simply finds  $\mathcal{G} = G$ ,  $\varepsilon = 3$ , and  $\xi = 1$ . There are various analytical solutions to the dynamics of (2). The most widely used in pulsar astronomy is the quasi-Keplerian parametrization by Damour and Deruelle [42]. It forms the basis of pulsar-timing models for relativistic binary pulsars, as we will discuss in more details in Section 1.4.

Beyond the first post-Newtonian level there is no fully generic framework for the gravitational dynamics of a binary system. However, one can find equations of motion valid for a general class of gravity theories, like in [43] where a framework based on multi-scalar-tensor theories is introduced to discuss tests of relativistic gravity to the second post-Newtonian level, or in [44] where the explicit equations of motion for non-spinning compact objects to 2.5 post-Newtonian order for a general class of scalar-tensor theories of gravity are given.

### 1.3 Gravitational spin effects in binary pulsars

In relativistic gravity theories, in general, the proper rotation of the bodies of a binary system directly affects their orbital and spin dynamics. Equations of motion for spinning bodies in GR have been developed by numerous authors, and in the meantime go way beyond the leading order contributions (for reviews and references see, e.g., [45, 35, 46, 47]). For present day pulsar-timing experiments it is sufficient to have a look at the post-Newtonian leading order contributions. There one finds three contributions: the spin-orbit (SO) interaction between the pulsar's spin  $\mathbf{S}_p$  and the orbital angular momentum  $\mathbf{L}$ , the SO interaction between the companion's spin  $\mathbf{S}_c$  and the orbital angular momentum, and finally the spin-spin interaction between the spin of the pulsar and the spin of the companion [45].

Spin-spin interaction will remain negligible in binary pulsar experiments for the foreseeable future. They are many orders of magnitude below the second post-Newtonian and spin-orbit effects [48], and many orders of magnitude below the

measurement precision of present timing experiments. For this reason, we will not further discuss spin-spin effects here.

For a boost-invariant gravity theory, the (acceleration-dependent) Lagrangian for the spin-orbit interaction has the following general form (summation over spatial indices  $i, j$ )

$$L_{\text{SO}}(\mathbf{x}_A, \mathbf{v}_A, \mathbf{a}_A) = \frac{1}{c^2} \sum_A S_A^{ij} \left[ \frac{1}{2} v_A^i a_A^j + \sum_{B \neq A} \frac{\Gamma_A^B m_B}{r_{AB}^3} (v_A^i - v_B^i)(x_A^j - x_B^j) \right], \quad (3)$$

where  $S_A^{ij} \equiv \varepsilon^{ijk} S_A^k$  is the antisymmetric spin tensor of body  $A$  [49, 35, 40]. The coupling function  $\Gamma_A^B$  can also account for strong-field effects in the spin-orbit coupling. In GR  $\Gamma_A^B = 2G$ . For bodies with negligible gravitational self-energy, one finds in the framework of the *parametrized post-Newtonian (PPN) formalism*<sup>2</sup>  $\Gamma_A^B = (\gamma_{\text{PPN}} + 1)G$ , a quantity that is actually most tightly constrained by the light-bending and Shapiro-delay experiments in the Solar system, which test  $\gamma_{\text{PPN}}$  [8, 9, 10, 12].

In binary pulsars, spin-orbit coupling has two effects. On the one hand, it adds spin-dependent terms to the equations of motion (1), which cause a Lense-Thirring precession of the orbit (for GR see [45, 50]). So far this contribution could not be tested in binary pulsar experiments. Prospects of its measurement will be discussed in the future outlook in Section 8. On the other hand it leads to secular changes in the orientation of the spins of the two bodies (geodetic precession), most importantly the observed pulsar in a pulsar binary [51, 45, 52]. As we discuss in more details in Section 3, a change in the rotational axis of the pulsar causes changes in the observed emission properties of the pulsar, as the line-of-sight gradually cuts through different regions of the magnetosphere.

As can be derived from (3), to first order in GR the geodetic precession of the pulsar, averaged over one orbit, is given by ( $\hat{\mathbf{L}} \equiv \mathbf{L}/|\mathbf{L}|$ )

$$\boldsymbol{\Omega}_p^{\text{SO}} = \frac{n_b}{1 - e^2} \left( 2 + \frac{3m_c}{2m_p} \right) \frac{m_p m_c}{M^2} \frac{V_b^2}{c^2} \hat{\mathbf{L}}, \quad (4)$$

where  $n_b \equiv 2\pi/P_b$  and  $V_b \equiv (GMn_b)^{1/3}$ .

It is expected that in alternative theories relativistic spin precession generally depends on self-gravitational effects, meaning, the actual precession may depend on the compactness of a self-gravitating body. For the class of theories that lead to the Lagrangian (3), equation (4) modifies to

$$\boldsymbol{\Omega}_p^{\text{SO}} = \frac{n_b}{1 - e^2} \left[ \frac{\Gamma_p^c}{\mathcal{G}} + \left( \frac{\Gamma_p^c}{\mathcal{G}} - \frac{1}{2} \right) \frac{m_c}{m_p} \right] \frac{m_p m_c}{M^2} \frac{V_b^2}{c^2} \hat{\mathbf{L}}, \quad (5)$$

---

<sup>2</sup>The PPN formalism uses 10 parameters to parametrize in a generic way deviations from GR at the post-Newtonian level, within the class of metric gravity theories (see [5] for details).

where  $\mathcal{V}_b \equiv (\mathcal{G}Mn_b)^{1/3}$  is the strong-field generalization of  $V_b$ .

Effects from spin-induced quadrupole moments are negligible as well. For double neutron-star systems they are many orders of magnitude below the second post-Newtonian and spin-orbit effects, due to the small extension of the bodies [48]. If the companion is a more extended star, like a white dwarf or a main-sequence star, the rotationally-induced quadrupole moment might become important. A prime example is PSR J0045–7319, where the quadrupole moment of the fast rotating companion causes a significant precession of the pulsar orbit [53]. For all the binary pulsars discussed here, the quadrupole moments of pulsar and companion are (currently) negligible.

Finally, certain gravitational phenomena, not present in GR, can even lead to a spin precession of isolated pulsars, for instance, a violation of the local Lorentz invariance and a violation of the local position invariance in the gravitational sector, as we will discuss in more details in Sections 5 and 6.

#### 1.4 Phenomenological approach to relativistic effects in binary pulsar observations

For binary pulsar experiments that test the quasi-stationary strong-field regime (G2) and the gravitational wave damping (GW), a phenomenological parametrization, the so-called ‘parametrized post-Keplerian’ (PPK) formalism, has been introduced by Damour [54] and extended by Damour and Taylor [40]. The PPK formalism parametrizes all the observable effects that can be extracted independently from binary pulsar timing and pulse-structure data. Consequently, the PPK formalism allows to obtain theory-independent information from binary pulsar observations by fitting for a set of *Keplerian* and *post-Keplerian parameters*.

The description of the orbital motion is based on the quasi-Keplerian parametrization of Damour & Deruelle, which is a solution to the first post-Newtonian equations of motion [42, 55]. The corresponding *Roemer delay* in the arrival time of the pulsar signals is

$$\Delta_{\text{R}} = x \sin \omega [\cos U - e(1 + \delta_r)] + x \cos \omega [1 - e^2(1 + \delta_\theta)^2]^{1/2} \sin U, \quad (6)$$

where the eccentric anomaly  $U$  is linked to the proper time of the pulsar  $T$  via the Kepler equation

$$U - e \sin U = 2\pi \left[ \left( \frac{T - T_0}{P_b} \right) - \frac{\dot{P}_b}{2} \left( \frac{T - T_0}{P_b} \right)^2 \right]. \quad (7)$$

The five Keplerian parameters  $P_b$ ,  $e$ ,  $x$ ,  $\omega$ , and  $T_0$  denote the orbital period, the orbital eccentricity, the projected semi-major axis of the pulsar orbit, the longitude

of periastron, and the time of periastron passage, respectively. The post-Keplerian parameter  $\delta_r$  is not separately measurable, i.e. it can be absorbed into other timing parameters, and the post-Keplerian parameter  $\delta_\theta$  has not been measured up to now in any of the binary pulsar systems. The relativistic precession of periastron changes the the longitude of periastron  $\omega$  according to

$$\omega = \omega_0 + \dot{\omega} \frac{P_b}{\pi} \arctan \left[ \left( \frac{1+e}{1-e} \right)^{1/2} \tan \frac{U}{2} \right], \quad (8)$$

meaning, that averaged over a full orbit, the location of periastron shifts by an angle  $\dot{\omega}P_b$ . The parameter  $\dot{\omega}$  is the corresponding post-Keplerian parameter. A change in the orbital period, due to the emission of gravitational waves, is parametrized by the post-Keplerian parameter  $\dot{P}_b$ . Correspondingly, one has post-Keplerian parameters for the change in the orbital eccentricity and the projected semi-major axis:

$$e = e_0 + \dot{e}(T - T_0), \quad (9)$$

$$x = x_0 + \dot{x}(T - T_0). \quad (10)$$

Besides the Roemer delay  $\Delta_R$ , there are two purely relativistic effects that play an important role in pulsar timing experiments. In an eccentric orbit, one has a changing time dilation of the “pulsar clock” due to a variation in the orbital velocity of the pulsar and a change of the gravitational redshift caused by the gravitational field of the companion. This so-called *Einstein delay* is a periodic effect, whose amplitude is given by the post-Keplerian parameter  $\gamma$ , and to first order can be written as

$$\Delta_E = \gamma \sin U. \quad (11)$$

For sufficiently edge-on and/or eccentric orbits the propagation delay suffered by the pulsar signals in the gravitational field of the companion becomes important. This so-called *Shapiro delay*, to first order, reads

$$\Delta_S = -2r \ln \left[ 1 - e \cos U - s \sin \omega (\cos U - e) - s \cos \omega (1 - e^2)^{1/2} \sin U \right], \quad (12)$$

where the two post-Keplerian parameters  $r$  and  $s$  are called *range* and *shape* of the Shapiro delay. The latter is linked to the inclination of the orbit with respect to the line of sight,  $i$ , by  $s = \sin i$ . It is important to note, that for  $i \rightarrow 90^\circ$  equation (12) breaks down and higher order corrections are needed. But so far, equation (12) is fully sufficient for the timing observations of known pulsars [56].

Concerning the post-Keplerian parameters related to quasi-stationary effects, for the wide class of boost-invariant gravity theories one finds that they can be

expressed as functions of the Keplerian parameters, the masses, and parameters generically accounting for gravitational self-field effects (cf. equation (2)) [40, 5]:

$$\dot{\omega} = \frac{n_b}{1-e^2} \left( \varepsilon - \frac{\xi}{2} + \frac{1}{2} \right) \frac{\mathcal{V}_b^2}{c^2}, \quad (13)$$

$$\gamma = \frac{e}{n_b} \left( \frac{G_{0c}}{\mathcal{G}} + \mathcal{K}_p^c + \frac{m_c}{M} \right) \frac{m_c}{M} \frac{\mathcal{V}_b^2}{c^2}, \quad (14)$$

$$r = \frac{1 + \varepsilon_{0c}}{4} \frac{G_{0c} m_c}{c^3}, \quad (15)$$

$$s = x n_b \frac{M}{m_c} \frac{c}{\mathcal{V}_b}, \quad (16)$$

plus  $\Omega^{\text{SO}}$  from equation (5). Here we have listed only those parameters that play a role in this review. For a complete list and a more detailed discussion, the reader is referred to [40]. The quantities  $G_{0c}$  and  $\varepsilon_{0c}$  are related to the interaction of the companion with a test particle or a photon. The parameter  $\mathcal{K}_p^c$  accounts for a possible change in the moment of inertia of the pulsar due to a change in the local gravitational constant. In GR one finds  $\mathcal{G} = G_{0c} = G$ ,  $\varepsilon = \varepsilon_{0c} = 3$ ,  $\xi = 1$  and  $\mathcal{K}_p^c = 0$ . Consequently

$$\dot{\omega}^{\text{GR}} = \frac{3n_b}{1-e^2} \frac{V_b^2}{c^2}, \quad (17)$$

$$\gamma^{\text{GR}} = \frac{e}{n_b} \left( 1 + \frac{m_c}{M} \right) \frac{m_c}{M} \frac{V_b^2}{c^2}, \quad (18)$$

$$r^{\text{GR}} = \frac{Gm_c}{c^3}, \quad (19)$$

$$s^{\text{GR}} = x n_b \frac{M}{m_c} \frac{c}{V_b}. \quad (20)$$

These parameters are independent of the internal structure of the neutron star(s), due to the effacement of the internal structure, a property of GR [38, 35]. For most alternative gravity theories this is not the case. For instance, in the mono-scalar-tensor theories  $T_1(\alpha_0, \beta_0)$  of [57, 58], one finds<sup>3</sup>

$$\dot{\omega}^{T_1} = \frac{n_b}{1-e^2} \left( \frac{3 - \alpha_p \alpha_c}{1 + \alpha_p \alpha_c} - \frac{m_p \alpha_p^2 \beta_c + m_c \alpha_c^2 \beta_p}{2M(1 + \alpha_p \alpha_c)^2} \right) \frac{\mathcal{V}_b^2}{c^2}, \quad (21)$$

$$\gamma^{T_1} = \frac{e}{n_b} \left( \frac{1 + k_p \alpha_c}{1 + \alpha_p \alpha_c} + \frac{m_c}{M} \right) \frac{m_c}{M} \frac{\mathcal{V}_b^2}{c^2}, \quad (22)$$

---

<sup>3</sup>The mono-scalar-tensor theories  $T_1(\alpha_0, \beta_0)$  of [57, 58] have a conformal coupling function  $A(\varphi) = \alpha_0(\varphi - \varphi_0) + \beta_0(\varphi - \varphi_0)^2/2$ . The Jordan-Fierz-Brans-Dicke gravity is the sub-class with  $\beta_0 = 0$ , and  $\alpha_0^2 = (2\omega_{\text{BD}} + 3)^{-1}$ .

$$r^{T_1} = \frac{G_* m_c}{c^3}, \quad (23)$$

$$s^{T_1} = x n_b \frac{M}{m_c} \frac{c}{\mathcal{V}_b}, \quad (24)$$

where  $\mathcal{V}_b = [G_*(1 + \alpha_p \alpha_c) M n_b]^{1/3}$ . The body-dependent quantities  $\alpha_p$  and  $\alpha_c$  denote the effective scalar coupling of pulsar and companion respectively, and  $\beta_A \equiv \partial \alpha_A / \partial \varphi_0$  where  $\varphi_0$  denotes the asymptotic value of the scalar field at spatial infinity. The quantity  $k_p$  is related to the moment of inertia  $I_p$  of the pulsar via  $k_p \equiv -\partial \ln I_p / \partial \varphi_0$ . For a given equation of state, the parameters  $\alpha_A$ ,  $\beta_A$ , and  $k_A$  depend on the fundamental constants of the theory, e.g.  $\alpha_0$  and  $\beta_0$  in  $T_1(\alpha_0, \beta_0)$ , and the mass of the body. As we will demonstrate later, these “gravitational form factors” can assume large values in the strong gravitational fields of neutron stars. Depending on the value of  $\beta_0$ , this is even the case for a vanishingly small  $\alpha_0$ , where there are practically no measurable deviations from GR in the Solar system. In fact, even for  $\alpha_0 = 0$ , a neutron star, above a certain  $\beta_0$ -dependent critical mass, can have an effective scalar coupling  $\alpha_A$  of order unity. This non-perturbative strong-field behavior, the so-called “spontaneous scalarization” of a neutron star, was discovered 20 years ago by Damour and Esposito-Farèse [57].

Finally, there is the post-Keplerian parameter  $\dot{P}_b$ , related to the damping of the orbit due to the emission of gravitational waves. We have seen above that in alternative gravity theories the back reaction from the gravitational wave emission might enter the equations of motion already at the 1.5 post-Newtonian level, giving rise to a  $\dot{P}_b \propto \mathcal{V}_b^3 / c^3$ . To leading order one finds in mono-scalar-tensor gravity the dipolar contribution from the scalar field [59, 60, 58]:

$$\dot{P}_b = -2\pi \frac{m_p m_c}{M^2} \frac{1 + e^2/2}{(1 - e^2)^{5/2}} \frac{\mathcal{V}_b^3}{c^3} \frac{(\alpha_p - \alpha_c)^2}{1 + \alpha_p \alpha_c} + \mathcal{O}(\mathcal{V}_b^5 / c^5). \quad (25)$$

As one can see, the change in the orbital period due to dipolar radiation depends strongly on the difference in the effective scalar coupling  $\alpha_A$ . Binary pulsar systems with a high degree of asymmetry in the compactness of their components are therefore ideal to test for dipolar radiation. An order unity difference in the effective scalar coupling would lead to a change in the binary orbit, which is several orders of magnitude ( $\sim c^2 / \mathcal{V}_b^2$ ) stronger than the quadrupolar damping predicted by GR.

At the 2.5 post-Newtonian level ( $\propto \mathcal{V}_b^5 / c^5$ ), in general, there are several contributions entering the  $\dot{P}_b$  calculation:

- Monopolar waves for eccentric orbits.
- Higher order contributions to the dipolar wave damping.

- Quadrupolar waves from the tensor field, and the fields that are also responsible for the monopolar and/or dipolar waves.

For scalar-tensor gravity these expressions can be found in [61]. For GR one finds from the well-known *quadrupole formula* [17, 62]:

$$\dot{P}_b^{\text{GR}} = -\frac{192\pi}{5} \frac{m_p m_c}{M^2} \frac{1 + 73e^2/24 + 37e^4/96}{(1 - e^2)^{7/2}} \frac{V_b^5}{c^5}. \quad (26)$$

Apart from a change in the orbital period, gravitational wave damping will also affect other post-Keplerian parameters. While gravitational waves carry away orbital energy and angular momentum, Keplerian parameters like the eccentricity and the semi-major axis of the pulsar orbit change as well. The corresponding post-Keplerian parameters are  $\dot{e}$  and  $\dot{x}$  respectively. However, these changes affect the arrival times of the pulsar signals much less than the  $\dot{P}_b$ , and therefore do (so far) not play a role in the radiative tests with binary pulsars.

As already mentioned in Section 1.2, there is no generic connection between the higher-order gravitational wave damping effects and the parameters  $\mathcal{G}$ ,  $\varepsilon$ , and  $\xi$  of the modified Einstein-Infeld-Hoffmann formalism. Such higher order, mixed radiative and strong-field effects depend in a complicated way on the structure of the gravity theory [40].

The post-Keplerian parameters are at the foundation of many of the gravity tests conducted with binary pulsars. As shown above, the exact functional dependence differs for given theories of gravity. A priori, the masses of the pulsar and the companion are undetermined, but they represent the only unknowns in this set of equations. Hence, once two post-Keplerian parameters are measured, the corresponding equations can be solved for the two masses, and the values for other post-Keplerian parameters can be predicted for an assumed theory of gravity. Any further post-Keplerian measurement must therefore be consistent with that prediction, otherwise the assumed theory has to be rejected. In other words, if  $N \geq 3$  post-Keplerian parameters can be measured, a total of  $N - 2$  independent tests can be performed. The method is very powerful, as any additionally measured post-Keplerian parameter is potentially able to fail the prediction and hence to falsify the tested theory of gravity. The standard graphical representation of such tests, as will become clear below, is the mass-mass diagram. Every measured post-Keplerian parameter defines a curve of certain width (given by the measurement uncertainty of the post-Keplerian parameter) in a  $m_p$ - $m_c$  diagram. A theory has passed a binary pulsar test, if there is a region in the mass-mass diagram that agrees with all post-Keplerian parameter curves.



## 2 Gravitational wave damping

### 2.1 The Hulse-Taylor pulsar

The first binary pulsar to ever be observed happened to be a rare double neutron star system. It was discovered by Russell Hulse and Joseph Taylor in summer 1974 [19]. The pulsar, PSR B1913+16, has a rotational period of 59 ms and is in a highly eccentric ( $e = 0.62$ ) 7.75-hour orbit around an unseen companion. Shortly after the discovery of PSR B1913+16, it has been realized that this system may allow the observation of gravitational wave damping within a time span of a few years [63, 64].

The first relativistic effect seen in the timing observations of the Hulse-Taylor pulsar was the secular advance of periastron  $\dot{\omega}$ . Thanks to its large value of 4.2 deg/yr, this effect was well measured already one year after the discovery [65]. Due to the, a priori, unknown masses of the system, this measurement could not be converted into a quantitative gravity test. However, assuming GR is correct, equation (17) gives the total mass  $M$  of the system. From the modern value given in table 2 one finds  $M = m_p + m_c = 2.828378 \pm 0.000007 M_\odot$  [31].<sup>4</sup>

It took a few more years to measure the Einstein delay (11) with good precision. In a single orbit this effect is exactly degenerate with the Roemer delay, and only due to the relativistic precession of the orbit these two delays become separable [63, 67]. By the end of 1978, the timing of PSR B1913+16 yielded a measurement of the post-Keplerian parameter  $\gamma$ , which is the amplitude of the Einstein delay [68]. Together with the total mass from  $\dot{\omega}^{\text{GR}}$ , equation (18) can now be used to calculate the individual masses. With the modern value for  $\gamma$  from table 2, and the total mass given above, one finds the individual masses  $m_p = 1.4398 \pm 0.0002 M_\odot$  and  $m_c = 1.3886 \pm 0.0002 M_\odot$  for pulsar and companion respectively [31].

With the knowledge of the two masses,  $m_p$  and  $m_c$ , the binary system is fully determined, and further GR effects can be calculated and compared with the observed values, providing an intrinsic consistency check of the theory. In fact, Taylor *et al.* [68] reported the measurement of a decrease in the orbital period  $\dot{P}_b$ , consistent with the quadrupole formula (26). This was the first proof for the existence of gravitational waves as predicted by GR. In the meantime the  $\dot{P}_b$  is measured with a precision of 0.04% (see table 2). However, this is not the precision with which the validity of the quadrupole formula is verified in the PSR B1913+16 system. The observed  $\dot{P}_b$  needs to be corrected for extrinsic effects, most notably the differential Galactic acceleration and the Shklovskii effect, to obtain the intrinsic value

---

<sup>4</sup>Strictly speaking, this is the total mass of the system scaled with an unknown Doppler factor  $D$ , i.e.  $M^{\text{observed}} = D^{-1} M^{\text{intrinsic}}$  [40]. For typical velocities,  $D - 1$  is expected to be of order  $10^{-4}$ , see for instance [66]. In gravity tests based on post-Keplerian parameters, the factor  $D$  drops out and is therefore irrelevant [55].

caused by gravitational wave damping [69, 70]. The extrinsic contribution due to the Galactic gravitational field (acceleration  $\mathbf{g}$ ) and the proper motion (transverse angular velocity in the sky  $\mu$ ) are given by

$$\delta\dot{P}_b^{\text{ext}} = \frac{P_b}{c} \left[ \hat{\mathbf{K}}_0 \cdot (\mathbf{g}_{\text{PSR}} - \mathbf{g}_\odot) + \mu^2 d \right], \quad (27)$$

where  $\hat{\mathbf{K}}_0$  is the unit vector pointing towards the pulsar, which is at a distance  $d$  from the Solar system. For PSR B1913+16,  $P_b$  and  $\hat{\mathbf{K}}_0$  are measured with very high precision, and also  $\mu$  is known with good precision ( $\sim 8\%$ ). However, there is a large uncertainty in the distance  $d$ , which is also needed to calculate the Galactic acceleration of the PSR B1913+16 system,  $\mathbf{g}_{\text{PSR}}$ , in equation (27). Due to its large distance, there is no direct parallax measurement for  $d$ , and estimates for  $d$  are based on model dependent methods, like the measured column density of free electrons between PSR B1913+16 and the Earth. Such methods are known to have large systematic uncertainties, and for this reason the distance to PSR B1913+16 is not well known:  $d = 9.9 \pm 3.1$  kpc [71, 31]. In addition, there are further uncertainties, e.g. in the Galactic gravitational potential and the distance of the Earth to the Galactic center. Accounting for all these uncertainties leads to an agreement between  $\dot{P}_b - \delta\dot{P}_b^{\text{ext}}$  and  $\dot{P}_b^{\text{GR}}$  at the level of about 0.3% [31]. The corresponding mass-mass diagram is given in figure 4. As the precision of the radiative test with PSR B1913+16 is limited by the model-dependent uncertainties in equation (27), it is not expected that this test can be significantly improved in the near future.

Finally, besides the mass-mass diagram, there is a different way to illustrate the test of gravitational wave damping with PSR B1913+16. According to equation (7), the change in the orbital period, i.e. the post-Keplerian parameter  $\dot{P}_b$ , is measured from a shift in the time of periastron passage, where  $U$  is a multiple of  $2\pi$ . One finds for the shift in periastron time, as compared to an orbit with zero decay

$$\Delta T = \frac{1}{2} P_b \dot{P}_b n^2 + \mathcal{O}(P_b \dot{P}_b^2 n^3), \quad (28)$$

where  $n = 0, 1, 2, \dots$  denotes the number of the periastron passage, and is given by  $n \simeq (T - T_0)/P_b$ . Equation (28) represents a parabola in time, which can be calculated with high precision using the masses that come from  $\dot{\omega}^{\text{GR}}$  and  $\gamma^{\text{GR}}$  (see above). On the other hand, the observed cumulative shift in periastron can be extracted from the timing observations with high precision. A comparison of observed and predicted cumulative shift in the time of the periastron passage is given in figure 5.

Table 2: Observed orbital timing parameters of PSR B1913+16, based on the Damour-Deruelle timing model (taken from [31]). Figures in parentheses represent estimated uncertainties in the last quoted digit.

$T_0$	time of periastron passage (MJD)	52144.90097841(4)
$x$	projected semi-major axis of the pulsar orbit (s)	2.341782(3)
$e$	orbital eccentricity	0.6171334(5)
$P_b$	orbital period at $T_0$ (d)	0.322997448911(4)
$\omega_0$	longitude of periastron at $T_0$ (deg)	292.54472(6)
$\dot{\omega}$	secular advance of periastron (deg/yr)	4.226598(5)
$\gamma$	amplitude of Einstein delay (ms)	4.2992(8)
$\dot{P}_b$	secular change of orbital period	$-2.423(1) \times 10^{-12}$

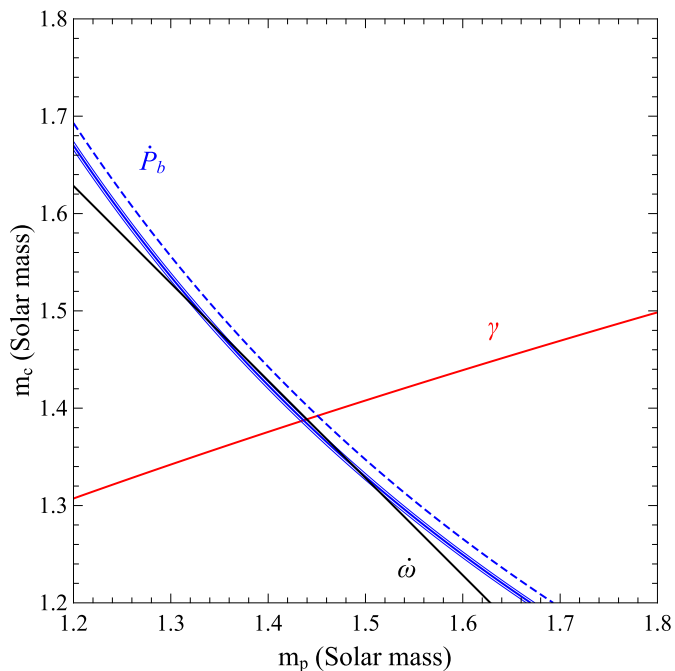


Figure 4: Mass-mass diagram for PSR B1913+16 based on GR and the three observed post-Keplerian parameters  $\dot{\omega}$  (black),  $\gamma$  (red) and  $\dot{P}_b$  (blue). The dashed  $\dot{P}_b$  curve is based on the observed  $\dot{P}_b$ , without corrections for Galactic and Shklovskii effects. The solid  $\dot{P}_b$  curve is based on the corrected (intrinsic)  $\dot{P}_b$ , where the thin lines indicate the one-sigma boundaries. Values are taken from table 2.

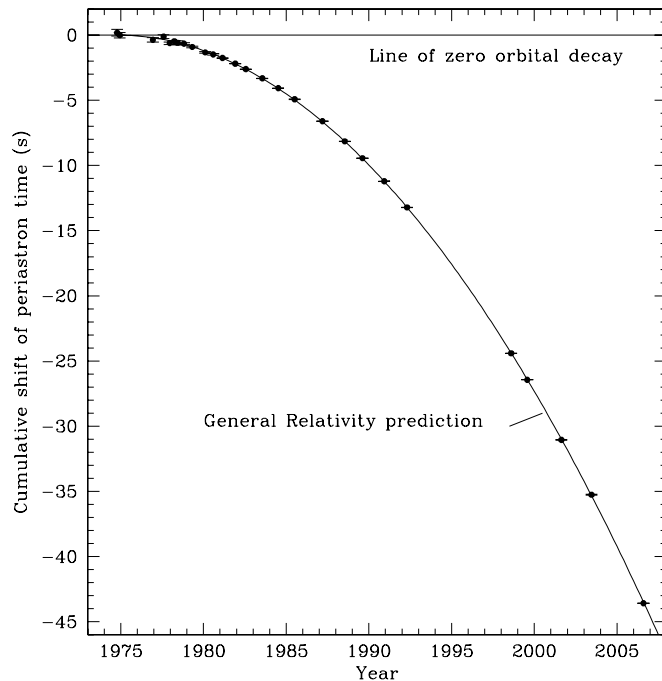


Figure 5: Shift in the time of periastron passage of PSR B1913+16 due to gravitational wave damping. The parabola represents the GR prediction and the data points the timing measurements, with (vertical) error bars mostly too small to be resolved. The observed shift in periastron time is a direct measurement of the change in the world-line of the pulsar due to the back-reaction of the emitted gravitational waves (cf. figure 3). The corresponding spatial shift amounts to about 20 000 km. Figure is taken from [31].

## 2.2 The Double Pulsar — The best test for Einstein’s quadrupole formula, and more

In 2003 a binary system was discovered where, at first, one member was identified as a pulsar with a 23 ms period [72]. About half a year later, the companion was also recognized as a radio pulsar with a period of 2.8 s [73]. Both pulsars, known as PSRs J0737–3039A and J0737–3039B, respectively, (or *A* and *B* hereafter), orbit each other in less than 2.5 hours in a mildly eccentric ( $e = 0.088$ ) orbit. As a result, the system is not only the first and only double neutron star system where both neutron stars are visible as active radio pulsars, but it is also the most relativistic binary pulsar laboratory for gravity known to date (see figure 6). Just to give an example for the strength of relativistic effects, the advance of periastron,  $\dot{\omega}$ , is 17

degrees per year, meaning that the eccentric orbit does a full rotation in just 21 years. In this subsection, we briefly discuss the properties of this unique system, commonly referred to as the *Double Pulsar*, and highlight some of the gravity tests that are based on the radio observations of this system. For detailed reviews of the Double Pulsar see [74, 75].

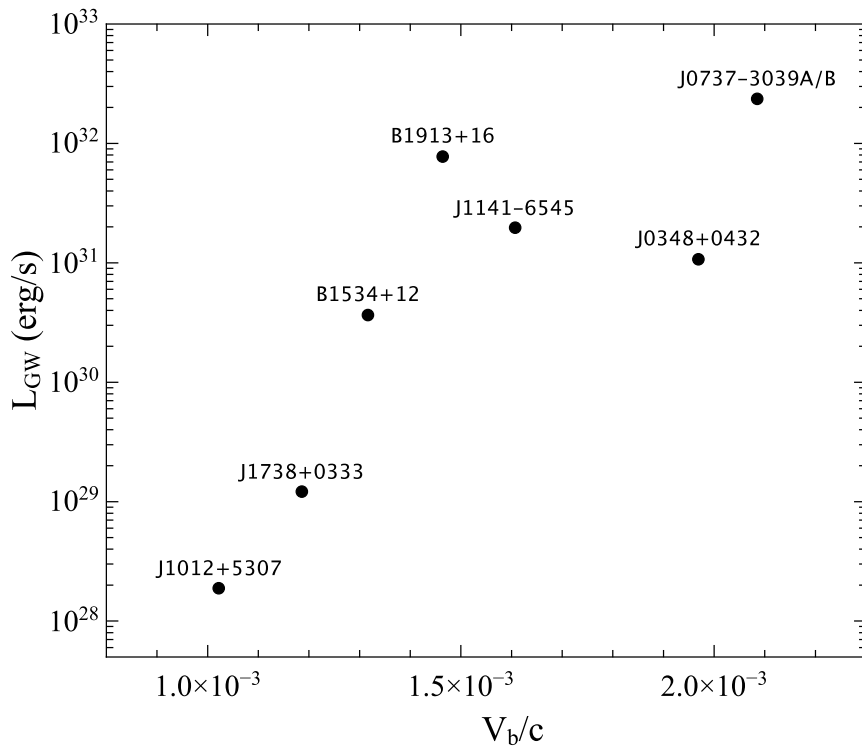


Figure 6: Short-orbital-period ( $P_b < 1$  day) binary pulsars used for gravity tests. The velocity  $V_b$  (divided by the speed of light  $c$ ) is a direct measure for the strength of post-Newtonian effects in the orbital dynamics. The gravitational wave luminosity  $L_{GW}$  is an indicator for the strength of radiative effects that cause secular changes to the orbital elements due to gravitational wave damping.

In the Double Pulsar system a total of six post-Keplerian parameters have been measured by now. Five arise from four different relativistic effects visible in pulsar timing [76], while a sixth one can be determined from the effects of geodetic precession, which will be discussed in detail in Section 3.2 below. The relativistic precession of the orbit,  $\dot{\omega}$ , was measured within a few days after timing of the system commenced, and by 2006 it was already known with a precision of 0.004% (see

table 3). At the same time the measurement of the amplitude of Einstein delay,  $\gamma$ , reached 0.7% (see table 3). Due to the periastron precession of 17 degrees per year, the Einstein delay was soon well separable from the Roemer delay. Two further post-Keplerian parameters came from the detection of the Shapiro delay: the *shape* and *range* parameters  $s$  and  $r$ . They were measured with a precision of 0.04% and 5%, respectively (see table 3). From the measured value  $s = \sin i = 0.99974_{-0.00039}^{+0.00016}$  ( $i = 88.7_{-0.8}^{+0.5}$ ) one can already see how exceptionally edge-on this system is.<sup>5</sup> Finally, the decrease of the orbital period due to gravitational wave damping was measured with a precision of 1.4% just three years after the discovery of the system (see table 3).

Table 3: A selection of observed orbital timing parameters of the Double Pulsar, based on the Damour-Deruelle timing model (taken from [76]). All post-Keplerian parameters below are obtained from the timing of pulsar  $A$ . The timing precision for pulsar  $B$  is considerably lower, and allows only for a, in comparison, low precision measurement ( $\sim 0.3\%$ ) of  $\dot{\omega}$  [76]. Figures in parentheses represent estimated uncertainties in the last quoted digit.

$x_A \equiv a_A \sin i/c$	projected semi-major axis of pulsar $A$ (s)	1.415032(1)
$x_B \equiv a_B \sin i/c$	projected semi-major axis of pulsar $B$ (s)	1.5161(16)
$e$	orbital eccentricity	0.0877775(9)
$P_b$	orbital period (d)	0.10225156248(5)
$\dot{\omega}$	secular advance of periastron (deg/yr)	16.89947(68)
$\gamma$	amplitude of Einstein delay for $A$ (ms)	0.3856(26)
$\dot{P}_b$	secular change of orbital period	$-1.252(17) \times 10^{-12}$
$s$	<i>shape</i> of Shapiro delay for $A$	0.99974(−39, +16)
$r$	<i>range</i> of Shapiro delay for $A$ ( $\mu\text{s}$ )	6.21(33)

A unique feature of the Double Pulsar is its nature as a “dual-line source”, i.e. we measure the orbits of both neutron stars at the same time. Obviously, the sizes of the two orbits are not independent from each other as they orbit a common center of mass. In GR, up to first post-Newtonian order the relative size of the orbits is identical to the inverse ratio of masses. Hence, by measuring the orbits of the two pulsars (relative to the centre of mass), we obtain a precise measurement of the mass ratio. This ratio is directly observable, as the orbital inclination angle is obviously identical for both pulsars, i.e.

$$R \equiv \frac{m_A}{m_B} = \frac{a_B}{a_A} = \frac{a_B \sin i/c}{a_A \sin i/c} \equiv \frac{x_B}{x_A}. \quad (29)$$

<sup>5</sup>The only binary pulsar known to be (most likely) even more edge-on is PSR J1614–2230 with  $s = \sin i = 0.999894 \pm 0.000005$  ( $i = 89.17^\circ \pm 0.02^\circ$ ) [77]. For this wide-orbit system ( $P_b \approx 8.7$  d), however, no further post-Keplerian parameter is known that could be used in a gravity test.

This expression is not just limited to GR. In fact, it is valid up to first post-Newtonian order and free of any explicit strong-field effects in any Lorentz-invariant theory of gravity (see [41] for a detailed discussion). Using the parameter values of table 3, one finds that in the Double Pulsar the masses are nearly equal with  $R = 1.0714 \pm 0.0011$ .

As it turns out, all the post-Keplerian parameters measured from timing are consistent with GR. In addition, the region of allowed masses agrees well with the measured mass ratio  $R$  (see figure 7). One has to keep in mind, that the test presented here is based on data published in 2006 [76]. In the meantime continued timing lead to a significant decrease in the uncertainties of the post-Keplerian parameters of the Double pulsar. This is especially the case for  $\dot{P}_b$ , for which the uncertainty typically decreases with  $T_{\text{obs}}^{-2.5}$  [78],  $T_{\text{obs}}$  being the total time span of timing observations. The new results will be published in an upcoming publication (Kramer *et al.*, in prep.). As reported in [28], presently the Double Pulsar provides the best test for the GR quadrupole formalism for gravitational wave generation, with an uncertainty well below the 0.1% level. As discussed above, the Hulse-Taylor pulsar is presently limited by uncertainties in its distance. This raises the valid question, at which level such uncertainties will start to limit the radiative test with the Double Pulsar as well. Compared to the Hulse-Taylor pulsar, the Double Pulsar is much closer to Earth. Because of this, a direct distance estimate of  $1.15^{+0.22}_{-0.16}$  kpc based on a parallax measurement with long-baseline interferometry was obtained [79]. Thus, with the current accuracy in the measurement of distance and transverse velocity, GR tests based on  $\dot{P}_b$  can be taken to the 0.01% level. We will come back to this in Section 8, where we discuss some future tests with the Double Pulsar.

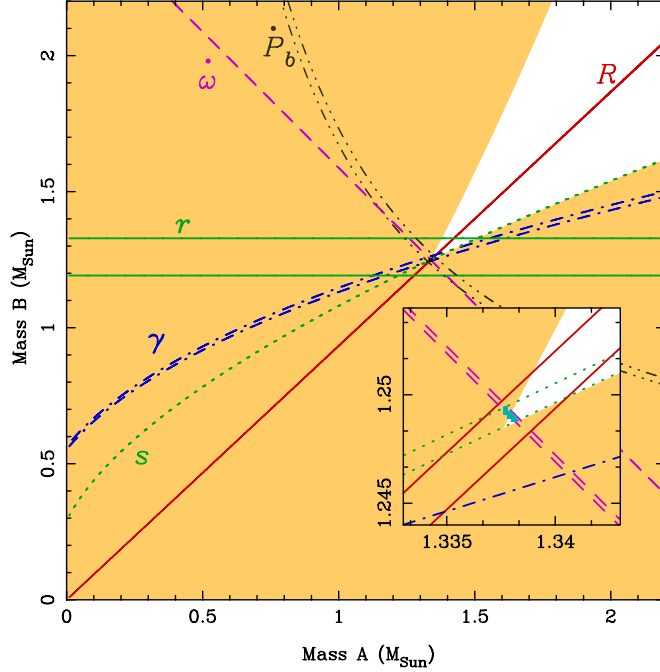


Figure 7: GR mass-mass diagram based on timing observations of the Double Pulsar. The orange areas are excluded simply by the fact that  $\sin i \leq 1$ . The figure is taken from [75] ( $\Omega_{\text{SO}}$  lines removed) and based on the timing solution published in [76].

With the large number of post-Keplerian parameters and the known mass ratio, the Double Pulsar is the most over-constrained binary pulsar system. For this reason, one can do more than just testing specific gravity theories. The Double Pulsar allows for certain generic tests on the orbital dynamics, time dilation, and photon propagation of a spacetime with two strongly self-gravitating bodies [75]. First, the fact that the Double Pulsar gives access to the mass ratio,  $R$ , in any Lorentz-invariant theory of gravity, allows us to determine  $m_A/M = R/(1 + R) = 0.51724 \pm 0.00026$  and  $m_B/M = 1/(1 + R) = 0.48276 \pm 0.00026$ . With this information at hand, the measurement of the shape of the Shapiro delay  $s$  can be used to determine  $\mathcal{V}_b$  via equation (16):  $\mathcal{V}_b/c = (2.0854 \pm 0.0014) \times 10^{-3}$ . At this point, the measurement of the post-Keplerian parameters  $\dot{\omega}$ ,  $\gamma$ , and  $r$  (equations (13), (14), (15)) can be used to impose restrictions on the “strong-field” parameters of Lagrangian (2) [75]:

$$\frac{2\varepsilon - \xi}{5} = 0.9995 \pm 0.0016, \quad (30)$$

$$\frac{G_{0B}}{\mathcal{G}} + \mathcal{K}_A^B = 1.005 \pm 0.010, \quad (31)$$



$$\frac{\varepsilon_{0B} + 1}{4} \frac{G_{0B}}{\mathcal{G}} = 1.009 \pm 0.054 . \quad (32)$$

This is in full agreement with GR, which predicts one for all three of these expressions. Consequently, nature cannot deviate much from GR in the quasi-stationary strong-field regime of gravity (G2 in figure 1).

### 2.3 PSR J1738+0333 — The best test for scalar-tensor gravity

The best “pulsar clocks” are found amongst the fully recycled millisecond pulsars, which have rotational periods less than about 10 ms (see e.g. [80]). A result of the stable mass transfer between companion and pulsar in the past — responsible for the recycling of the pulsar — is a very efficient circularization of the binary orbit, that leads to a pulsar-white dwarf system with very small residual eccentricity [81]. For such systems, the post-Keplerian parameters  $\dot{\omega}$  and  $\gamma$  are generally not observable. There are a few cases where the orbit is seen sufficiently edge-on, so that a measurement of the Shapiro delay gives access to the two post-Keplerian parameters  $r$  and  $s$  with good precision (see e.g. [82], which was the first detection of a Shapiro delay in a binary pulsar). With these two parameters the system is then fully determined, and in principle can be used for a gravity test in combination with a third measured (or constrained) post-Keplerian parameter (e.g.  $\dot{P}_b$ ). Besides the Shapiro delay parameters, some of the circular binary pulsar systems offer a completely different access to their masses, which is not solely based on the timing observations in the radio frequencies. If the companion star is bright enough for optical spectroscopy, then we have a dual-line system, where the Doppler shifts in the spectral lines can be used, together with the timing observations of the pulsar, to determine the mass ratio  $R$ . Furthermore, if the companion is a white dwarf, the spectroscopic information in combination with models of the white dwarf and its atmosphere can be used to determine the mass of the white dwarf  $m_c$ , ultimately giving the mass of the pulsar via  $m_p = R m_c$ . As we will see in this and the following subsection, two of the best binary pulsar systems for gravity tests have their masses determined through such a combination of radio and optical astronomy.

PSR J1738+0333 was discovered in 2001 [83]. It has a spin period  $P$  of 5.85 ms and is a member of a low-eccentricity ( $e < 4 \times 10^{-7}$ ) binary system with an orbital period  $P_b$  of just 8.5 hours. The companion is an optically bright low-mass white dwarf (see figure 8). Extensive timing observation over a period of 10 years allowed a determination of astrometric, spin and orbital parameters with high precision [30], most notably

- A change in the orbital period of  $(-17.0 \pm 3.1) \times 10^{-15}$ .

- A timing parallax, which gives a model independent distance estimate of  $d = 1.47 \pm 0.10$  kpc.

The latter is important to correct for the Shklovskii effect and the differential Galactic acceleration to obtain the intrinsic  $\dot{P}_b$  (cf. equation (27)). Additional spectroscopic observations of the white dwarf gave the mass ratio  $R = 8.1 \pm 0.2$  and the companion mass  $m_c = 0.181^{+0.007}_{-0.005} M_\odot$ , and consequently the pulsar mass  $m_p = 1.47^{+0.07}_{-0.06} M_\odot$  [84]. It is important to note, that the mass determination for PSR B1738+0333 is free of any explicit strong-field contributions, since this is the case for the mass ratio [41], and certainly for the mass of the white dwarf, which is a weakly self-gravitating body, i.e. a gravity regime that has been well tested in the Solar system (G1 in figure 1).

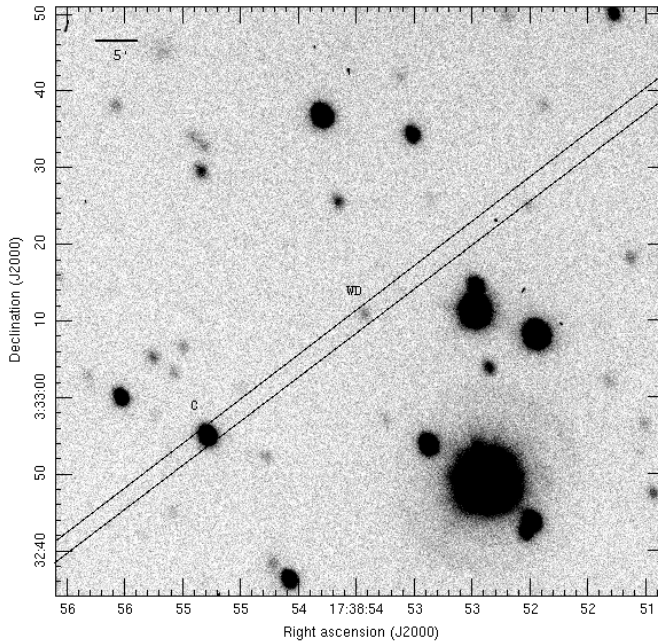


Figure 8: Optical finding chart for the PSR J1738+0333 companion. Indicated are the white dwarf companion (WD), the slit orientation used during the observation and the comparison star (C) that was included in the slit. The white dwarf is sufficiently bright to allow for high signal-to-noise spectroscopy (see [84] for details, where this figure is taken from).

After using equation (27) to correct for the Shklovskii contribution,  $\delta\dot{P}_b = P_b \mu^2 d/c = (8.3^{+0.6}_{-0.5}) \times 10^{-15}$ , and the contribution from the Galactic differential

acceleration,  $\delta\dot{P}_b = (0.58^{+0.16}_{-0.14}) \times 10^{-15}$ , one finds an intrinsic orbital period change due to gravitational wave damping of  $\dot{P}_b^{\text{intr}} = (-25.9 \pm 3.2) \times 10^{-15}$ . This value agrees well with the prediction of GR, as can be seen in figure 9.

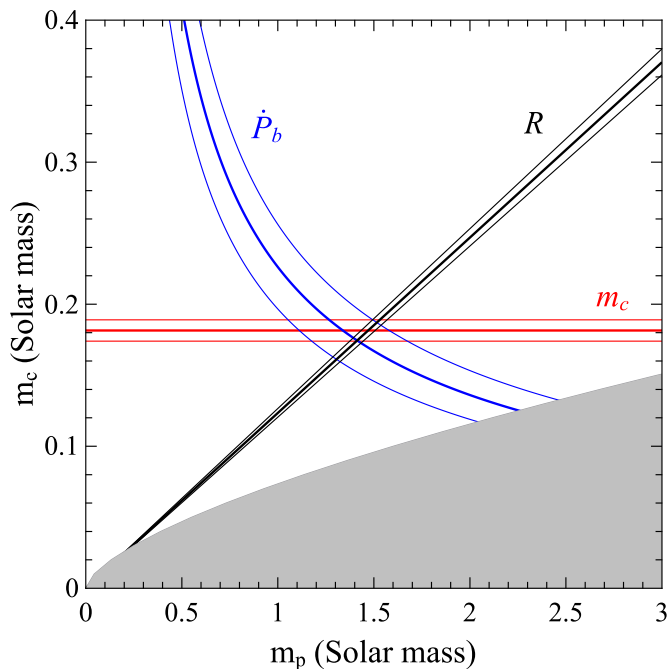


Figure 9: GR mass-mass diagram based on the timing observations of PSR J1738+0333 and the optical observations of its white-dwarf companion respectively. The thin lines indicate the one-sigma errors of the measured parameters. The grey area is excluded by the condition  $\sin i \leq 1$ .

The radiative test with PSR J1738+0333 represents a  $\sim 15\%$  verification of GR's quadrupole formula. A comparison with the  $< 0.1\%$  test from the Double Pulsar (see Section 2.2) raises the valid question of whether the PSR J1738+0333 experiment is teaching us something new about the nature of gravity and the validity of GR. To address this question, let's have a look at equation (25). Dipolar radiation can be a strong source of gravitational wave damping, if there is a sufficient difference between the effective coupling parameters  $\alpha_p$  and  $\alpha_c$  of pulsar and companion respectively. For the Double Pulsar, where we have two neutron stars with  $m_p \approx m_c$ , one generally expects that  $\alpha_p \approx \alpha_c$ , and therefore the effect of dipolar radiation would be strongly suppressed. On the other hand, in the PSR J1738+0333 system there is a large difference in the compactness of the two bodies. For the weakly self-gravitating

white-dwarf companion  $\alpha_c \simeq \alpha_0$ , i.e. it assumes the weak-field value<sup>6</sup>, while the strongly self-gravitating pulsar can have an  $\alpha_p$  that significantly deviates from  $\alpha_0$ . In fact, as discussed in Section 1.4,  $\alpha_p$  can even be of order unity in the presence of effects like strong-field scalarization. In the absence of non-perturbative strong-field effects one can do a first order estimation  $(\alpha_p - \alpha_c) \propto (\epsilon_p - \epsilon_c) + \mathcal{O}(\epsilon^2)$ . For the Double Pulsar one finds  $(\epsilon_p - \epsilon_c)^2 \approx 6 \times 10^{-5}$ , which is significantly smaller than for the PSR J1738+0333 system, which has  $(\epsilon_p - \epsilon_c)^2 \approx 0.012$ .<sup>7</sup> As a consequence, the orbital decay of asymmetric systems like PSR J1738+0333 could still be dominated by dipolar radiation, even if the Double Pulsar agrees with GR. For this reason, PSR J1738+0333 is particularly useful to test gravity theories that violate the strong equivalence principle and therefore predict the emission of dipolar radiation. A well known class of gravity theories, where this is the case, are scalar-tensor theories. As it turns out, PSR J1738+0333 is currently the best test system for these alternatives to GR (see figure 10). In terms of equation (25), one finds

$$|\alpha_p - \alpha_c| < 2 \times 10^{-3} \quad (95\% \text{ confidence}) , \quad (33)$$

where for the weakly self-gravitating white dwarf companion  $\alpha_c \simeq \alpha_0$ . This limit can be interpreted as a generic limit on dipolar radiation, where  $\alpha_p - \alpha_c$  is the difference of some hypothetical (scalar- or vector-like) “gravitational charges” [39].

---

<sup>6</sup>From the Cassini experiment [12] one obtains  $|\alpha_0| < 3 \times 10^{-3}$  (95% confidence).

<sup>7</sup>These numbers are based on the equation of state MPA1 in [85]. Within GR, MPA1 has a maximum neutron-star mass of  $2.46 M_\odot$ , which can also account for the high-mass candidates of [86, 87, 88].

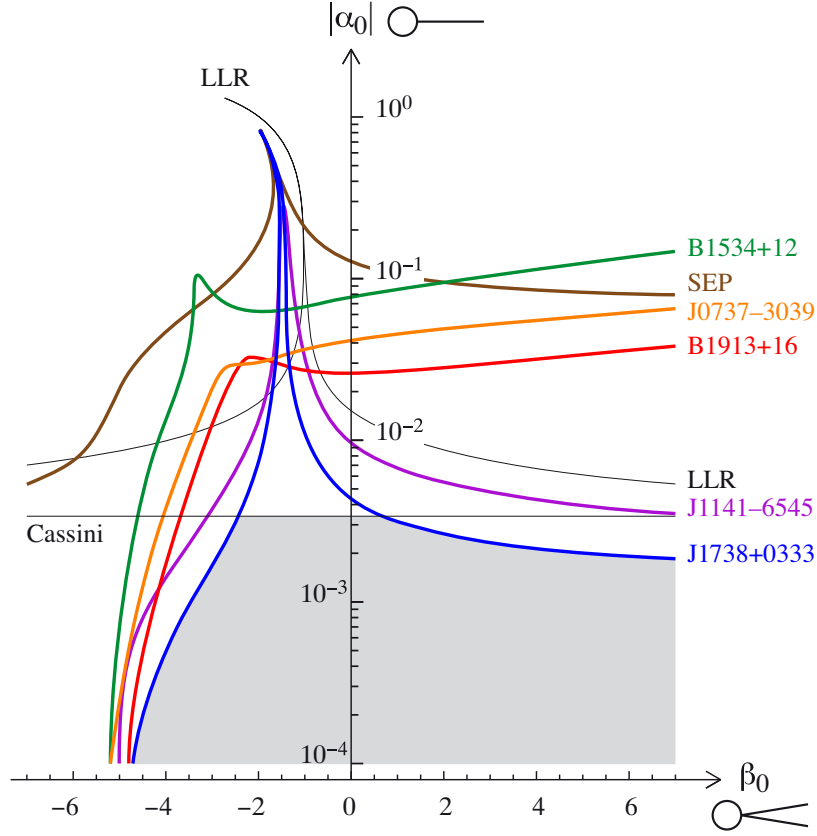


Figure 10: Constraints on the class of  $T_1(\alpha_0, \beta_0)$  scalar-tensor theories of [57, 58], from different binary pulsar and Solar system (Cassini and Lunar Laser Ranging) experiments. The grey area indicates the still allowed  $T_1$  theories, and includes GR ( $\alpha_0 = \beta_0 = 0$ ). It is obvious that PSR J1738+0333 is the most constraining experiment for most of the  $\beta_0$  range, and is even competitive with Cassini in testing the Jordan-Fierz-Brans-Dicke theory ( $\beta_0 = 0$ ). As can be clearly seen, the double neutron-star systems PSR B1534+12 [89], PSR B1913+16 (Hulse-Taylor pulsar) and PSR J0737–3039A/B (Double Pulsar) are considerably less constraining, as explained in the text. PSR J1141–6545 is also well suited for a dipolar radiation test [90], since it also has a white dwarf companion [91]. Figure is taken from [30].

## 2.4 PSR J0348+0432 — A massive pulsar in a relativistic orbit

PSR J0348+0432 was discovered in 2007 in a drift scan survey using the Green Bank radio telescope (GBT) [92, 93]. PSR J0348+0432 is a mildly recycled radio-pulsar with a spin period of 39 ms. Soon it was found to be in a 2.46-hour orbit with a low-

mass white-dwarf companion. In fact, the orbital period is only 15 seconds longer than that of the Double Pulsar, which by itself makes this already an interesting system for gravity. Initial timing observations of the binary yielded an accurate astrometric position, which allowed for an optical identification of its companion [94]. As it turned out, the companion is a relatively bright white dwarf with a spectrum that shows deep Balmer lines. Like in the case of PSR J1738+0333, one could use high-resolution optical spectroscopy to determine the mass ratio  $R = 11.70 \pm 0.13$  (see figure 11) and the companion mass  $m_c = 0.172 \pm 0.003 M_\odot$ . For the mass of the pulsar one then finds  $m_p = R m_c = 2.01 \pm 0.04 M_\odot$ , which is presently the highest, well determined neutron star mass, and only the second neutron star with a well determined mass close to  $2 M_\odot$ .<sup>8</sup>

---

<sup>8</sup>The first well determined two Solar mass neutron star is PSR J1614–2230 [77], which is in a wide orbit and therefore does not provide any gravity test.

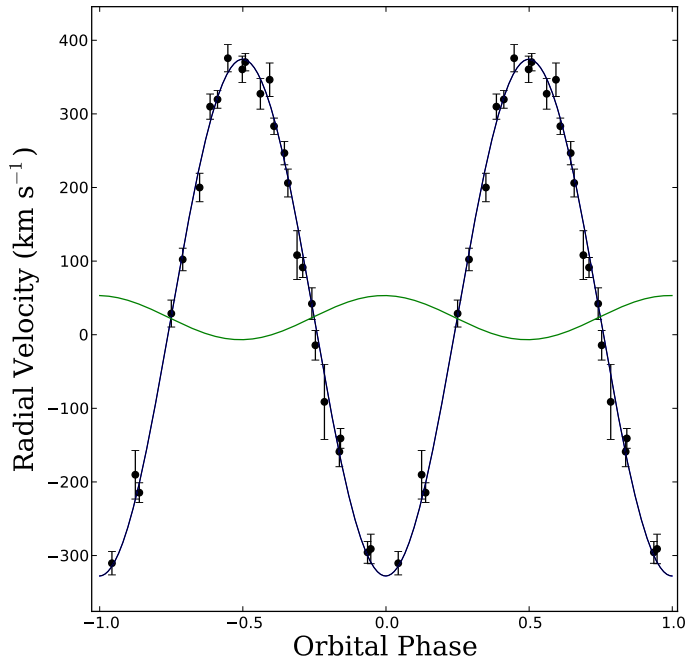


Figure 11: Spectroscopically measured radial velocities for the white-dwarf companion of PSR J0348+0432. For illustration purposes the data are plotted twice. The fitted sinusoidal curve (blue) has an amplitude of  $351 \pm 4$  km/s. As a comparison, the sinusoidal green line shows the radial velocity of the pulsar as derived from the timing solution. The amplitude of the green line is known with very high precision:  $30.008235 \pm 0.000016$  km/s. The ratio of the amplitudes gives the mass ratio  $R$ . Figure is taken from [94].

Since its discovery there have been regular timing observations of PSR J0348+0432 with three of the major radio telescopes in the world, the 100-m Green Bank Telescope, the 305-m radio telescope at the Arecibo Observatory, and the 100-m Effelsberg radio telescope. Based on the timing data, in 2013 Antoniadis *et al.* [94] reported the detection of a decrease in the orbital period of  $\dot{P}_b = (-2.73 \pm 0.45) \pm 10^{-13}$  that is in full agreement with GR (see figure 12). In numbers:

$$\dot{P}_b / \dot{P}_b^{\text{GR}} = 1.05 \pm 0.18 . \quad (34)$$

As it turns out, using the distance inferred from the photometry of the white dwarf ( $d \sim 2.1$  kpc) corrections due to the Shklovskii effect and differential acceleration in

the Galactic potential (see equation (27)) are negligible compared to the measurement uncertainty in  $\dot{P}_b$ .

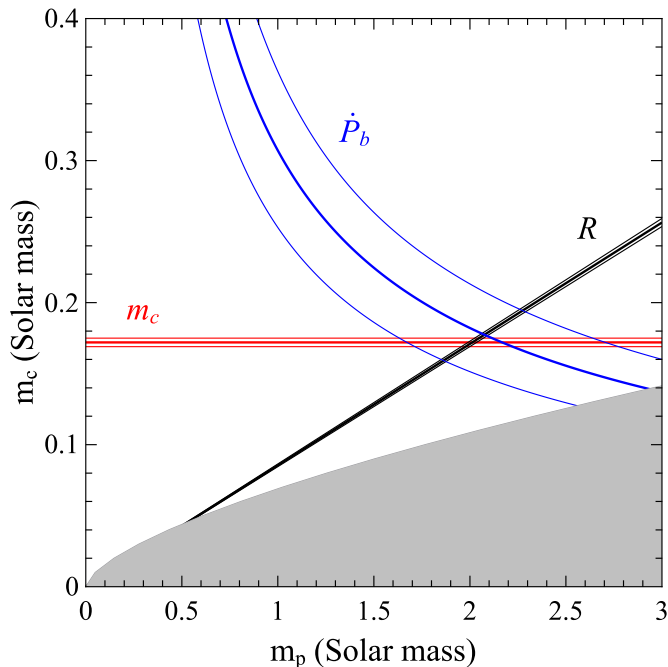


Figure 12: GR mass-mass diagram based on timing and optical observations of the PSR J0348+0432 system. The thin lines indicate the one-sigma errors of the measured parameters. The grey area is excluded by the condition  $\sin i \leq 1$ .

Like PSR 1738+0333, PSR J0348+0432 is a system with a large asymmetry in the compactness of the components, and therefore well suited for a dipolar radiation test. Using equation (25), the limit (34) can be converted into a limit on additional gravitational scalar or vector charges:

$$|\alpha_p - \alpha_0| < 5 \times 10^{-3} \quad (95\% \text{ confidence}). \quad (35)$$

This limit is certainly weaker than the limit (34), but it has a new quality as it tests a gravity regime in neutron stars that has not been tested before. Gravity tests before [94] were confined to “canonical” neutron star masses of  $\sim 1.4 M_\odot$ . PSR J0348+0432 for the first time allows a test of the relativistic motion of a massive neutron star, which in terms of gravitational self-energy lies clearly outside the tested region (see figure 13).



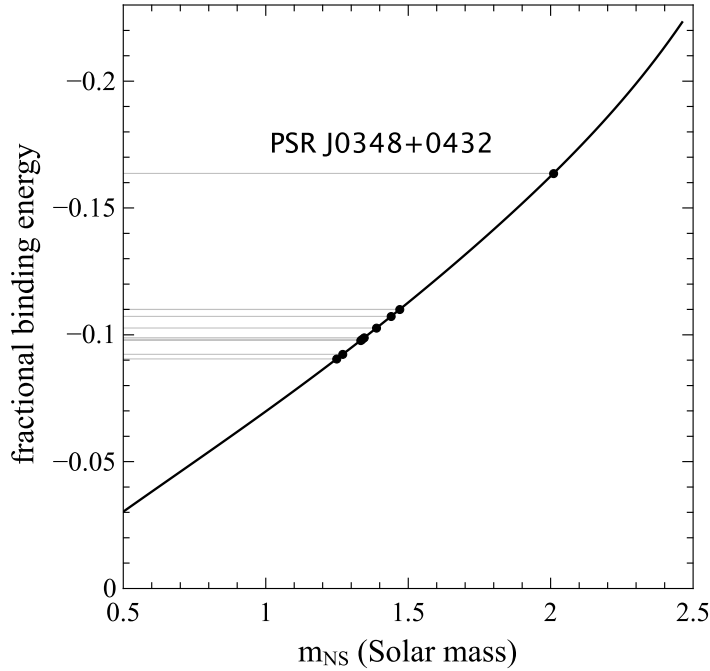


Figure 13: Fractional gravitational binding energy of a neutron star as a function of its (inertial) mass, based on equation of state MPA1 [85]. The plot clearly shows the prominent position of PSR J0348+0432. The other dots indicate the neutron star masses of the individual test systems in figure 10.

Although an increase in fractional binding energy of about 50% does not seem much, in the highly non-linear gravity regime of neutron stars it could make a significant difference. To demonstrate this, [94] used the scalar-tensor gravity  $T_1(\alpha_0, \beta_0)$  of [57, 58], which is known to behave strongly non-linear in the gravitational fields of neutron stars, in particular for  $\beta_0 < -4.0$ . As shown in figure 14, PSR J0348+0432 excludes a family of scalar-tensor theories that predict significant deviations from GR in massive neutron stars and were not excluded by previous experiments, most notably the test done with PSR J1738+0333. To further illustrate this in a mass-mass diagram, figure 15 shows a gravity theory with strong-field scalarization in massive neutron stars that passes the PSR J1738+0333 experiment, but is falsified by PSR J0348+0432.

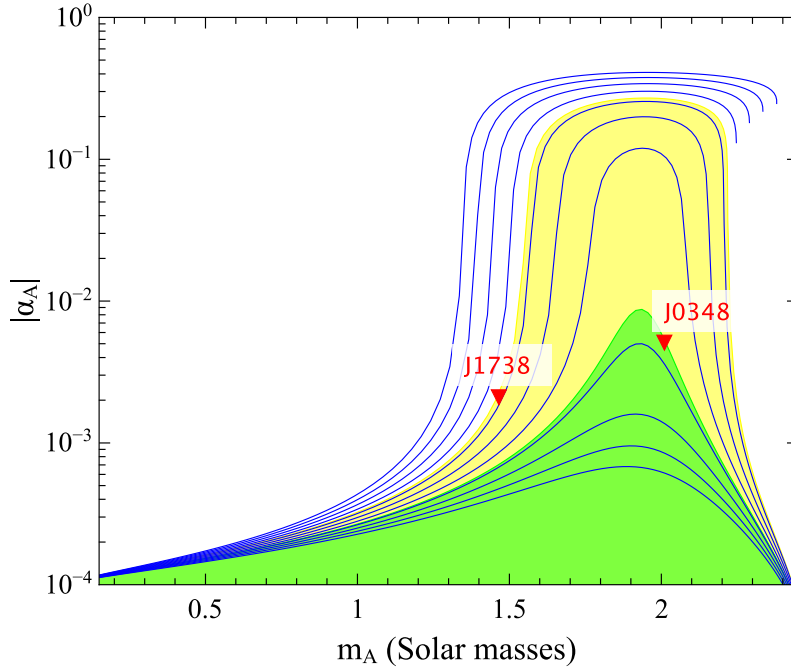


Figure 14: Effective scalar coupling as a function of the neutron-star mass, in the  $T_1(\alpha_0, \beta_0)$  mono-scalar-tensor gravity theory of [57, 58]. For the linear coupling of matter to the scalar field we have chosen  $\alpha_0 = 10^{-4}$ , a value well below the sensitivity of any near-future Solar system experiment, like GAIA [95]. The blue curves correspond to stable neutron-star configurations for different values of the quadratic coupling  $\beta_0$ :  $-5$  to  $-4$  (top to bottom) in steps of  $0.1$ . The yellow area indicates the parameter space still allowed by the limit (33) [label ‘J1738’], whereas only the green area is in agreement with the limit (35) [label ‘J0348’]. The plot shows clearly how the massive pulsar PSR J0348+0432 probes deep into a new gravity regime. Neutron-star calculations are based on equation of state MPA1 [85] (see [94] for a different equation-of-state).

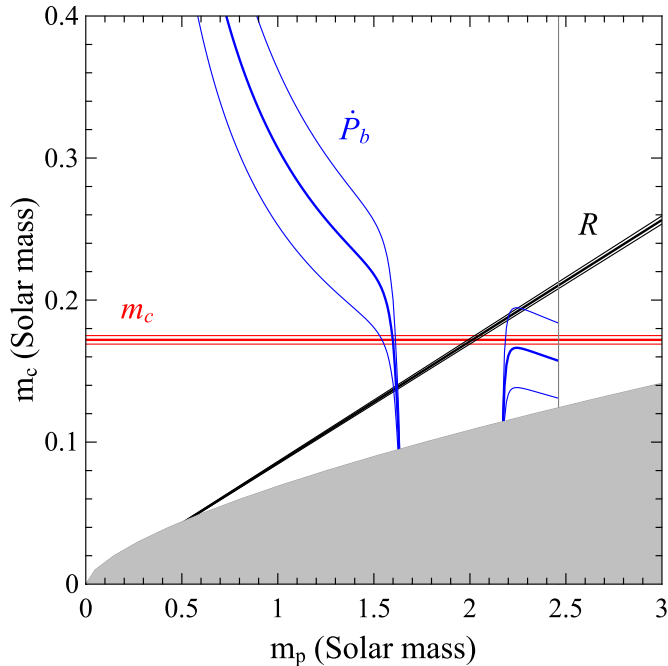


Figure 15: Mass-mass diagram based on timing and optical observations of the PSR J0348+0432 system, for the mono-scalar-tensor gravity  $T_1(10^{-4}, -4.5)$ . The thin lines indicate the one-sigma errors of the measured parameters. The vertical grey line is at the maximum mass of a neutron star for the given theory and equation-of-state (MPA1). The grey area is excluded by the condition  $\sin i \leq 1$ . Obviously  $T_1(10^{-4}, -4.5)$  is clearly falsified by this test, as there is no common region for the curves of the three parameters  $m_c$ ,  $R$  and  $\dot{P}_b$ .

With PSR J0348+0432, gravity tests now cover a range of neutron star masses from  $1.25 M_\odot$  (PSR J0737–3039B) to  $2 M_\odot$ . No significant deviation from GR in the orbital motion of these neutron stars was found. These findings have interesting implications for the upcoming ground-based gravitational wave experiments, as we will briefly discuss in the next subsection.

## 2.5 Implications for gravitational wave astronomy

The first detection of gravitational waves from astrophysical sources by ground-based laser interferometers, like LIGO<sup>9</sup> and VIRGO<sup>10</sup>, will mark the beginning of a new

<sup>9</sup>[www.ligo.org](http://www.ligo.org)

<sup>10</sup>[www.cascina.virgo.infn.it](http://www.cascina.virgo.infn.it)

era of gravitational wave astronomy [96]. One of the most promising sources for these detectors are merging compact binaries, consisting of neutron stars and black holes, whose orbits are decaying towards a final coalescence due to gravitational wave damping. While the signal sweeps in frequency  $f$  through the detectors' typical sensitive bandwidth  $[f_{\text{in}}, f_{\text{out}}]$  from about 20 Hz to a few kHz, the gravitational wave signal will be deeply buried in the broadband noise of the detectors [96]. To detect the signal, one will have to apply a matched filtering technique, i.e. correlate the output of the detector with a template wave form. Consequently, it is crucial to know the binary's orbital phase with high accuracy for searching and analyzing the signals from in-spiraling compact binaries. Typically, one aims to lose less than one gravitational wave cycle in a signal with  $\sim 10^4$  cycles. For this reason, within GR such calculations for the phase evolution of compact binaries have been conducted with great effort to cover many post-Newtonian orders including spin-orbit and spin-spin contributions (see [36, 97] for reviews). Table 4 illustrates the importance of the individual corrections to the number of cycles spent in the LIGO/VIRGO band<sup>11</sup> for two merging non-spinning neutron stars. For a later comparison, the two neutron-star masses are chosen to be  $2 M_{\odot}$  and  $1.25 M_{\odot}$ , the highest and lowest neutron-star masses observed.

Table 4: Contributions to the accumulated number of gravitational wave cycles in the frequency band of 20 Hz to 1350 Hz for a  $2 M_{\odot}/1.25 M_{\odot}$  neutron-star pair (cf. equations (235),(236) in [36]). The frequency of 1350 Hz corresponds to the innermost circular orbit of the merging binary system [36].

	correction to LO	number of cycles
LO (leading order)	—	4158.6
1pN	$(v/c)^2$	196.4
1.5pN	$(v/c)^3$	-123.6
2pN	$(v/c)^4$	7.2
2.5pN	$(v/c)^5$	-10.3
3pN	$(v/c)^6$	2.4
3.5pN	$(v/c)^7$	-0.9

If the gravitational interaction between two compact masses is different from GR, the phase evolution over the last few thousand cycles, which fall into the bandwidth of the detectors, deviates from the (GR) template. This will degrade the ability

<sup>11</sup>The advanced LIGO/VIRGO gravitational wave detectors are expected to have a lower end seismic noise cut-off at about 10 Hz [98]. For a low signal-to-noise ratio the low-frequency cut-off is considerably higher. In this review, we adapt a value of 20 Hz as the minimum frequency. The maximum frequency of a few kHz is not important here, since the frequency of the innermost circular orbit is well below the upper limit of the LIGO/VIRGO band.

to accurately determine the parameters of the merging binary, or in the worst case even prevent the detection of the signal. In scalar-tensor gravity, for instance, the evolution of the phase is modified because the system can now lose additional energy to dipolar waves [99, 100]. Depending on the difference between the effective scalar couplings of the two bodies,  $\alpha_A$  and  $\alpha_B$ , the 1.5 post-Newtonian dipolar contribution to the equations of motion could drive the gravitational wave signal many cycles away from the GR template. For this reason, it is desirable that potential deviations from GR in the interaction of two compact objects can be tested and constrained prior to the start of the advanced gravitational wave detectors. With its location at the high end of the measured neutron-star masses, PSR J0348+0432 with its limit (35) plays a particularly important role in such constraints.

The change in the number of cycles that fall into the frequency band of a gravitational wave detector due to a dipolar contribution is given, to leading order, by [99, 100]

$$\Delta N \approx -\frac{25}{21504\pi} \left(\frac{m_A m_B}{M^2}\right)^{2/5} (\alpha_A - \alpha_B)^2 \left(u_{\text{in}}^{-7/3} - u_{\text{out}}^{-7/3}\right), \quad (36)$$

where  $u \equiv \pi(GM c^{-3})f$ , and  $\mathcal{M} \equiv (m_A m_B)^{3/5} M^{-1/5}$  is the chirp mass. Equation (36) is based on the assumption that  $\alpha_0$ ,  $\alpha_A$  and  $\alpha_B$  are considerably smaller than unity, which is supported by binary pulsar experiments. For a  $2/1.25 M_\odot$  double neutron-star merger, one finds from equation (36) and the limit (35)

$$|\Delta N(f_{\text{in}} = 20 \text{ Hz}, f_{\text{out}} = f_{\text{ICO}})| < 0.4, \quad (37)$$

where  $f_{\text{ICO}} \approx 1350 \text{ Hz}$  is the gravitational wave frequency of the innermost circular orbit (cf. [36]). The exact value of  $f_{\text{ISCO}}$  does not play an important role in equation (36), since  $f_{\text{in}} \ll f_{\text{ICO}}$ . This result is based on the extreme assumption, that the light neutron star has an effective scalar coupling which corresponds to the well constrained weak-field limit, i.e.  $\alpha_B = \alpha_0$ . If the companion of the  $2 M_\odot$  neutron star is a  $10 M_\odot$  black hole, then the constraints on  $\Delta N$  that can be derived from binary pulsar experiments are even tighter (see [94]). A comparison with table 4 shows that the limit (37) is already below the contribution of the highest order correction calculated.

As explained in [94], binary pulsar experiment cannot exclude significant deviations associated with short-range fields (e.g. massive scalar fields), which could still impact the mergers for ground-based gravitational wave detectors. Also, there is the possibility of the occurrence of effects like dynamical scalarization that, depending on the specifics of the theory and the masses, could start to influence the merger at  $f < f_{\text{ICO}}$  [101], and consequently limit the validity of (37) to a smaller frequency

band. Nevertheless, the constraints on dipolar radiation obtained from binary pulsars provide added confidence in the use of elaborate GR templates to search for the signals of compact merging binaries in the LIGO/VIRGO data sets.

### 3 Geodetic precession

A few months after the discovery of the Hulse-Taylor pulsar, Damour and Ruffini [51] proposed a test for geodetic precession in that system. If the pulsar spin is sufficiently tilted with respect to the orbital angular momentum, the spin direction should gradually change over time (see Section 1.3). A change in the orientation of the spin-axis of the pulsar with respect to the line-of-sight should lead to changes in the observed pulse profile. These pulse-profile changes manifest themselves in various forms [102], such as changes in the amplitude ratio or separation of pulse components [103, 104], the shape of the characteristic swing of the linear polarization [105], or the absolute value of the position angle of the polarization in the sky [75]. In principle, such changes could allow for a measurement of the precession rate and by this yield a test of GR. In practice, it turned out to be rather difficult to convert changes in the pulse profile into a quantitative test for the precession rate. Indeed, the Hulse-Taylor pulsar, in spite of prominent profile changes due to geodetic precession [103, 104], does not (yet) allow for a quantitative test of geodetic precession. This is mostly due to uncertainties in the orientation of the magnetic axis and the intrinsic beam shape [106].

Profile and polarization changes due to geodetic precession have been observed in other binary pulsars as well [107, 108], but again did not lead to a quantitative gravity test. A complete list of binary pulsars that up to date show signs of geodetic precession can be found in [28]. Out of the six pulsars listed in [28], so far only two allowed for quantitative constraints on their rate of geodetic precession. These two binary pulsars will be discussed in more details in the following.

#### 3.1 PSR B1534+12

PSR B1534+12 is a 38 ms pulsar, which was discovered in 1991 [109]. It is a member of an eccentric ( $e = 0.27$ ) double neutron-star system with an orbital period of about 10 hours. Subsequent timing observations lead to the determination of five post-Keplerian parameters:  $\dot{\omega}$ ,  $\gamma$ ,  $\dot{P}_b$ , and  $r$ ,  $s$  from the Shapiro delay [89]. The large uncertainty in the distance to this system still prevents its usage in a gravitational wave test, since the observed  $\dot{P}_b$  has a large Shklovskii contribution, which one cannot properly correct for. The other four post-Keplerian parameters are nevertheless useful to test quasi-stationary strong-field effects. However, these tests are generally less constraining than tests from other pulsars (see e.g. figure 10).

Continued observations of PSR B1534+12 with the 305-m Arecibo radio telescope revealed systematic changes in the the observed pulsar profile by about 1% per year, as well as changes in the polarization properties of the pulsar [110]. As outlined above, such changes are expected from geodetic precession. Using equation (4) and the parameters from [89], one finds that GR predicts a precession rate of

$$\Omega^{\text{SO}} = 0.51 \text{ deg/yr} \quad (38)$$

for PSR B1534+12.

Besides the secular changes visible in the high signal-to-noise ratio pulse profile and polarization data of PSR B1534+12, Stairs *et al.* [105] reported the detection of special-relativistic aberration of the revolving pulsar beam due to orbital motion. Aberration periodically shifts the observed angle between the line of sight and spin axis of PSR B1534+12 by an amount that depends on the orientation of the pulsar spin, and therefore contains additional geometrical information. Combining these observations, Stairs *et al.* [105] were able to determine the system geometry, including the misalignment between the spin of PSR B1534+12 and the angular momentum of the binary motion, and constrain the rate of geodetic precession to

$$\begin{aligned} \Omega^{\text{SO}} &= 0.44_{-0.16}^{+0.48} \text{ deg/yr} && (68\% \text{ confidence}) , \\ \Omega^{\text{SO}} &= 0.44_{-0.24}^{+4.6} \text{ deg/yr} && (95\% \text{ confidence}) . \end{aligned} \quad (39)$$

Although the uncertainties are comparably large, these were the first beam-model-independent constraints on the geodetic precession rate of a binary pulsar. As can be seen, these model-independent constraints on the precession rate are consistent with the prediction by GR, as given in equation (38).

### 3.2 The Double Pulsar

In Section 2.2, we have seen the Double Pulsar as one of the most exciting “laboratories” for relativistic gravity, with a wealth of relativistic effects measured, allowing the determination of 5 post-Keplerian parameters from timing observations:  $\dot{\omega}$ ,  $\gamma$ ,  $\dot{P}_b$ ,  $r$ ,  $s$ . Calculating the inclination angle of the orbit  $i$  from  $s = \sin i$ , one finds that the line-of-sight is inclined with respect to the plane of the binary orbit by just about  $1.3^\circ$  [76]. As a consequence, during the superior conjunction the signals of pulsar  $A$  pass pulsar  $B$  at a distance of only 20 000 km. This is small compared to the extension of pulsar  $B$ ’s magnetosphere, which is roughly given by the radius of the light-cylinder<sup>12</sup>  $r_{\text{lc}} \equiv cP/2\pi \sim 130\,000$  km. And indeed, at every superior

---

<sup>12</sup>The light-cylinder is defined as the surface where the co-rotating frame reaches the speed of light.

conjunction pulsar  $A$  gets eclipsed for about 30 seconds due to absorption by the plasma in the magnetosphere of pulsar  $B$  [73]. A detailed analysis revealed that during every eclipse the light curve of pulsar  $A$  shows flux modulations that are spaced by half or integer numbers of pulsar  $B$ 's rotational period [111] (see figure 16). This pattern can be understood by absorbing plasma that co-rotates with pulsar  $B$  and is confined within the closed field lines of the magnetic dipole of pulsar  $B$ . As such, the orientation of pulsar  $B$ 's spin is encoded in the observed light curve of pulsar  $A$  [112]. Over the course of several years, Breton *et al.* [112] observed characteristic shifts in the eclipse pattern, that can be directly related to a precession of the spin of pulsar  $B$ . From this analysis, Breton *et al.* were able to derive a precession rate of

$$\Omega^{\text{SO}} = 4.77_{-0.65}^{+0.66} \text{ deg/yr} . \quad (40)$$

The measured rate of precession is consistent with that predicted by GR ( $\Omega_{\text{GR}}^{\text{SO}} = 5.07 \text{ deg/yr}$ ) within its one-sigma uncertainty. This is the sixth(!) post-Keplerian parameter measured in the Double-Pulsar system (see figure 17). Furthermore, for the coupling function  $\Gamma_B^A$ , which parametrizes strong-field deviation in alternative gravity theories (see equation (5)), one finds

$$\Gamma_B^A/\mathcal{G} = 1.90 \pm 0.22 , \quad (41)$$

which agrees with the GR value  $\Gamma_B^A/G = 2$ . Although the geodetic precession of a gyroscope was confirmed to better than 0.3% by the Gravity Probe B experiment [14], the clearly less precise test with Double Pulsar  $B$  (13%) for the first time gives a good measurement of this effect for a strongly self-gravitating ‘‘gyroscope’’, and by this represents a qualitatively different test.



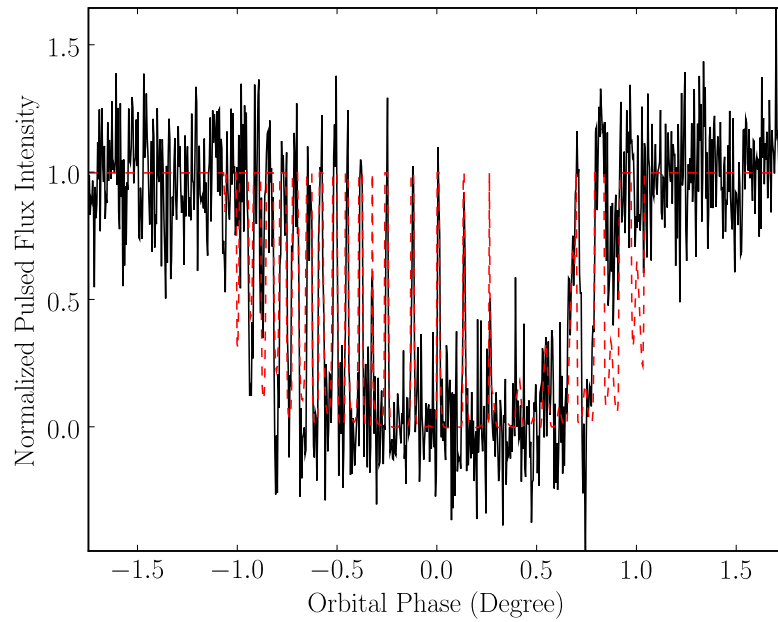


Figure 16: Average eclipse profile of pulsar *A* observed at 820 MHz over a 5-day period around 11 April 2007 (black line). The model based on a co-rotating magnetosphere gives a good explanation of the eclipse profile (red dashed line). Figure is taken from [112].

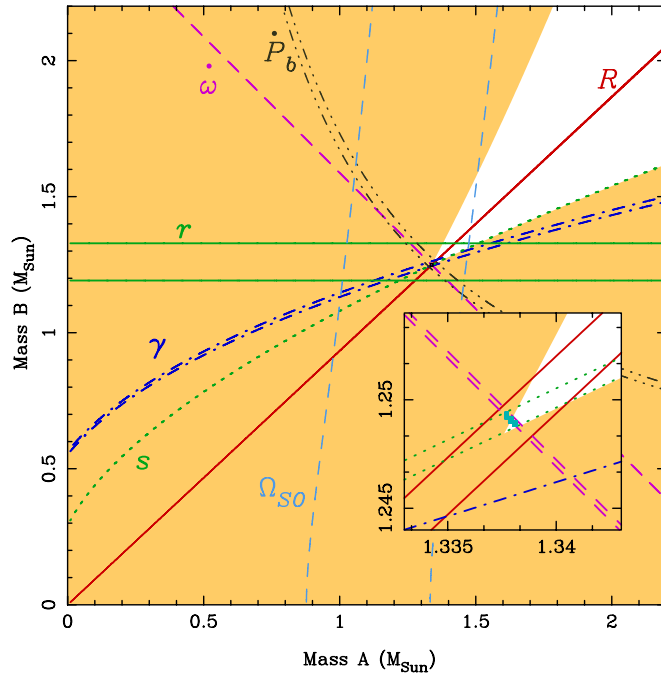


Figure 17: GR mass-mass diagram for the Double Pulsar. Same as in Section 2.2 (figure 7), plus the inclusion of the constraints from the geodetic precession of pulsar  $B$  ( $\Omega_{SO}$ ). Figure is taken from [75].

The geodetic precession of pulsar  $B$  not only changes the pattern of the flux modulations observed during the eclipse of pulsar  $A$ , it also changes the orientation of pulsar  $B$ 's emission beam with respect to our line-of-sight. As a result of this, geodetic precession has by now turned pulsar  $B$  in such a way, that since 2009 it is no longer seen by radio telescopes on Earth [113]. From their model, Perera *et al.* [113] predicted that the reappearance of pulsar  $A$  is expected to happen around 2035 with the same part of the beam, but could be as early as 2014 if one assumes a symmetric beam shape.

Finally, for pulsar  $A$  GR predicts a precession rate of 4.78 deg/yr, which is comparable to that of pulsar  $B$ . However, since the light-cylinder radius of pulsar  $A$  ( $\sim 1000$  km) is considerably smaller than that of pulsar  $B$ , there are no eclipses that could give insight into the orientation of its spin. Moreover, long-term pulse profile observations indicate that the misalignment between the spin of pulsar  $A$  and the orbital angular momentum is less than  $3.2^\circ$  (95% confidence) [114]. For such a close alignment, geodetic precession is not expected to cause any significant changes in the spin direction (cf. equations (4) and (5)). This, on the other hand, is good news

for tests based on timing observations. One does not expect a complication in the analysis of the pulse arrival times due to additional modeling of a changing pulse profile, like this is, for instance, the case in PSR J1141–6545 [90].

## 4 The strong equivalence principle

The strong equivalence principle (SEP) extends the weak equivalence principle (WEP) to the universality of free fall (UFF) of self-gravitating bodies. In GR, WEP and SEP are fulfilled, i.e. in GR the world line of a body is independent of its chemical composition and gravitational binding energy. Therefore, a detection of a SEP violation would directly falsify GR. On the other hand, alternative theories of gravity generally violate SEP. This is also the case for most metric theories of gravity [5]. For a weakly self-gravitating body in a weak external gravitational field one can simply express a violation of SEP as a difference between inertial and gravitational mass that is proportional to the gravitational binding energy  $E_{\text{grav}}$  of the mass:

$$\frac{m_G}{m_I} \simeq 1 + \eta \frac{E_{\text{grav}}}{m_I c^2} \equiv 1 + \eta \epsilon . \quad (42)$$

The Nordtvedt parameter  $\eta$  is a theory dependent constant. In the parameterized post-Newtonian (PPN) framework,  $\eta$  is given as a combination of different PPN parameters (see [5] for details). As a consequence of (42), the Earth ( $\epsilon \approx -5 \times 10^{-10}$ ) and the Moon ( $\epsilon \approx -2 \times 10^{-11}$ ) would fall differently in the gravitational field of the Sun (Nordtvedt effect [115]). The parameter  $\eta$  is therefore tightly constrained by the lunar-laser-ranging (LLR) experiments to  $\eta = (3.0 \pm 3.6) \times 10^{-4}$ , which is in perfect agreement with GR where  $\eta = 0$  [116].

In view of the smallness of the self-gravity of Solar system bodies, the LLR experiment says nothing about strong-field aspects of SEP. SEP could still be violated in extremely compact objects, like neutron stars, meaning that a neutron star would feel a different acceleration in an external gravitational field than weakly self-gravitating bodies. For such a strong-field SEP violation, the best current limits come from millisecond pulsar-white dwarf systems with wide orbits. If there is a violation of UFF by neutron stars, then the gravitational field of the Milky Way would polarize the binary orbit [117]. In comparison with the LLR experiment, such tests have two disadvantages: i) the much weaker polarizing external field ( $|\mathbf{g}| \sim 2 \times 10^{-8} \text{ cm/s}^2$ , as compared to the  $\sim 0.6 \text{ cm/s}^2$  of the Solar gravitational field at the location of the Earth-Moon system), and ii) the significantly lower precision in the ranging, which is of the order of a few  $10^3 \text{ cm}$  for the best pulsar experiments ( $\sim 1 \text{ cm}$  for LLR). This is almost completely counterbalanced by the gravitational binding energy of the neutron star, which is a large fraction of its total

inertial mass energy ( $\epsilon \sim -0.1$ ) and more than eight orders of magnitude larger than that of the Earth. This results in experiments with comparable limits on a SEP violation, which nonetheless are complementary since they probe different regimes of binding energy. The recent discovery of a millisecond pulsar in a hierarchical triple (see [118] and Ransom *et al.*, in prep.) might allow for a significant improvement in testing SEP, as it combines a strong external field  $\mathbf{g}$  with a large fractional binding energy  $\epsilon$ .

Since beyond the first post-Newtonian approximation there is no general PPN formalism available, discussions of gravity tests in this regime are done in various theory-specific frameworks. A particularly suitable example for a framework that allows a detailed investigation of higher order/strong-field deviations from GR, is the above mentioned two-parameter class of mono-scalar-tensor theories  $T_1(\alpha_0, \beta_0)$  of [57, 58], which for certain values of  $\beta_0$  exhibit significant strong-field deviations from GR, and a correspondingly strong violation of SEP for neutron stars. To illustrate this violation of SEP, it is sufficient to look at the leading ‘‘Newtonian’’ terms in the equations of motion of a three body system with masses  $m_a$  ( $a = 1, 2, 3$ ) [61]:

$$\ddot{\mathbf{x}}_a = - \sum_{b \neq a} \mathcal{G}_{ab} m_b \frac{\mathbf{x}_a - \mathbf{x}_b}{|\mathbf{x}_a - \mathbf{x}_b|^3}, \quad (43)$$

where the body-dependent effective gravitational constant  $\mathcal{G}_{ab}$  is related to the bare gravitational constant  $G_*$  by

$$\mathcal{G}_{ab} = G_*(1 + \alpha_a \alpha_b). \quad (44)$$

As mentioned above, for a neutron star  $\alpha_a$  can significantly deviate from the weak-field value  $\alpha_0 \ll 1$ . The structure dependence of the effective gravitational constant  $\mathcal{G}_{ab}$  has the consequence that the pulsar does not fall in the same way as its companion, in the gravitational field of our Galaxy. For a binary pulsar with a non-compact companion, e.g. a white dwarf, that effect should be most prominent. Since both the white dwarf and the Galaxy are weakly self-gravitating bodies, their effective scalar coupling can be approximated by  $\alpha_0$ , and one finds from equation (43)

$$\ddot{\mathbf{x}}_{\text{PSR}} - \ddot{\mathbf{x}}_{\text{WD}} \simeq -G(1 + \delta_{\text{P00}})M \frac{\mathbf{x}_{\text{PSR}} - \mathbf{x}_{\text{WD}}}{|\mathbf{x}_{\text{PSR}} - \mathbf{x}_{\text{WD}}|^3} + \delta_{\text{P00}} \mathbf{g} + \mathbf{a}_{\text{PN}}, \quad (45)$$

where  $\delta_{\text{P00}} \equiv (\alpha_{\text{PSR}} - \alpha_0)\alpha_0$ , and where  $\mathbf{g}$  is the gravitational acceleration caused by the Galaxy at the location of the binary pulsar.<sup>13</sup> Also, the contribution from post-Newtonian dynamics, term  $\mathbf{a}_{\text{PN}}$ , has been added, whose most important consequence is the secular precession of periastron,  $\dot{\omega}_{\text{PN}}$ . The  $\mathbf{g}$ -related term reflects the

<sup>13</sup>Here we used  $G \equiv G^*(1 + \alpha_0^2)$ , and we dropped terms of order  $\alpha_0^3$  and smaller.

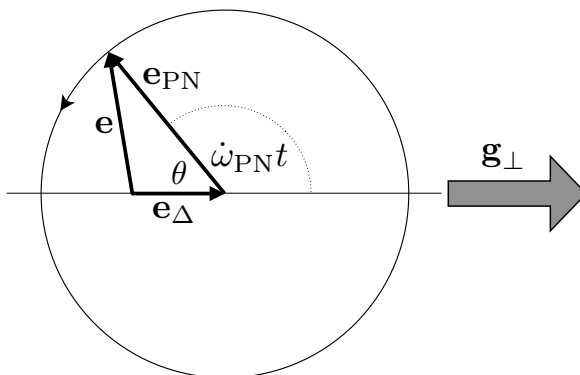


Figure 18: Time evolution of the orbital eccentricity vector  $\mathbf{e} = \mathbf{e}_{\text{PN}} + \mathbf{e}_{\Delta}$  for a small-eccentricity binary, in the presence of a SEP violation. The vector  $\mathbf{g}_{\perp}$  represents the projection of the external acceleration in the orbital plane.

violation of SEP, which modifies the orbital dynamics of binary pulsars. This can be confronted with pulsar observations to test for a violation of SEP. In the following we briefly discuss different tests of SEP with binary pulsars. For a more complete review of the topic of this section see [119]. The discussion below is not specific to scalar-tensor gravity, and the quantity  $\delta_{\text{P}00}$  can be generically seen as the difference between inertial and gravitational mass.

#### 4.1 The Damour-Schäfer test

In 1991, when Damour and Schäfer first investigated the orbital dynamics of a binary pulsar under the influence of a SEP violation [117], only four binary pulsars were known in the Galactic disk. Two of these (PSR B1913+16 and PSR B1957+20) were clearly inadequate for that test, not only because of the compactness of their orbits, but also because PSR B1913+16 is member of a double neutron star system that lacks the required amount of asymmetry in the binding energy, necessary for a stringent test of a SEP violation, and PSR B1957+20 is a so called “black-widow” pulsar, where the companion suffers significant irregular mass losses, due to the irradiation by the pulsar. The remaining systems were PSR B1855+09 [82] and PSR B1953+29 [120]. Both of these systems have wide orbits with small eccentricities,  $e = 2.2 \times 10^{-5}$  and  $e = 3.3 \times 10^{-4}$  respectively.

Damour and Schäfer found for small-eccentricity binary systems that a violation of SEP leads to a characteristic polarization of the orbit, which is best represented by a vector addition where the end-point of the observed eccentricity vector  $\mathbf{e}(t)$  evolves along a circle in an eccentric way (see figure 18). The polarizing eccentricity

$\mathbf{e}_\Delta$  is proportional to  $\delta_{P00}$  and therefore, a limit on  $|\mathbf{e}_\Delta|$  would directly pose a limit on  $\delta_{P00}$ . Unfortunately neither  $e_{PN}$  nor  $\theta$  in figure 18 are measurable quantities. Also, a direct test for a change in  $\mathbf{e}(t)$  is in many cases not feasible, as the expected changes are much too small compared to the available measurement precision from timing (we will discuss exceptions below). In their test, Damour and Schäfer realized if one excludes small  $\theta$  values with a given probability, one can set an upper limit on  $|\mathbf{e}_\Delta|$  without knowing  $e_{PN}$ . This is the basic idea behind the Damour-Schäfer test. The angle  $\theta$  can be assumed to have a uniform probability distribution in the range  $[0^\circ, 360^\circ)$  if the following two conditions are met:

- DS1)** The system should have a sufficient age, so that one can assume that the relativistic precession of the orbit will have caused the eccentricity vector to have made many turns since the system's birth, thereby effectively randomizing the relative orientation  $\theta \equiv \pi - \dot{\omega}_{PN}t$  (cf. equation (48) below).
- DS2)** The rate of periastron advance  $\dot{\omega}_{PN}$  should be appreciably larger than the angular velocity of the pulsar's rotation of the Galaxy with which  $\mathbf{g}$  rotates in the reference frame of the binary system. As a result, the projection of the Galactic acceleration vector onto the orbit can be considered constant.

Only if these conditions are met, the Damour-Schäfer test can be applied. Both of the systems considered in [117] fulfill these two criteria. Damour and Schäfer derived 90% confidence limits of  $|\delta_{P00}| < 5.6 \times 10^{-2}$  and  $|\delta_{P00}| < 1.1 \times 10^{-2}$ , from PSR B1855+09 and PSR B1953+29 respectively.

Once the eccentricity of a wide binary pulsar system is measured, there is generally little one can do to improve the Damour-Schäfer test with that system. Significant improvement of the Damour-Schäfer test has to come from the discovery of a new system. The larger the orbital period and the smaller the orbital eccentricity, the tighter a limit can be derived from a Damour-Schäfer test. In fact, the figure-of-merit for this test is  $P_b^2/e$ . In the meantime, quite a few suitable systems have been discovered (see e.g. table 4 in [121]). However, one cannot just pick the one with the best figure-of-merit from that ensemble, as this introduces a selection bias, since it is possible that the small eccentricity of the selected system is actually the result of a SEP violation where by chance  $\theta$  is small. In fact, if one has a large number of systems, there is a high probability that there are systems with small  $\theta$  [122, 119]. In this case, one has to properly combine all the systems in a statistical test. The latest results based on a proper statistical treatment can be found in [123, 121] which give 95% confidence limits of order  $5 \times 10^{-3}$ . The slightly better limit in [121] has a caveat by including PSR J1711–4322, which has a large figure-of-merit but neither fulfills condition DS1 nor DS2. Concerning DS2, as shown in [124], PSR J1711–4322 is at

a location in the Galactic plane where  $\dot{\omega}_{\text{PN}}$  is close, or even equal to the Galactic rotation. This can lead to a highly non-uniform evolution of  $\theta(t)$ .

## 4.2 Direct tests

There is an underlying assumption in the Damour-Schäfer test for multiple systems, which is related to the mass dependence of a SEP violation. Constraining a  $\delta_{\text{P00}}$  from a set of pulsar-white dwarf systems in a generic way, requires the assumption that  $\delta_{\text{P00}}$  is practically independent of the mass of the neutron star, as these systems have different pulsar masses. Even in the absence of a non-perturbative behavior, where to first order  $\delta_{\text{P00}}$  is proportional to  $\epsilon$  (cf. equation (42)), we can have deviations from that assumption of order 30% along the range of observed neutron star masses. And in the presence of non-perturbative strong-field effects, like the spontaneous scalarization mentioned above, this assumption is strongly violated. For this reason it is desirable to have direct tests, based on long term timing observations of individual systems, used to directly constrain  $\dot{e}$  (see [119] for details). As it requires a number of conditions to be met, like high timing precision and knowledge on the orbital orientation, only few systems turn out to be suitable at present. In [119] two binary pulsar systems have been identified as particularly suitable for a direct test of a SEP violation: PSR J1713+0747 and PSR J1903+0327. While the work on PSR J1713+0747 is still in progress, preliminary results for PSR J1903+0327 have been published in [119]. PSR J1903+0327 is a millisecond pulsar with good timing precision in a wide ( $x = 105.593 \text{ lt-s}$ ), highly eccentric ( $e = 0.44$ ) orbit [125, 32]. The pulsar is comparably massive ( $m_p = 1.67 M_\odot$ ) and the companion is a Sun-like main sequence star. At present, the limit from PSR J1903+0327 ( $\sim \text{few } \%$ ) cannot compete with the results of the Damour-Schäfer test mentioned above. But these limits are expected to improve with time, just by continuous timing observations.

In summary, there are several advantages of a direct test [119] compared to the Damour-Schäfer test:

- The tests are conducted for specific neutron star masses, and therefore are meaningful even in the presence of a non-perturbative strong-field behavior.
- The test no longer requires probabilistic consideration for unknown angles, and therefore cannot only set an upper limit, but also has the potential to detect a SEP violation.
- There are hardly any relevant additional effects, that lead to a non-zero  $\dot{e}$ . For wide binary orbits,  $\dot{e}$  from gravitational wave damping is absolutely negligible. Therefore the precision of this test is expected to just keep on improving with time, at least for the foreseeable future.

- We do not need to restrict our sample to systems with small eccentricities. In fact, in an eccentric system the violation of SEP would not only cause a change in the orbital eccentricity ( $\dot{e}$ ) but also, depending on the orientation, change the inclination of the orbital plane, which leads to a change in the projected semi-major axis ( $\dot{x}$ ). This allows for a unique cross-check, since the ratio  $\dot{x}/(x\dot{e})$  for a SEP violation only depends on the orientation and the eccentricity of the pulsar orbit [119].

## 5 Local Lorentz invariance of gravity

Some alternative gravity theories allow the Universal matter distribution to single out the existence of a preferred frame, which breaks the symmetry of local Lorentz invariance (LLI) for the gravitational interaction. In the post-Newtonian parametrization of semi-conservative gravity theories, LLI violation is characterized by two parameters,  $\alpha_1$  and  $\alpha_2$  [5]. Non-vanishing  $\alpha_1$  and  $\alpha_2$  modify the dynamics of self-gravitating systems that move with respect to the preferred frame (preferred-frame effects). In GR one finds  $\alpha_1 = \alpha_2 = 0$ .

As the most natural preferred frame, generally one chooses the frame associated with the isotropic cosmic microwave background (CMB), meaning that the preferred frame is assumed to be fixed by the global matter distribution of the Universe. From the five-year Wilkinson Microwave Anisotropy Probe (WMAP) satellite experiment, a CMB dipole measurement with high precision was obtained [126]. The CMB dipole corresponds to a motion of the Solar system with respect to the CMB with a velocity of  $369.0 \pm 0.9$  km/s in direction of Galactic longitude and latitude  $(l, b) = (263.99^\circ \pm 0.14^\circ, 48.26^\circ \pm 0.03^\circ)$ . The numbers quoted in the next two sub-sections, will be with respect to the CMB frame. A generalization to other frames is straightforward, and was done in some of the references cited below.

The most important (weak-field) constraints on preferred-frame effects do come from Lunar Laser Ranging (LLR) [127],

$$\alpha_1 = (-0.7 \pm 1.8) \times 10^{-4} \quad (95\% \text{ CL}) , \quad (46)$$

and the alignment of the Sun's spin with the total angular momentum of the planets in the Solar system [128],

$$|\alpha_2| < 2.4 \times 10^{-7} . \quad (47)$$

### 5.1 Constraints on $\hat{\alpha}_1$ from binary pulsars

In binary pulsars, the isotropic violation of Lorentz invariance in the gravitational sector should lead to characteristic preferred frame effects in the binary dynamics, if



the barycenter of the binary is moving relative to the preferred frame with a velocity  $\mathbf{w}$ . For small-eccentricity binaries, the effects induced by  $\hat{\alpha}_1$  and  $\hat{\alpha}_2$  (the hat indicates possible modifications by strong-field effects) decouple, and can therefore be tested independently [129, 130].

In case of a non-vanishing  $\hat{\alpha}_1$ , the observed eccentricity vector  $\mathbf{e}$  of a small-eccentricity binary pulsar is a vectorial superposition of a ‘rotating eccentricity’  $\mathbf{e}_R(t)$  and a fixed ‘forced eccentricity’  $\mathbf{e}_F$ :  $\mathbf{e}(t) = \mathbf{e}_F + \mathbf{e}_R(t)$  [129]. The rotating eccentricity has a constant length  $e_R$ , and rotates with the relativistic precession of periastron,  $\dot{\omega}$ , in the orbital plane. This is identical to the dynamics caused by a violation of the strong equivalence principle (cf. Section 4), with the forced eccentricity this time pointing into the direction of  $\hat{\mathbf{L}} \times \mathbf{w}$ . As a consequence, the binary orbit changes from a less to a more eccentric configuration and back on a time scale of

$$T_{\dot{\omega}} \equiv \frac{2\pi}{\dot{\omega}} \simeq (1140 \text{ yr}) \left( \frac{P_b}{1 \text{ day}} \right)^{5/3} \left( \frac{M}{2M_\odot} \right)^{-2/3}, \quad (48)$$

where we have assumed that the true  $\dot{\omega}$  does not deviate significantly from the one predicted by GR (equation (17)), an assumption that is well justified by other binary-pulsar experiments, like the generic tests in the Double Pulsar (cf. Section 2.2).

The forced eccentricity  $\mathbf{e}_F$  is determined by the strength of the preferred frame effect. Its magnitude is approximately given by

$$e_F \simeq 0.093 \hat{\alpha}_1 \frac{m_p - m_c}{M} \left( \frac{M}{2M_\odot} \right)^{-1/3} \left( \frac{P_b}{1 \text{ day}} \right)^{1/3} \left( \frac{w \sin \psi}{300 \text{ km/s}} \right), \quad (49)$$

where  $\psi$  is the angle between  $\mathbf{w}$  and  $\hat{\mathbf{L}}$  (see [129] for a detailed expression). The observation of small eccentricities in binary pulsars, like  $e \sim 10^{-7}$  for PSR J1738+0333 does not directly constrain  $\hat{\alpha}_1$ . The orientation of the a priori unknown intrinsic  $\mathbf{e}_R$  could be such, that it compensates for a large  $\mathbf{e}_F$ . If the system is sufficiently old, one can assume a uniform probability distribution in  $[0^\circ, 360^\circ)$  for  $\theta(t)$ . Like in the Damour-Schäfer test for SEP, one can now set a probabilistic upper limit on  $e_F$ , and by this on  $\hat{\alpha}_1$ , by excluding  $\theta$  values close to alignment of  $\mathbf{e}_R$  and  $\mathbf{e}_F$ . Based on this method, [129] found a limit of  $|\hat{\alpha}_1| < 5 \times 10^{-4}$  with 90% confidence.

But even if  $\theta$  happens to be close to  $0^\circ$ , due to the relativistic precession it will not remain there, and a large  $e_F$  cannot remain hidden for ever. In fact, if  $\dot{\omega}$  is sufficiently large (greater than  $\sim 1^\circ$  per year) a significant change in the orbital eccentricity should become observable over time scales of a few years, even if at the start of the observation there was a complete cancellation between  $\mathbf{e}_R$  and  $\mathbf{e}_F$ . This can be used to constrain  $\hat{\alpha}_1$  [130]. Hence, in contrast to the SEP test of Section 4.1, one now looks for suitable binary pulsars with short orbital periods. The best such test comes from PSR J1738+0333 (see Section 2.3). This binary pulsar is ideal for this test for several reasons:

- The orbit has an extremely small, well constrained eccentricity of  $\sim 10^{-7}$  [30].
- The (calculated) relativistic precession of periastron is about  $1.6^\circ/\text{yr}$ , and the binary has been observed by now for about 10 years [30]. Hence,  $\theta(t)$  has covered an angle of  $16^\circ$  in that time.
- The 3D velocity with respect to the Solar system is known with good precision from timing and optical observations, meaning that one can compute  $\mathbf{w}$  [84, 30].
- The orientation of the system is such, that the unknown angle of the ascending node  $\Omega$  has little influence on the  $\hat{\alpha}_1$  limit, hence there is no need for probabilistic considerations to exclude certain values of  $\Omega$  [130].

Consequently, PSR J1738+0333 leads to the best constraints of  $\alpha_1$ -like violations of the local Lorentz invariance of gravity, giving [130]

$$\hat{\alpha}_1 = -0.4_{-3.1}^{+3.7} \times 10^{-5} \quad (95\% \text{ confidence}) . \quad (50)$$

This limit is not only five times better than the current most stringent limit on  $\alpha_1$  obtained in the Solar system (cf. equation (46)), it is also sensitive to potential deviations related to the strong self-gravity of the pulsar. For non-perturbative deviations one can, for illustration purposes, do an expansion with respect to the fractional binding energy  $\epsilon$  of the neutron star,

$$\hat{\alpha}_1 = \alpha_1 + \mathcal{C}_1 \epsilon + \mathcal{O}(\epsilon^2) . \quad (51)$$

Since  $\epsilon \sim -0.1$  for PSR J1738+0333, we get tight constraints for  $\mathcal{C}_1$ , a parameter that is virtually unconstrained by the LLR experiment, since  $\epsilon \sim -5 \times 10^{-10}$  for the Earth.

## 5.2 Constraints on $\hat{\alpha}_2$ from binary and solitary pulsars

In the presence of a non-vanishing  $\hat{\alpha}_2$ , a small-eccentricity binary system experiences a precession of the orbital angular momentum around the fixed direction  $\mathbf{w}$  with an angular frequency

$$\begin{aligned} \Omega_{\hat{\alpha}_2}^{\text{prec}} &= -\hat{\alpha}_2 \frac{\pi}{P_b} \left( \frac{w}{c} \right)^2 \cos \psi \\ &\simeq -(0.066^\circ/\text{yr}) \hat{\alpha}_2 \left( \frac{P_b}{1 \text{ day}} \right)^{-1} \left( \frac{w}{300 \text{ km/s}} \right)^2 \cos \psi , \end{aligned} \quad (52)$$

where  $\psi$  is the angle between the orbital angular momentum and  $\mathbf{w}$  [130]. In binary pulsars, such a precession should become visible as a secular change in the projected

semi-major axis of the pulsar orbit,  $\dot{x}$ , which is an observable timing parameter. The two binary pulsars PSRs J1012+5307 and J1738+0333 turn out to be particularly useful for such a test, since both of them have optically bright white dwarf companions, which allowed the determination of the masses in the system, and the 3D systemic velocity with respect to the preferred frame [131, 132, 84].

Unfortunately, in general, the orientation of a binary pulsar orbit with respect to  $\mathbf{w}$  and the line-of-sight cannot be fully determined from timing observations. As a consequence, one cannot directly test  $\hat{\alpha}_2$  from observed constraints for  $\dot{x}$ . In fact, since the longitude of the ascending node  $\Omega$  is not measured, neither for PSR J1012+5307 nor for PSR J1738+0333, the orientation of these systems could in principle be such, that an  $\hat{\alpha}_2$ -induced precession would not lead to a significant  $\dot{x}$ . Assuming a random distribution of  $\Omega$  in the interval  $[0^\circ, 360^\circ)$ , one can use probabilistic considerations to exclude such unfavorable orientations. A detailed discussion of this test can be found in [130], where the following 95% confidence limits are derived

$$\begin{aligned} |\hat{\alpha}_2| &< 3.6 \times 10^{-4} && \text{from PSR J1012+5307,} \\ |\hat{\alpha}_2| &< 2.9 \times 10^{-4} && \text{from PSR J1738+0333,} \\ |\hat{\alpha}_2| &< 1.8 \times 10^{-4} && \text{from PSRs J1012+5307 and J1738+0333 combined.} \end{aligned} \tag{53}$$

It is important to note, that for the last limit, based on the statistical combination of the two systems, one has to assume that  $\hat{\alpha}_2$  has only a weak functional dependence on the neutron-star mass in the range of  $1.3 - 2.0 M_\odot$ .

The limit for  $\hat{\alpha}_2$  obtained from binary pulsars are still several orders of magnitude weaker than the  $\alpha_2$  limit which Nordtvedt derived in 1987 from the alignment of the Sun's spin with the orbital planes of the planets [128]. In the same paper, Nordtvedt pointed out that solitary fast-rotating pulsars could be used in a similar way to obtain tight constraints for  $\alpha_2$ . This can be directly seen from equation (52), which holds for a rotating self-gravitating star if  $P_b$  is replaced by the rotational period  $P$  of the star. While the five-billion-year base-line for the Solar experiment is typically a factor of  $\sim 10^9$  longer than the observational time-span  $T_{\text{obs}}$  of pulsars, for millisecond pulsars  $P$  is  $\sim 10^9$  shorter than the rotational period of the Sun. In fact, the first millisecond pulsar PSR B1937+21, discovered in 1982 [133], by now has a figure of merit  $T_{\text{obs}}/P$  that is  $\sim 10$  times larger than that of the Sun.

The precession of a solitary pulsar due to a non-vanishing  $\hat{\alpha}_2$  would lead to characteristic changes in the observed pulse profile over time-scales of years, just like in the case of binary pulsars that experience geodetic precession (cf. Section 3). Consequently, a non-detection of such changes can be converted into constraints for  $\hat{\alpha}_2$ . Recently, Shao *et al.* [134] used the two solitary millisecond pulsars PSRs B1937+21 and J1744-1134 for such an experiment. For both pulsars they utilized a consis-

tent set of data, taken over a time span of approximately 15 years with the same observing system at the 100-m Effelsberg radio telescope. The continuity in the observing system was key for an optimal comparison of the high signal-to-noise ratio profiles over time. As it turns out, both pulsars, PSRs B1937+21 and J1744–1134, do not show any detectable profile evolution in the last 15 years. As an example of such a non-detection see figure 19, which shows two pulse profiles of PSR B1937+21 obtained at different epochs.

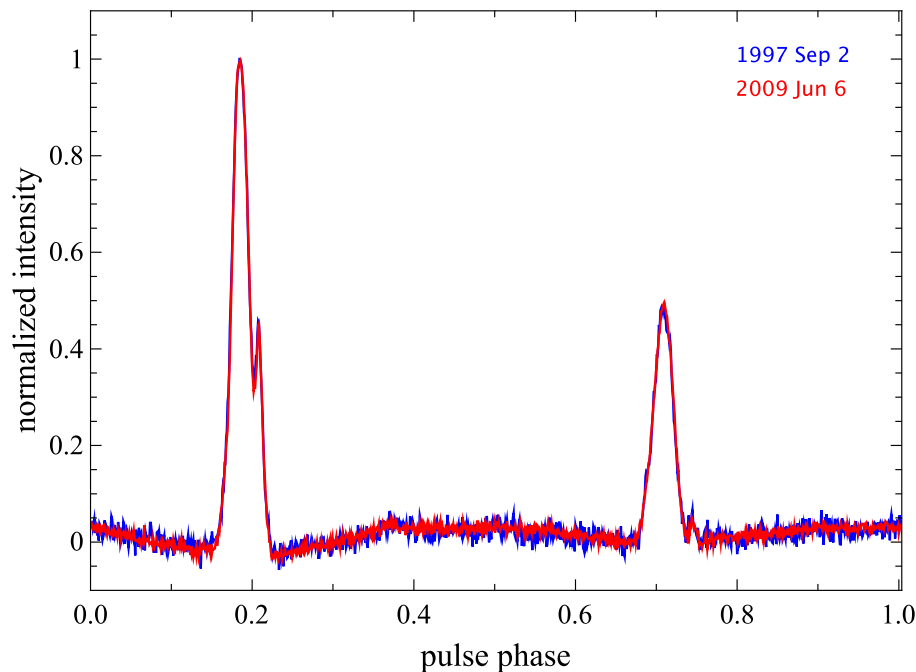


Figure 19: Comparison of two pulse profiles of PSR B1937+21 obtained at two different epochs. The blue one was obtained on September 2, 1997, while the red one was obtained on June 6, 2009. The main peak is aligned and scaled to have the same intensity. There exists no visible difference within the noise level. Profiles were taken from [134].

Similarly to the  $\hat{\alpha}_2$  test with the binary pulsars, there are unknown angles in the orientation of the pulsar spin, for which certain values have to be excluded based on probabilistic considerations. From extensive Monte-Carlo simulations Shao *et al.* found with 95% confidence

$$|\hat{\alpha}_2| < 2.5 \times 10^{-8} \quad \text{from PSR B1937+21,}$$

$$\begin{aligned}
|\hat{\alpha}_2| &< 1.5 \times 10^{-8} && \text{from PSR J1744–1134,} \\
|\hat{\alpha}_2| &< 1.6 \times 10^{-9} && \text{from PSRs B1937+21 and J1744–1134 combined.}
\end{aligned}
\tag{54}$$

These limits are significantly tighter than the  $\alpha_2$  limit from the Sun’s spin orientation. Like in the case of the  $\hat{\alpha}_1$  test (previous subsection), this test also covers potential deviations related to the strong self-gravity of the pulsar, and in the combination of the two pulsars, makes the assumption that  $\hat{\alpha}_2$  depends only weakly on the neutron-star mass.

An important difference to the aforementioned tests with binary pulsars is, that for solitary pulsars one cannot determine the radial velocity. It enters the determination of  $\mathbf{w}$  as a free parameter. However, as shown in [134], the unknown radial velocities for PSRs B1937+21 and J1744–1134 only have a marginal effect on the limits. For the limits above it was assumed that both pulsars are gravitationally bound in the Galactic potential. But even if one relaxes this assumption and allows for unphysically large radial velocities, exceeding 1000 km/s, the limits get weaker by at most  $\sim 40\%$ .

As a final remark, a combined test of  $\hat{\alpha}_1$  and  $\hat{\alpha}_2$  for the gravitational interaction of two strongly self-gravitating objects using the Double Pulsar, has been proposed in [135]. At the time of that publication, however, the observational time span was not long enough to disentangle potential preferred-frame effects from other orbital contributions. The large correlations with orbital parameters in the timing solution, lead to rather weak limits on  $\hat{\alpha}_1$  and  $\hat{\alpha}_2$  in the Double Pulsar.

### 5.3 Constraints on $\hat{\alpha}_3$ from binary pulsars

In non-conservative gravity theories, there is a third PPN parameter related to preferred-frame effects, denoted by  $\alpha_3$ , which identically vanishes in GR. Besides its association with preferred-frame effects,  $\alpha_3$  is also associated with a violation of the conservation of total momentum, the key feature of non-conservative gravity theories. Because of this, a non-zero  $\alpha_3$  leads to a self-acceleration for a self-gravitating rotating body. The acceleration is perpendicular to the angular rotation of the body,  $\boldsymbol{\Omega}$  and its motion with respect to the preferred frame,  $\mathbf{w}$ . The  $\alpha_3$ -induced acceleration is given by [5]

$$\mathbf{a}_{\alpha_3} = -\frac{\alpha_3}{3} \boldsymbol{\epsilon} \mathbf{w} \times \boldsymbol{\Omega}.
\tag{55}$$

The quantity  $\epsilon$  is the fractional binding energy of the body, as defined in equation (42). Due to their high binding energy ( $\epsilon \sim -0.1$ ) and their fast rotation ( $\Omega \sim 10^3$  rad/s), millisecond pulsars are ideal objects to probe for  $\alpha_3$  related effects. In fact, as shown in [136], millisecond pulsars in binary systems with a large orbital period  $P_b$  and a small eccentricity  $e$  are the best test systems for  $\hat{\alpha}_3$ , where the hat

indicates a strong-field generalization. As shown in [136],  $\mathbf{a}_{\alpha_3}$  has a polarizing effect on the binary orbit, analogous to the one induced by a SEP violation (cf. Section 4). Consequently a Damour-Schäfer test can be applied to constrain  $\alpha_3$ . The same requirements as in the SEP test (cf. DS1 and DS2 in Section 4) have to be met. DS2 is important, since the binary system should not move appreciably in the Galaxy during the build up of the polarization induced by  $\mathbf{a}_{\alpha_3}$ , otherwise the equations given in [136] do not apply. The latest limit, based on a proper statistical analysis of a large sample of known binary pulsars, comes from [121]:  $|\hat{\alpha}_3| < 5.5 \times 10^{-20}$  (95% confidence). PSR J1711–4322, which violates DS1 and DS2, has also been included in this analysis. However, due to its slow rotation ( $P = 103$  ms) it plays only a minor part in that test. The limit of [121] is more than a factor of  $\sim 10^{13}$  better than the best Solar system limit [5], and by far the tightest limit on any of the PPN parameters.

## 6 Local position invariance of gravity

The local position invariance (LPI) of gravity states that the outcome of any local gravitational experiment is independent of where and when it is performed. If the LPI is violated in the gravitational sector, the gravitational interaction of a localized self-gravitating system depends on the direction of its acceleration in the gravitational field of an external mass [5]. In such a scenario, the dynamics of the Solar system or a binary system depends on the overall matter distribution in our Galaxy, and one would experience a directional dependence in the locally measured gravitational constant. Within the PPN formalism, such an anisotropy is described by the *Whitehead parameter*  $\xi$  (not to be confused with the parameter  $\xi$  in equation (2)) [5]. It is interesting to note, that even for fully conservative theories of gravity one may have  $\xi \neq 0$ . In GR the gravitational interaction fulfills LPI and therefore GR has  $\xi = 0$ .

For small-eccentricity binaries,  $\xi$  primarily induces a precession of the orbital angular momentum around the direction of the external gravitational field,  $\mathbf{n}_G$ , with the angular velocity

$$\Omega^{\text{prec}} = -\xi \frac{2\pi}{P_b} \frac{\Phi_G}{c^2} \cos \psi , \quad (56)$$

where  $\Phi_G$  is the Newtonian Galactic potential at the position of the system, and  $\psi$  is the angle between the orbital angular momentum and  $\mathbf{n}_G$ . Due to the analogy with equation (52), one immediately sees that the same kind of analysis, as outlined in Section 5.2 for testing  $\hat{\alpha}_2$ , can be performed to constrain  $\hat{\xi}$ . Like in the previous section, the hat indicates the strong-field generalization of the PPN parameter. From

a combined analysis of PSRs J1012+5307 and J1738+0333 one obtains [137]

$$|\hat{\xi}| < 3.1 \times 10^{-4} \quad (95\% \text{ confidence}) . \quad (57)$$

This limit surpasses the weak-field limit on  $\xi$  obtained from the non-detection of anomalous Earth tides by about one order of magnitude.

A non-vanishing  $\xi$  would also affect an isolated rotating body [128]. Like for a binary system, the angular momentum, i.e. the spin, of a self-gravitating object with internal equilibrium should precess around  $\mathbf{n}_G$ . The precessional frequency is given by equation (56), if  $P_b$  is replaced by the rotational period  $P$  of the isolated body. Again, one has the analogy to the  $\hat{\alpha}_2$  tests of Section 5.2). Consequently, the same data and method used in the  $\hat{\alpha}_2$  test with solitary pulsars can be used to constrain  $|\hat{\xi}|$ . One obtains with 95% confidence [138]:

$$\begin{aligned} |\hat{\xi}| &< 2.2 \times 10^{-8} && \text{from PSR B1937+21,} \\ |\hat{\xi}| &< 1.2 \times 10^{-7} && \text{from PSR J1744-1134,} \\ |\hat{\xi}| &< 3.9 \times 10^{-9} && \text{from PSRs B1937+21 and J1744-1134 combined.} \end{aligned} \quad (58)$$

These limits are significantly (up to three orders of magnitude) better than the limit obtained from the Solar spin [128, 138].

As mentioned above, a violation of the LPI for gravity is directly related to a directional dependence of the local gravitational constant  $G$ . Consequently, the limits (58) can straightforwardly be converted into limits on an anisotropy of  $G$ . Corresponding to the combined limit from PSRs B1937+21 and J1744-1134 in (58), one finds

$$\left| \frac{\Delta G}{G} \right|^{\text{anisotropy}} < 4 \times 10^{-16} \quad (95\% \text{ confidence}) , \quad (59)$$

which is the most constraining limit on the anisotropy of  $G$  [138].

## 7 A varying gravitational constant

The locally measured Newtonian gravitational constant  $G$  may vary with time as the Universe evolves. In fact, this is expected for most alternatives to GR that violate the strong equivalence principle [5]. By now there are various tests to constrain a change in the gravitational constant on different time scales. Some tests probe a change over the cosmological history, i.e.  $G(t)$ , others a present change, i.e. today's  $\dot{G}$  (see [139] for a review).

In a binary system, a time variation of  $G$  changes the orbital period  $P_b$ . If the gravitational binding energy of the masses is small, like for Solar system bodies, this change is to first order given by [140]

$$\frac{\dot{P}_b}{P_b} = -\frac{\dot{n}_b}{n_b} = -2\frac{\dot{G}}{G}, \quad (60)$$

and the semi-major axis of the relative motion changes according to

$$\frac{\dot{a}}{a} = -\frac{\dot{G}}{G}. \quad (61)$$

In the Solar system, the Lunar Laser Ranging (LLR) experiment gives the best limit. Based on 39 years of LLR data, [141] derived a limit of

$$\frac{\dot{G}}{G} = (-0.7 \pm 3.8) \times 10^{-13} \text{ yr}^{-1} = (-0.001 \pm 0.005) H_0. \quad (62)$$

The value for the Hubble constant  $H_0 = 67.8 \text{ km/s/Mpc}$  is taken from [142].

Equation (60) is not applicable to binary pulsars. Contrary to weakly self-gravitating bodies, in binary pulsars the dependence on the gravitational self-energy cannot be neglected [143]. A change in  $G$  changes the gravitational binding energy of a self-gravitating body, and by this its mass. While such a change is negligible in the Earth-Moon system, since the fractional binding energy is very small for these bodies ( $\epsilon_{\text{Earth}} \approx -5 \times 10^{-10}$ ), it is significant for neutron stars, where the gravitational self-energy accounts for a significant fraction of the mass ( $\epsilon_{\text{NS}} \sim -0.1$ ). A detailed calculation can be found in [143], which shows that for a binary pulsar system equation (60) has to be modified to

$$\frac{\dot{P}_b}{P_b} = -2\frac{\dot{G}}{G} \left[ 1 - \left( 1 + \frac{m_c}{2M} \right) s_p - \left( 1 + \frac{m_p}{2M} \right) s_c \right], \quad (63)$$

where the ‘‘sensitivity’’

$$s_A \equiv - \left. \frac{\partial(\ln m_A)}{\partial(\ln G)} \right|_N \quad (64)$$

measures how the mass of body  $A$  changes with a change of the local gravitational constant  $G$ , for a fixed baryon number  $N$  (see [5] for details). For a given mass, the sensitivity of a neutron star depends on the equation of state and on the specifics of the gravity theory. Figure 20 shows the sensitivity for Jordan-Fierz-Brans-Dicke gravity, for different  $\alpha_0$  (i.e.  $\omega_{\text{BD}}$ ) and two different equations of state. If the companion of the pulsar is a weakly self-gravitating star, like a white dwarf,  $s_c$  becomes negligible and equation (63) simplifies to

$$\frac{\dot{P}_b}{P_b} \simeq -2\frac{\dot{G}}{G} \left[ 1 - \left( 1 + \frac{m_c}{2M} \right) s_p \right]. \quad (65)$$



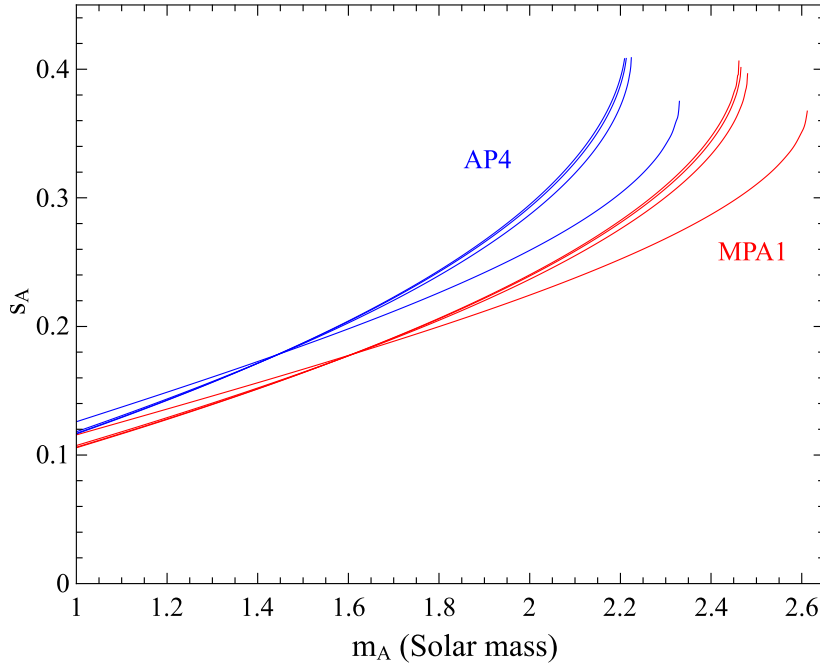


Figure 20: Sensitivity  $s_A$  for Jordan-Fierz-Brans-Dicke theory, i.e.  $T_1(\alpha_0, 0)$ , and for two different equations of state (red: MPA1 [85], blue: AP4 [144]). For each equation of state four lines have been calculated, corresponding to  $|\alpha_0| = 0.5, 0.2, 0.1, 0.01$  as the maximum mass decreases. For  $|\alpha_0| < 0.01$ ,  $s_A$  is practically independent of  $\alpha_0$ .

The currently best pulsar limit for a change in the gravitational constant comes from the pulsar-white dwarf system PSR J0437–4715 ( $P_b = 5.74$  d). A direct confrontation of equation (65) with the timing observations of that pulsar yields [145]

$$\frac{\dot{G}}{G} = \frac{(-5 \pm 26) \times 10^{-13}}{1 - 1.1s_p} \text{ yr}^{-1} \quad (95\% \text{ confidence}). \quad (66)$$

The factor  $(1 - 1.1s_p)$  weakens the limit by typically 30%, and has been neglected in [145]. As pointed out in [132], the limit (66) has the following caveat. It is generally expected that a gravity theory with a varying gravitational constant also predicts the existence of dipolar gravitational waves, that modify  $\dot{P}_b$ , and could in principle even balance a significant part of a decrease in  $G$ . In fact, just to give an example, in Jordan-Fierz-Brans-Dicke theory  $\dot{P}_b^{\dot{G}} \sim -\dot{P}_b^{\text{dipole}}$  for binary pulsar-white dwarf systems that have orbital periods of  $\sim 10$  d, like PSR J0437–4715. In the absence of non-perturbative strong-field effects one finds for the change in the orbital period

of a pulsar-white dwarf system in a small-eccentricity orbit the combined expression (cf. equation (25))

$$\frac{\dot{P}_b - \dot{P}_b^{\text{GR}}}{P_b} \simeq -2 \frac{\dot{G}}{G} \left[ 1 - \left( 1 + \frac{m_c}{2M} \right) s_p \right] - \frac{4\pi^2}{P_b^2} \frac{G m_p m_c}{c^3 M} \kappa_D s_p^2 + \mathcal{O}(s_p^3). \quad (67)$$

The constant  $\kappa_D$  is a theory dependent constant, which is a priori unknown in generic test, where no specific gravity theory is applied. As proposed in [132], it is now possible to combine two pulsars with a sufficiently large difference in their orbital periods  $P_b$  to constrain  $\dot{G}$  and  $\kappa_D$  simultaneously. In [30], the best pulsar for testing dipolar radiation, PSR J1738+0333 (see Section 2.3), and the best pulsar for a  $\dot{G}$  test, PSR J0437–4715, have been combined to give joint constraints for a variation in  $G$  and dipolar radiation (see figure 21). In this generic test, one has to make certain reasonable assumptions about  $s_A$  and how it changes with mass  $m_A$ , since PSR J1738+0333 and PSR J0437–4715 have different masses (see [30] for details). As one can see from figure 21, the pulsar limit on  $\dot{G}$  is still somewhat weaker than the one from LLR (68), but obtained with a completely independent method.

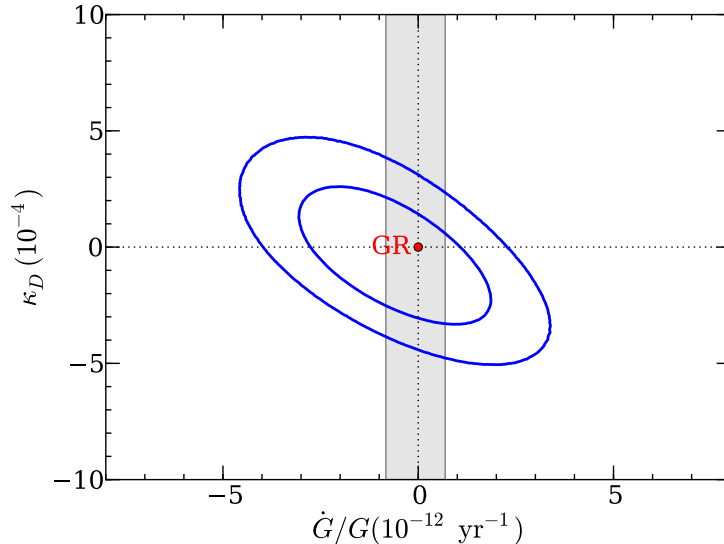


Figure 21: A joint  $\dot{G}$ - $\kappa_D$  test based on PSRs J1738+0333 and PSR J0437–4715. The inner blue contour includes 68.3% and the outer contour 95.4% of all probability. GR ( $\dot{G} = \kappa_D = 0$ ) is well within the inner contour and close to the peak of probability density. The grey band includes regions consistent with the one-sigma constraints for  $\dot{G}/G$  from LLR (equation (62)). Generally only the upper half of the diagram has physical meaning, as the radiation of dipolar gravitational waves is expected to make the system lose orbital energy. Figure is taken from [30].

Apart from providing an independent test for a varying gravitational constant, binary pulsar experiments can test for strong-field enhancements of  $\dot{G}$ . To illustrate this, we use scalar-tensor gravity, where a change in the locally measured gravitational constant  $G$  is the result of a change in the scalar field(s). More specifically, in the  $T_1(\alpha_0, \beta_0)$  theory of [57, 58], LLR tests for a variation of the gravitational constant that is given by

$$\frac{\dot{G}}{G} = 2 \left[ 1 + \frac{\beta_0}{1 + \alpha_0^2} \right] \alpha_0 \dot{\phi}_0 \quad (68)$$

(see equation (167) of [139]). For the effective gravitational constant between two strongly self-gravitating bodies (as measured in the physical Jordan-frame), equation (68) changes to

$$\frac{\dot{\mathcal{G}}}{\mathcal{G}} = 2 \left[ 1 + \frac{\alpha_A \beta_B + \alpha_B \beta_A}{2\alpha_0(1 + \alpha_A \alpha_B)} \right] \alpha_0 \dot{\phi}_0 . \quad (69)$$

In the presence of significant scalarization effects in the strong gravitational fields of neutron stars, the expression in square brackets of equation (69) can be considerably larger than the corresponding one in equation (68), even for  $\beta_0$  values which are not yet excluded by binary pulsar experiments (see figure 22). As a conclusion,  $\dot{G}$  tests with binary pulsars can be more sensitive than LLR tests in situations where a change in the gravitational constant gets enhanced by strong-field effects in neutron stars. The details depend on the specifics of the gravity theory and the mass of the neutron star. Also, a complete analysis needs to account for corresponding changes in the masses, i.e. the analogue to equation (63). We will not go into these details here.

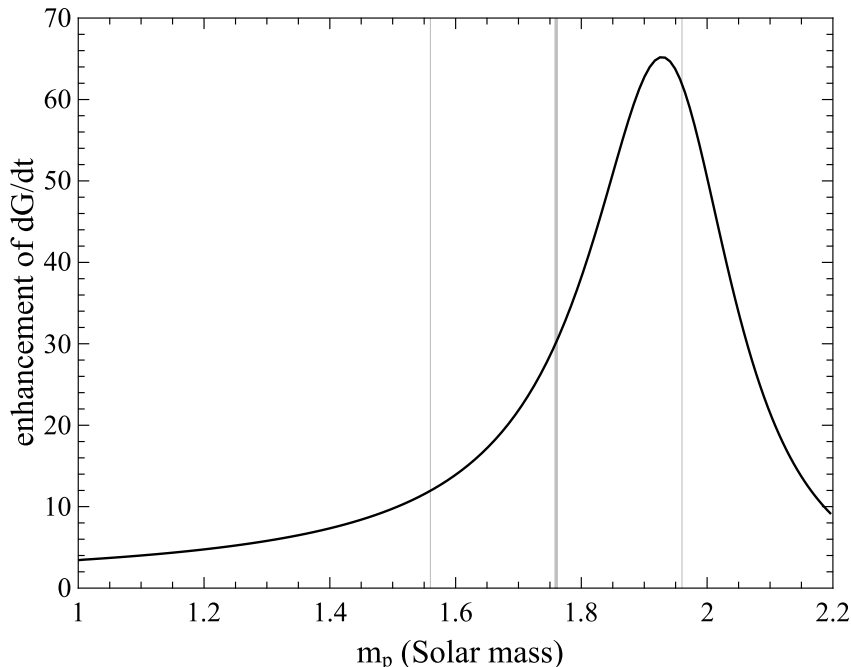


Figure 22: Enhancement of  $\dot{G}$  in a pulsar-white dwarf system as a function of the pulsar mass  $m_p$ . Figure shows the ratio  $(\dot{G}/\mathcal{G}) / (\dot{G}/G)$  as given in equations (68) and (69) for  $T_1(10^{-4}, -4.3)$  gravity, a theory which still passes the PSR J0348+0432 test (see figure 14). The grey vertical lines indicate the mass range for PSR J0437–4715 (mean and one-sigma uncertainties) [29]. PSR J1614–2230, with its mass of  $1.97 \pm 0.04 M_\odot$  and orbital period of 8.7 days [77], seems to be a promising future test for  $\dot{G}$ , once tight constraints on the intrinsic  $\dot{P}_b$  can be derived from the timing observations.

## 8 Summary and Outlook

With their discovery of the first binary pulsar four decades ago, Joseph Taylor and Russell Hulse opened a new field of experimental gravity, which has been an active field of research ever since. Besides the Hulse-Taylor pulsar, which led to the first confirmation of the existence of gravitational waves, astronomy has seen the discovery of many new binary pulsars suitable for precision gravity tests. Arguably, the most exciting discovery was the Double Pulsar in 2003, which by now provides the best test for GR’s quadrupole formalism of gravitational wave generation ( $< 0.1\%$  uncertainty), and the best test for the relativistic spin precession of a strongly self-gravitating body. In addition to this, it is the binary pulsar with the most post-Keplerian parameters measured, allowing for a number of generic constraints on strong-field deviations from GR. For certain aspects of gravity, binary pulsars with white dwarf companions have proven to be even better “test laboratories” than the Double Pulsar. These are gravitational phenomena, predicted by alternatives to GR, that depend on the difference in the compactness/binding energy of the two components, like gravitational dipolar radiation and a violation of the strong equivalence principle. By now, pulsar-white dwarf systems, like PSR J1738+0333, set quite stringent limits (coupling strength less than about  $10^{-3}$ ) on the existence of any additional “gravitational charges” associated with light or massless fields. The recent discovery of a massive pulsar in a relativistic binary system (PSR J0348+0432), for the first time allowed to test the orbital motion of a neutron star that is significantly more compact than pulsars of previous gravity tests. For certain aspects of gravity, solitary pulsars turned out to be ideal probes. The current best limits on the PPN parameters  $\alpha_2$ , related to the existence of a preferred frame for gravity, and  $\xi$ , related to a violation of local position invariance of the gravitational interaction, do come from pulse-profile observations of two solitary millisecond pulsars. In all these tests, pulsars go beyond Solar system tests, since they are also sensitive to deviations that occur only in the strong-field environment of neutron stars.

So far, GR has passed all these tests with flying colors. Will this continue forever? Is GR our final answer to the macroscopic description of gravity? Pulsar astronomy will certainly continue to investigate this question. Many of the tests mentioned here will simply improve by continued timing observations of the known pulsars. In fact, the measurement precision for some of the post-Keplerian parameters increases fast with time. For instance, in regular observations (with the same hardware) the uncertainty in the change of the orbital period  $\dot{P}_b$  decreases with  $T_{\text{obs}}^{-2.5}$ ,  $T_{\text{obs}}$  denoting the observing time span. Improvements in the hardware, like new broad-band receivers (e.g. [146]), will further boost the timing precision. For pulsars like PSR J1738+0333 and PSR J0348+0432 soon the modeling of the white dwarf will be the limiting factor, while for the Double Pulsar the corrections of the

external contributions to  $\dot{P}_b$  will be the challenging bit, in particular if one wants to reach the  $\sim 10^{-5}$  level at which higher order contributions to  $\dot{P}_b$  [147, 148] and the Lense-Thirring contribution to the orbital dynamics [45, 50] become relevant (see [75] for a detailed discussion). The upcoming next generation of radio telescopes, like the Five-hundred-meter Aperture Spherical radio Telescope (FAST) [149] and the The Square Kilometre Array (SKA) [150], certainly promise a big step towards this goal. With SKA, for many pulsars one can hope for a factor of 100 improvement in timing precision [151]. The SKA also promises to provide excellent direct distance measurements to pulsars, either directly by utilizing the long baselines of the SKA to form high angular resolution images, or by fitting for the timing parallax in the arrival times of the pulsar signals [152]. In combination with new models for the gravitational potential of our Galaxy, in particular after new missions like GAIA [153], one will be able to accurately determine the extrinsic “contaminations” of  $\dot{P}_b$  via equation (27), and by this know the intrinsic  $\dot{P}_b$ . This is key for any high precision gravitational wave test with binary pulsars, but also crucial to measure the Lense-Thirring drag in the Double Pulsar [75].

Reducing the parameter uncertainties for known pulsars is one way to push gravity tests forward, finding new, more relativistic systems is the other. Presently there are a number of pulsar surveys underway that promise the discovery of many new pulsars. New techniques, like acceleration searches [154] and high performance computing, e.g. Einstein@Home [155], promise the detection of pulsars in tight orbits, which generally cannot be found with traditional methods. There is considerable hope among pulsar astronomers, that this will finally also lead to the discovery of a pulsar-black hole system, occasionally called the “holy grail” of pulsar astronomy. Such a system is expected to provide a superb new probe of relativistic gravity and black hole properties, like the dragging of spacetime by the rotation of the black hole [156, 157, 158]. According to GR, for an astrophysical black hole (Kerr solution) there is an upper limit for its spin, given by  $S_{\max} = GM^2/c$ . It would pose an interesting challenge to GR, if the timing of a pulsar-black hole system indicates a spin  $S > S_{\max}$ . But even for gravity theories that predict the same properties for black holes as in GR, a pulsar-black hole system would constitute an excellent test system, due to the high grade of asymmetry in the strong-field properties of these two components (see [158] for simulations based on  $T_1(\alpha_0, \beta_0)$  scalar-tensor theories). A pulsar in a close orbit ( $P_b < 1$  yr) around the super-massive black hole ( $m_{\text{BH}} \approx 4 \times 10^6 M_\odot$ ) in the center of our Galaxy would be the ultimate test system, in that context. According to the mock data analysis in [159], for such a system a precise measurement of the quadrupole moment of the black hole, and therefore a test of the no-hair theorem, should be possible, provided that the environment of the pulsar orbit is sufficiently clean. Finding and timing a pulsar in the center of our Galaxy is certainly challenging. A promising result in that direction is the very

recent detection of radio signals from a magnetar near the Galactic center black hole [160], even if this pulsar is still too far away from the super-massive black hole ( $\sim 0.1$  pc) to probe its spacetime.

Until now, all gravitational wave tests are based on probing the near-zone of a binary spacetime by measuring how the back reaction of the gravitational radiation changes the world lines of the source masses. As outlined above, with the Double Pulsar this test has reached a precision of better than 0.1%. Presently there are considerable efforts to achieve a direct detection of gravitational waves, i.e. measure the far-field properties of such radiative spacetimes by using appropriate test masses. Ground based laser interferometric gravitational wave observatories, like LIGO and VIRGO, have mirrors with separations of a few kilometers. Their sensitivity is in the range from 10 Hz to few  $10^3$  Hz. Planned space-based detectors, like eLISA<sup>14</sup>, will have three drag-free satellites as test masses with a typical separation of  $\sim 10^6$  km, and should be sensitive to gravitational waves from about  $10^{-4}$  Hz to 0.1 Hz. For the ultra-low frequency band (few nano-Hz) pulsar timing arrays are currently the most promising detectors [161]. In these experiments the Earth/Solar system and a collection of very stable pulsars act as the test masses. A gravitational wave becomes apparent in a pulsar timing array by the changes it causes in the arrival times of the pulsar signals. Due to the fitting of the rotational frequency  $\nu$  and its time derivative  $\dot{\nu}$  for every pulsar, such a detector is only sensitive to wavelengths up to  $\sim cT_{\text{obs}}$ .<sup>15</sup> This leads to the special situation that the length of the “detector arms” is much larger than the wavelength. As a consequence, the observed timing signal contains two contributions, the so-called *pulsar term*, related to the impact of the gravitational wave on the pulsar when the radio signal is emitted, and the *Earth term* corresponding to the impact of the gravitational wave on the Earth during the arrival of the radio signal at the telescope [164, 165]. The most promising source in the nano-Hz frequency band is a stochastic gravitational wave background, as a result of many mergers of super-massive black hole binaries in the past history of the Universe [166, 167]. With the large number of “detector arms”, pulsar timing arrays have enough information to explore the properties of the nano-Hz gravitational wave background in details, once its signal is clearly detected in the data. Are there more than the two Einsteinian polarization modes (alternative metric theories can have up to six)? Is the propagation speed of nano-Hz gravitational waves frequency depended? Does the graviton carry mass? These are some of the main questions that can be addressed with pulsar timing arrays [168, 169]. The isolation of a single source in the pulsar timing array data would give us a unique opportunity to

---

<sup>14</sup>[www.elisascience.org/](http://www.elisascience.org/)

<sup>15</sup>It has been suggested to use the orbital period of binary pulsars to test for gravitational waves of considerably longer wavelength [162, 163].

study the merger evolution of a super-massive black hole binary, since the signal in the Earth term and the signal in the pulsar term show two different states of the system, which are typically several thousand years apart [170]. For these kind of gravity experiments, however, we might have to wait till the full SKA has collected a few years of data, which probably brings us close to the year 2030.

## References

- [1] A. Einstein. Die Feldgleichungen der Gravitation. *Sitzungsberichte der Königlich Preussischen Akademie der Wissenschaften (Berlin)*, pages 844–847, 1915.
- [2] A. Einstein. Erklärung der Perihelbewegung des Merkur aus der allgemeinen Relativitätstheorie. *Sitzungsberichte der Königlich Preussischen Akademie der Wissenschaften (Berlin)*, pages 831–839, 1915.
- [3] H. Seeliger. Über die Anomalien in der Bewegung der innern Planeten. *Astronomische Nachrichten*, 201:273, 1915.
- [4] A. Einstein. Die Grundlage der allgemeinen Relativitätstheorie. *Annalen der Physik*, 354:769–822, 1916.
- [5] C. M. Will. *Theory and Experiment in Gravitational Physics*. Cambridge University Press, Cambridge, 1993.
- [6] F. W. Dyson, A. S. Eddington, and C. Davidson. A Determination of the Deflection of Light by the Sun’s Gravitational Field, from Observations Made at the Total Eclipse of May 29, 1919. *Royal Society of London Philosophical Transactions Series A*, 220:291–333, 1920.
- [7] M. Froeschle, F. Mignard, and F. Arenou. Determination of the PPN Parameter gamma with the HIPPARCOS Data. In R. M. Bonnet, E. Høg, P. L. Bernacca, L. Emiliani, A. Blaauw, C. Turon, J. Kovalevsky, L. Lindegren, H. Hassan, M. Bouffard, B. Strim, D. Heger, M. A. C. Perryman, and L. Wolter, editors, *Hipparcos - Venice '97*, volume 402 of *ESA Special Publication*, pages 49–52, 1997.
- [8] D. E. Lebach, B. E. Corey, I. I. Shapiro, M. I. Ratner, J. C. Webber, A. E. E. Rogers, J. L. Davis, and T. A. Herring. Measurement of the Solar Gravitational Deflection of Radio Waves Using Very-Long-Baseline Interferometry. *Phys. Rev. Lett.*, 75:1439–1442, 1995.



- [9] S. S. Shapiro, J. L. Davis, D. E. Lebach, and J. S. Gregory. Measurement of the Solar Gravitational Deflection of Radio Waves using Geodetic Very-Long-Baseline Interferometry Data, 1979–1999. *Phys. Rev. Lett.*, 92:121101, 2004.
- [10] E. Fomalont, S. Kopeikin, G. Lanyi, and J. Benson. Progress in Measurements of the Gravitational Bending of Radio Waves Using the VLBA. *Astrophys. J.*, 699:1395–1402, 2009.
- [11] I. I. Shapiro. Fourth Test of General Relativity. *Phys. Rev. Lett.*, 13:789–791, 1964.
- [12] B. Bertotti, L. Iess, and P. Tortora. A test of general relativity using radio links with the Cassini spacecraft. *Nature*, 425:374–376, 2003.
- [13] K. Nordtvedt. 30 years of lunar laser ranging and the gravitational interaction. *Class. Quantum Grav.*, 16:A101–A112, 1999.
- [14] C. W. F. Everitt, D. B. Debra, B. W. Parkinson, J. P. Turneare, J. W. Conklin, M. I. Heifetz, G. M. Keiser, A. S. Silbergleit, T. Holmes, J. Kolodziejczak, M. Al-Meshari, J. C. Mester, B. Muhlfelder, V. G. Solomonik, K. Stahl, P. W. Worden, Jr., W. Bencze, S. Buchman, B. Clarke, A. Al-Jadaan, H. Al-Jibreen, J. Li, J. A. Lipa, J. M. Lockhart, B. Al-Suwaidan, M. Taber, and S. Wang. Gravity Probe B: Final Results of a Space Experiment to Test General Relativity. *Phys. Rev. Lett.*, 106:221101, 2011.
- [15] I. Ciufolini and E. C. Pavlis. A confirmation of the general relativistic prediction of the Lense-Thirring effect. *Nature*, 431:958–960, 2004.
- [16] A. Einstein. Näherungsweise Integration der Feldgleichungen der Gravitation. *Sitzungsberichte der Königlich Preußischen Akademie der Wissenschaften (Berlin)*, pages 688–696, 1916.
- [17] A. Einstein. Über Gravitationswellen. *Sitzungsberichte der Königlich Preußischen Akademie der Wissenschaften (Berlin)*, pages 154–167, 1918.
- [18] D. Kennefick. *Traveling at the Speed of Thought: Einstein and the Quest for Gravitational Waves*. Princeton University Press, Princeton and Oxford, 2007.
- [19] R. A. Hulse and J. H. Taylor. Discovery of a pulsar in a binary system. *Astrophys. J.*, 195:L51–L53, 1975.
- [20] J. J. Hermes, M. Kilic, W. R. Brown, D. E. Winget, C. Allende Prieto, A. Gianninas, A. S. Mukadam, A. Cabrera-Lavers, and S. J. Kenyon. Rapid Orbital

- Decay in the 12.75-minute Binary White Dwarf J0651+2844. *Astrophys. J.*, 757:L21, 2012.
- [21] A. Hewish, S. J. Bell, J. D. H. Pilkington, P. F. Scott, and R. A. Collins. Observation of a Rapidly Pulsating Radio Source. *Nature*, 217:709–713, 1968.
- [22] R. N. Manchester, G. B. Hobbs, A. Teoh, and M. Hobbs. The Australia Telescope National Facility Pulsar Catalogue. *Astrophys. J.*, 129:1993–2006, 2005. <http://www.atnf.csiro.au/research/pulsar/psrcat/>.
- [23] Duncan R. Lorimer. Binary and millisecond pulsars. *Living Rev. Relativity*, 8, 2005. <http://www.livingreviews.org/lrr-2005-7>.
- [24] G. Hobbs, W. Coles, R. N. Manchester, M. J. Keith, R. M. Shannon, D. Chen, M. Bailes, N. D. R. Bhat, S. Burke-Spolaor, D. Champion, A. Chaudhary, A. Hotan, J. Khoo, J. Kocz, Y. Levin, S. Osłowski, B. Preisig, V. Ravi, J. E. Reynolds, J. Sarkissian, W. van Straten, J. P. W. Verbiest, D. Yardley, and X. P. You. Development of a pulsar-based time-scale. *Mon. Not. R. Astron. Soc.*, 427:2780–2787, 2012.
- [25] I. H. Stairs. Testing General Relativity with Pulsar Timing. *Living Rev. Relativity*, 6, 2003. <http://www.livingreviews.org/lrr-2003-5>.
- [26] D. R. Lorimer and M. Kramer. *Handbook of Pulsar Astronomy*. Cambridge University Press, Cambridge, 2004.
- [27] R. T. Edwards, G. B. Hobbs, and R. N. Manchester. TEMPO2, a new pulsar timing package - II. The timing model and precision estimates. *Mon. Not. R. Astron. Soc.*, 372:1549–1574, 2006.
- [28] M. Kramer. Probing gravitation with pulsars. *Proceedings of the International Astronomical Union*, 8:19–26, 2012.
- [29] J. P. W. Verbiest, M. Bailes, W. van Straten, G. B. Hobbs, R. T. Edwards, R. N. Manchester, N. D. R. Bhat, J. M. Sarkissian, B. A. Jacoby, and S. R. Kulkarni. Precision Timing of PSR J0437–4715: An Accurate Pulsar Distance, a High Pulsar Mass, and a Limit on the Variation of Newton’s Gravitational Constant. *Astrophys. J.*, 679:675–680, 2008.
- [30] P. C. C. Freire, N. Wex, G. Esposito-Farèse, J. P. W. Verbiest, M. Bailes, B. A. Jacoby, M. Kramer, I. H. Stairs, J. Antoniadis, and G. H. Janssen. The relativistic pulsar-white dwarf binary PSR J1738+0333 - II. The most stringent test of scalar-tensor gravity. *Mon. Not. R. Astron. Soc.*, 423:3328–3343, 2012.

- [31] J. M. Weisberg, D. J. Nice, and J. H. Taylor. Timing Measurements of the Relativistic Binary Pulsar PSR B1913+16. *Astrophys. J.*, 722:1030–1034, 2010.
- [32] P. C. C. Freire, C. G. Bassa, N. Wex, I. H. Stairs, D. J. Champion, S. M. Ransom, P. Lazarus, V. M. Kaspi, J. W. T. Hessels, M. Kramer, J. M. Cordes, J. P. W. Verbiest, P. Podsiadlowski, D. J. Nice, J. S. Deneva, D. R. Lorimer, B. W. Stappers, M. A. McLaughlin, and F. Camilo. On the nature and evolution of the unique binary pulsar J1903+0327. *Mon. Not. R. Astron. Soc.*, 412:2763–2780, 2011.
- [33] A. W. Hotan, M. Bailes, and S. M. Ord. High-precision baseband timing of 15 millisecond pulsars. *Mon. Not. R. Astron. Soc.*, 369:1502–1520, 2006.
- [34] D. J. Champion, G. B. Hobbs, R. N. Manchester, R. T. Edwards, D. C. Backer, M. Bailes, N. D. R. Bhat, S. Burke-Spolaor, W. Coles, P. B. Demorest, R. D. Ferdman, W. M. Folkner, A. W. Hotan, M. Kramer, A. N. Lommen, D. J. Nice, M. B. Purver, J. M. Sarkissian, I. H. Stairs, W. van Straten, J. P. W. Verbiest, and D. R. B. Yardley. Measuring the Mass of Solar System Planets Using Pulsar Timing. *Astrophys. J.*, 720:L201–L205, 2010.
- [35] T. Damour. The problem of motion in Newtonian and Einsteinian gravity. In S.W. Hawking and W. Israel, editors, *Three Hundred Years of Gravitation*, pages 128–198. Cambridge University Press, Cambridge; New York, 1987.
- [36] L. Blanchet. Gravitational Radiation from Post-Newtonian Sources and Inspiralling Compact Binaries. *Living Rev. Relativity*, 9, 2006.
- [37] Toshifumi Futamase and Yousuke Itoh. The Post-Newtonian Approximation for Relativistic Compact Binaries. *Living Rev. Relativity*, 10, 2007. <http://www.livingreviews.org/lrr-2007-2>.
- [38] T. Damour. Gravitational radiation and the motion of compact bodies. In N. Deruelle and T. Piran, editors, *Gravitational Radiation*, pages 59–144, Amsterdam, Netherlands; New York, U.S.A., 1983. North-Holland; Elsevier.
- [39] J.-M. Gérard and Y. Wiaux. Gravitational dipole radiations from binary systems. *Phys. Rev. D*, 66:024040, 2002.
- [40] T. Damour and J. H. Taylor. Strong-field tests of relativistic gravity and binary pulsars. *Phys. Rev. D*, 45:1840–1868, 1992.
- [41] T. Damour. Binary Systems as Test-Beds of Gravity Theories. In M. Colpi, P. Casella, V. Gorini, U. Moschella, and A. Possenti, editors, *Astrophysics and*

- Space Science Library*, volume 359 of *Astrophysics and Space Science Library*, pages 1–41, 2009.
- [42] T. Damour and N. Deruelle. General Relativistic Celestial Mechanics of Binary Systems. I. The post-Newtonian motion. *Ann. Inst. Henri Poincaré Phys. Théor.*, 43:107–132, 1985.
  - [43] T. Damour and G. Esposito-Farèse. Testing gravity to second post-Newtonian order: A field-theory approach. *Phys. Rev. D*, 53:5541–5578, 1996.
  - [44] S. Mirshekari and C. M. Will. Compact binary systems in scalar-tensor gravity: Equations of motion to 2.5 post-Newtonian order. *Phys. Rev. D*, 87:084070, 2013.
  - [45] B. M. Barker and R. F. O’Connell. Gravitational two-body problem with arbitrary masses, spins, and quadrupole moments. *Phys. Rev. D*, 12:329–335, 1975.
  - [46] V. A. Brumberg. *Essential relativistic celestial mechanics*. Adam Hilger, Bristol, England and New York, 1991.
  - [47] J. Hartung, J. Steinhoff, and G. Schäfer. Next-to-next-to-leading order post-Newtonian linear-in-spin binary Hamiltonians. *Annalen der Physik*, 525:359–394, 2013.
  - [48] N. Wex. The second post-Newtonian motion of compact binary-star systems with spin. *Class. Quantum Grav.*, 12:983–1005, 1995.
  - [49] T. Damour. Problème des deux corps et freinage de rayonnement en relativité générale. *C. R. Acad. Sci. Paris, Série II*, 294:1355–1357, 1982.
  - [50] T. Damour and G. Schäfer. Higher order relativistic periastron advances in binary pulsars. *Nuovo Cimento B*, 101:127, 1988.
  - [51] T. Damour and R. Ruffini. Certain new verifications of general relativity made possible by the discovery of a pulsar belonging to a binary system. *Academie des Sciences Paris Comptes Rendus Serie Sciences Mathematiques*, 279:971–973, 1974.
  - [52] G. Börner, J. Ehlers, and E. Rudolph. Relativistic spin precession in two-body systems. *Astron. Astrophys.*, 44:417–420, 1975.
  - [53] V. M. Kaspi, M. Bailes, R. N. Manchester, B. W. Stappers, and J. F. Bell. Evidence from a precessing pulsar orbit for a neutron-star birth kick. *Nature*, 381:584–586, 1996.

- [54] T. Damour. Strong-field tests of general relativity and the binary pulsar. In A. Coley, C. Dyer, and T. Tupper, editors, *Proceedings of the 2nd Canadian Conference on General Relativity and Relativistic Astrophysics*, pages 315–334, 1988.
- [55] T. Damour and N. Deruelle. General relativistic celestial mechanics of binary systems. II. The post-Newtonian timing formula. *Ann. Inst. Henri Poincaré Phys. Théor.*, 44:263–292, 1986.
- [56] M. Ali. Relativistic Propagation Effects in Binary Pulsar Signals for Next Generation Radio Telescopes. Master thesis, University of Bonn, Germany, 2011.
- [57] T. Damour and G. Esposito-Farèse. Nonperturbative strong-field effects in tensor-scalar theories of gravitation. *Phys. Rev. Lett.*, 70:2220–2223, 1993.
- [58] T. Damour and G. Esposito-Farèse. Tensor-scalar gravity and binary-pulsar experiments. *Phys. Rev. D*, 54:1474–1491, 1996.
- [59] D. M. Eardley. Observable effects of a scalar gravitational field in a binary pulsar. *Astrophys. J.*, 196:L59–L62, 1975.
- [60] C. M. Will. Gravitational radiation from binary systems in alternative metric theories of gravity — Dipole radiation and the binary pulsar. *Astrophys. J.*, 214:826–839, 1977.
- [61] T. Damour and G. Esposito-Farèse. Tensor-multi-scalar theories of gravitation. *Class. Quantum Grav.*, 9:2093–2176, September 1992.
- [62] P.C. Peters. Gravitational radiation and the motion of two point masses. *Phys. Rev.*, 136:B1224–B1232, 1964.
- [63] V. A. Brumberg, I. B. Zeldovich, I. D. Novikov, and N. I. Shakura. Component masses and inclination of binary systems containing a pulsar, determined from relativistic effects. *Sov. Astronomy Lett.*, 1:2–4, 1975.
- [64] R. V. Wagoner. Test for the existence of gravitational radiation. *Astrophys. J.*, 196:L63–L65, 1975.
- [65] J. H. Taylor, R. A. Hulse, L. A. Fowler, G. E. Gullahorn, and J. M. Rankin. Further observations of the binary pulsar PSR 1913+16. *Astrophys. J.*, 206:L53–L58, 1976.

- [66] N. Wex, V. Kalogera, and M. Kramer. Constraints on Supernova Kicks from the Double Neutron Star System PSR B1913+16. *Astrophys. J.*, 528:401–409, 2000.
- [67] R. Blandford and S. A. Teukolsky. On the Measurement of the Mass of PSR 1913+16. *Astrophys. J.*, 198:L27–L29, 1975.
- [68] J. H. Taylor, L. A. Fowler, and P. M. McCulloch. Measurements of general relativistic effects in the binary pulsar PSR 1913+16. *Nature*, 277:437–440, 1979.
- [69] I. S. Shklovskii. Possible Causes of the Secular Increase in Pulsar Periods. *Sov. Astronomy*, 13:562–565, 1970.
- [70] T. Damour and J. H. Taylor. On the orbital period change of the binary pulsar PSR 1913+16. *Astrophys. J.*, 366:501–511, 1991.
- [71] J. M. Weisberg, S. Stanimirović, K. Xilouris, A. Hedden, A. de la Fuente, S. B. Anderson, and F. A. Jenet. Arecibo H I Absorption Measurements of Pulsars and the Electron Density at Intermediate Longitudes in the First Galactic Quadrant. *Astrophys. J.*, 674:286–294, 2008.
- [72] M. Burgay, N. D’Amico, A. Possenti, R. N. Manchester, A. G. Lyne, B. C. Joshi, M. A. McLaughlin, M. Kramer, J. M. Sarkissian, F. Camilo, V. Kalogera, C. Kim, and D. R. Lorimer. An increased estimate of the merger rate of double neutron stars from observations of a highly relativistic system. *Nature*, 426:531–533, 2003.
- [73] A. G. Lyne, M. Burgay, M. Kramer, A. Possenti, R. N. Manchester, F. Camilo, M. A. McLaughlin, D. R. Lorimer, N. D’Amico, B. C. Joshi, J. Reynolds, and P. C. C. Freire. A Double-Pulsar System: A Rare Laboratory for Relativistic Gravity and Plasma Physics. *Science*, 303:1153–1157, 2004.
- [74] M. Kramer and I. H. Stairs. The Double Pulsar. *Annual Review of Astronomy and Astrophysics*, 46:541–572, 2008.
- [75] M. Kramer and N. Wex. TOPICAL REVIEW: The double pulsar system: a unique laboratory for gravity. *Class. Quantum Grav.*, 26:073001, 2009.
- [76] M. Kramer, I. H. Stairs, R. N. Manchester, M. A. McLaughlin, A. G. Lyne, R. D. Ferdman, M. Burgay, D. R. Lorimer, A. Possenti, N. D’Amico, J. M. Sarkissian, G. B. Hobbs, J. E. Reynolds, P. C. C. Freire, and F. Camilo. Tests of General Relativity from Timing the Double Pulsar. *Science*, 314:97–102, 2006.

- [77] P. B. Demorest, T. Pennucci, S. M. Ransom, M. S. E. Roberts, and J. W. T. Hessels. A two-solar-mass neutron star measured using Shapiro delay. *Nature*, 467:1081–1083, 2010.
- [78] R. Blandford and S. A. Teukolsky. Arrival-time analysis for a pulsar in a binary system. *Astrophys. J.*, 205:580–591, 1976.
- [79] A. T. Deller, M. Bailes, and S. J. Tingay. Implications of a VLBI Distance to the Double Pulsar J0737-3039A/B. *Science*, 323:1327–1329, 2009.
- [80] J. P. W. Verbiest, M. Bailes, W. A. Coles, G. B. Hobbs, W. van Straten, D. J. Champion, F. A. Jenet, R. N. Manchester, N. D. R. Bhat, J. M. Sarkissian, D. Yardley, S. Burke-Spolaor, A. W. Hotan, and X. P. You. Timing stability of millisecond pulsars and prospects for gravitational-wave detection. *Mon. Not. R. Astron. Soc.*, 400:951–968, 2009.
- [81] E. S. Phinney. Pulsars as Probes of Newtonian Dynamical Systems. *Royal Society of London Philosophical Transactions Series A*, 341:39–75, 1992.
- [82] M. F. Ryba and J. H. Taylor. High-precision timing of millisecond pulsars. I - Astrometry and masses of the PSR 1855+09 system. *Astrophys. J.*, 371:739–748, 1991.
- [83] B. A. Jacoby. *Recycled pulsars*. PhD thesis, California Institute of Technology, California, USA, 2005.
- [84] J. Antoniadis, M. H. van Kerkwijk, D. Koester, P. C. C. Freire, N. Wex, T. M. Tauris, M. Kramer, and C. G. Bassa. The relativistic pulsar-white dwarf binary PSR J1738+0333 - I. Mass determination and evolutionary history. *Mon. Not. R. Astron. Soc.*, 423:3316–3327, 2012.
- [85] H. Müther, M. Prakash, and T. L. Ainsworth. The nuclear symmetry energy in relativistic Brueckner-Hartree-Fock calculations. *Physics Letters B*, 199:469–474, 1987.
- [86] P. C. C. Freire, S. M. Ransom, S. Bégin, I. H. Stairs, J. W. T. Hessels, L. H. Frey, and F. Camilo. Eight New Millisecond Pulsars in NGC 6440 and NGC 6441. *Astrophys. J.*, 675:670–682, 2008.
- [87] M. H. van Kerkwijk, R. P. Breton, and S. R. Kulkarni. Evidence for a Massive Neutron Star from a Radial-velocity Study of the Companion to the Black-widow Pulsar PSR B1957+20. *Astrophys. J.*, 728:95, 2011.

- [88] R. W. Romani, A. V. Filippenko, J. M. Silverman, S. B. Cenko, J. Greiner, A. Rau, J. Elliott, and H. J. Pletsch. PSR J1311–3430: A Heavyweight Neutron Star with a Flyweight Helium Companion. *Astrophys. J.*, 760:L36, 2012.
- [89] I. H. Stairs, S. E. Thorsett, J. H. Taylor, and A. Wolszczan. Studies of the Relativistic Binary Pulsar PSR B1534+12. I. Timing Analysis. *Astrophys. J.*, 581:501–508, 2002.
- [90] N. D. R. Bhat, M. Bailes, and J. P. W. Verbiest. Gravitational-radiation losses from the pulsar white-dwarf binary PSR J1141–6545. *Phys. Rev. D*, 77(12):124017, 2008.
- [91] J. Antoniadis, C. G. Bassa, N. Wex, M. Kramer, and R. Napiwotzki. A white dwarf companion to the relativistic pulsar PSR J1141–6545. *Mon. Not. R. Astron. Soc.*, 412:580–584, 2011.
- [92] J. Boyles, R. S. Lynch, S. M. Ransom, I. H. Stairs, D. R. Lorimer, M. A. McLaughlin, J. W. T. Hessels, V. M. Kaspi, V. I. Kondratiev, A. Archibald, A. Berndsen, R. F. Cardoso, A. Cherry, C. R. Epstein, C. Karako-Argaman, C. A. McPhee, T. Pennucci, M. S. E. Roberts, K. Stovall, and J. van Leeuwen. The Green Bank Telescope 350 MHz Drift-scan survey. I. Survey Observations and the Discovery of 13 Pulsars. *Astrophys. J.*, 763:80, 2013.
- [93] R. S. Lynch, J. Boyles, S. M. Ransom, I. H. Stairs, D. R. Lorimer, M. A. McLaughlin, J. W. T. Hessels, V. M. Kaspi, V. I. Kondratiev, A. M. Archibald, A. Berndsen, R. F. Cardoso, A. Cherry, C. R. Epstein, C. Karako-Argaman, C. A. McPhee, T. Pennucci, M. S. E. Roberts, K. Stovall, and J. van Leeuwen. The Green Bank Telescope 350 MHz Drift-scan Survey II: Data Analysis and the Timing of 10 New Pulsars, Including a Relativistic Binary. *Astrophys. J.*, 763:81, 2013.
- [94] J. Antoniadis, P. C. C. Freire, N. Wex, T. M. Tauris, R. S. Lynch, M. H. van Kerkwijk, M. Kramer, C. Bassa, V. S. Dhillon, T. Driebe, J. W. T. Hessels, V. M. Kaspi, V. I. Kondratiev, N. Langer, T. R. Marsh, M. A. McLaughlin, T. T. Pennucci, S. M. Ransom, I. H. Stairs, J. van Leeuwen, J. P. W. Verbiest, and D. G. Whelan. A Massive Pulsar in a Compact Relativistic Binary. *Science*, 340:448, April 2013.
- [95] D. Hobbs, B. Holl, L. Lindegren, F. Raison, S. Klioner, and A. Butkevich. Determining PPN  $\gamma$  with Gaia’s astrometric core solution. *Proceedings of the International Astronomical Union*, 5:315–319, 2009.



- [96] B. S. Sathyaprakash and B. F. Schutz. Physics, Astrophysics and Cosmology with Gravitational Waves. *Living Rev. Relativity*, 12, 2009. <http://www.livingreviews.org/lrr-2009-2>.
- [97] Luc Blanchet. Post-newtonian theory and the two-body problem. In Luc Blanchet, Alessandro Spallicci, and Bernard Whiting, editors, *Mass and Motion in General Relativity*, volume 162 of *Fundamental Theories of Physics*, pages 125–166. Springer Netherlands, 2011.
- [98] LIGO Scientific Collaboration, Virgo Collaboration, J. Aasi, J. Abadie, B. P. Abbott, R. Abbott, T. D. Abbott, M. Abernathy, T. Accadia, and F. Acernese, et al. Prospects for Localization of Gravitational Wave Transients by the Advanced LIGO and Advanced Virgo Observatories. *ArXiv e-prints*, 1304.0670, 2013.
- [99] C. M. Will. Testing scalar-tensor gravity with gravitational-wave observations of inspiralling compact binaries. *Phys. Rev. D*, 50:6058–6067, 1994.
- [100] T. Damour and G. Esposito-Farèse. Gravitational-wave versus binary-pulsar tests of strong-field gravity. *Phys. Rev. D*, 58(4):042001, 1998.
- [101] E. Barausse, C. Palenzuela, M. Ponce, and L. Lehner. Neutron-star mergers in scalar-tensor theories of gravity. *Phys. Rev. D*, 87:081506, 2013.
- [102] N. D. H. Dass and V. Radhakrishnan. The new binary pulsar and the observation of gravitational spin precession. *Astrophys. J.*, 16:L135–L139, 1975.
- [103] J. M. Weisberg, R. W. Romani, and J. H. Taylor. Evidence for geodetic spin precession in the binary pulsar 1913 + 16. *Astrophys. J.*, 347:1030–1033, 1989.
- [104] M. Kramer. Determination of the Geometry of the PSR B1913+16 System by Geodetic Precession. *Astrophys. J.*, 509:856–860, 1998.
- [105] I. H. Stairs, S. E. Thorsett, and Z. Arzoumanian. Measurement of Gravitational Spin-Orbit Coupling in a Binary-Pulsar System. *Phys. Rev. Lett.*, 93:141101, 2004.
- [106] J. M. Weisberg and J. H. Taylor. General Relativistic Geodetic Spin Precession in Binary Pulsar B1913+16: Mapping the Emission Beam in Two Dimensions. *Astrophys. J.*, 576:942–949, 2002.
- [107] R. N. Manchester, M. Kramer, I. H. Stairs, M. Burgay, F. Camilo, G. B. Hobbs, D. R. Lorimer, A. G. Lyne, M. A. McLaughlin, C. A. McPhee, A. Possenti, J. E. Reynolds, and W. van Straten. Observations and Modeling of Relativistic Spin Precession in PSR J1141–6545. *Astrophys. J.*, 710:1694–1709, 2010.

- [108] G. Desvignes, M. Kramer, I. Cognard, L. Kasian, J. van Leeuwen, I. Stairs, and G. Theureau. PSR J1906+0746: From relativistic spin-precession to beam modeling. *Proceedings of the International Astronomical Union*, 8:199–202, 2012.
- [109] A. Wolszczan. A nearby 37.9-ms radio pulsar in a relativistic binary system. *Nature*, 350:688–690, 1991.
- [110] I. H. Stairs, S. E. Thorsett, J. H. Taylor, and Z. Arzoumanian. Geodetic Precession in PSR B1534+12. In M. Kramer, N. Wex, and R. Wielebinski, editors, *IAU Colloq. 177: Pulsar Astronomy — 2000 and Beyond*, volume 202 of *Astronomical Society of the Pacific Conference Series*, pages 121–124, 2000.
- [111] M. A. McLaughlin, A. G. Lyne, D. R. Lorimer, A. Possenti, R. N. Manchester, F. Camilo, I. H. Stairs, M. Kramer, M. Burgay, N. D’Amico, P. C. C. Freire, B. C. Joshi, and N. D. R. Bhat. The Double Pulsar System J0737-3039: Modulation of A by B at Eclipse. *Astrophys. J.*, 616:L131–L134, 2004.
- [112] R. P. Breton, V. M. Kaspi, M. Kramer, M. A. McLaughlin, M. Lyutikov, S. M. Ransom, I. H. Stairs, R. D. Ferdman, F. Camilo, and A. Possenti. Relativistic Spin Precession in the Double Pulsar. *Science*, 321:104–107, 2008.
- [113] B. B. P. Perera, M. A. McLaughlin, M. Kramer, I. H. Stairs, R. D. Ferdman, P. C. C. Freire, A. Possenti, R. P. Breton, R. N. Manchester, M. Burgay, A. G. Lyne, and F. Camilo. The Evolution of PSR J0737–3039B and a Model for Relativistic Spin Precession. *Astrophys. J.*, 721:1193–1205, 2010.
- [114] R. D. Ferdman, I. H. Stairs, M. Kramer, R. P. Breton, M. A. McLaughlin, P. C. C. Freire, A. Possenti, B. W. Stappers, V. M. Kaspi, R. N. Manchester, and A. G. Lyne. The Double Pulsar: Evidence for Neutron Star Formation without an Iron Core-collapse Supernova. *Astrophys. J.*, 767:85, 2013.
- [115] K. Nordtvedt. Testing Relativity with Laser Ranging to the Moon. *Phys. Rev.*, 170:1186–1187, 1968.
- [116] J. Müller, F. Hofmann, and L. Biskupek. Testing various facets of the equivalence principle using lunar laser ranging. *Class. Quantum Grav.*, 29:184006, 2012.
- [117] T. Damour and G. Schäfer. New tests of the strong equivalence principle using binary-pulsar data. *Phys. Rev. Lett.*, 66:2549–2552, 1991.
- [118] R. Lynch. The hunt for new pulsars with the Green Bank Telescope. *Proceedings of the International Astronomical Union*, 8:41–46, 2012.

- [119] P. C. C. Freire, M. Kramer, and N. Wex. Tests of the universality of free fall for strongly self-gravitating bodies with radio pulsars. *Class. Quantum Grav.*, 29:184007, 2012.
- [120] V. Boriakoff, R. Buccheri, and F. Fauci. Discovery of a 6.1-ms binary pulsar PSR1953+29. *Nature*, 304:417–419, 1983.
- [121] M. E. Gonzalez, I. H. Stairs, R. D. Ferdman, P. C. C. Freire, D. J. Nice, P. B. Demorest, S. M. Ransom, M. Kramer, F. Camilo, G. Hobbs, R. N. Manchester, and A. G. Lyne. High-precision Timing of Five Millisecond Pulsars: Space Velocities, Binary Evolution, and Equivalence Principles. *Astrophys. J.*, 743:102, 2011.
- [122] N. Wex. Small-eccentricity binary pulsars and relativistic gravity. In M. Kramer, N. Wex, and R. Wielebinski, editors, *IAU Colloq. 177: Pulsar Astronomy — 2000 and Beyond*, volume 202 of *Astronomical Society of the Pacific Conference Series*, pages 113–116, 2000.
- [123] I. H. Stairs, A. J. Faulkner, A. G. Lyne, M. Kramer, D. R. Lorimer, M. A. McLaughlin, R. N. Manchester, G. B. Hobbs, F. Camilo, A. Possenti, M. Burgay, N. D’Amico, P. C. Freire, and P. C. Gregory. Discovery of Three Wide-Orbit Binary Pulsars: Implications for Binary Evolution and Equivalence Principles. *Astrophys. J.*, 632:1060–1068, 2005.
- [124] M. Kehl and A. Krieger. Auswirkungen der Verletzung des Starken Äquivalenzprinzips auf die Dynamik von Binärpulsaren im Gravitationsfeld der Milchstraße und in Kugelsternhaufen. Bachelor thesis, University of Bonn, Germany, 2012.
- [125] D. J. Champion, S. M. Ransom, P. Lazarus, F. Camilo, C. Bassa, V. M. Kaspi, D. J. Nice, P. C. C. Freire, I. H. Stairs, J. van Leeuwen, B. W. Stappers, J. M. Cordes, J. W. T. Hessels, D. R. Lorimer, Z. Arzoumanian, D. C. Backer, N. D. R. Bhat, S. Chatterjee, I. Cognard, J. S. Deneva, C.-A. Faucher-Giguère, B. M. Gaensler, J. Han, F. A. Jenet, L. Kasian, V. I. Kondratiev, M. Kramer, J. Lazio, M. A. McLaughlin, A. Venkataraman, and W. Vlemmings. An Eccentric Binary Millisecond Pulsar in the Galactic Plane. *Science*, 320:1309–1312, 2008.
- [126] G. Hinshaw, J. L. Weiland, R. S. Hill, N. Odegard, D. Larson, C. L. Bennett, J. Dunkley, B. Gold, M. R. Greason, N. Jarosik, E. Komatsu, M. R. Nolte, L. Page, D. N. Spergel, E. Wollack, M. Halpern, A. Kogut, M. Limon, S. S. Meyer, G. S. Tucker, and E. L. Wright. Five-Year Wilkinson Microwave

- Anisotropy Probe Observations: Data Processing, Sky Maps, and Basic Results. *Astrophys. J. Suppl.*, 180:225–245, 2009.
- [127] J. Müller, J. G. Williams, and S. G. Turyshev. Lunar Laser Ranging Contributions to Relativity and Geodesy. In H. Dittus, C. Lammerzahl, and S. G. Turyshev, editors, *Lasers, Clocks and Drag-Free Control: Exploration of Relativistic Gravity in Space*, volume 349 of *Astrophysics and Space Science Library*, pages 457–472, 2008.
- [128] K. Nordtvedt. Probing gravity to the second post-Newtonian order and to one part in  $10^7$  using the spin axis of the sun. *Astrophys. J.*, 320:871–874, 1987.
- [129] T. Damour and G. Esposito-Farèse. Testing local Lorentz invariance of gravity with binary-pulsar data. *Phys. Rev. D*, 46:4128–4132, 1992.
- [130] L. Shao and N. Wex. New tests of local Lorentz invariance of gravity with small-eccentricity binary pulsars. *Class. Quantum Grav.*, 29:215018, 2012.
- [131] P. J. Callanan, P. M. Garnavich, and D. Koester. The mass of the neutron star in the binary millisecond pulsar PSR J1012+5307. *Mon. Not. R. Astron. Soc.*, 298:207–211, 1998.
- [132] K. Lazaridis, N. Wex, A. Jessner, M. Kramer, B. W. Stappers, G. H. Janssen, G. Desvignes, M. B. Purver, I. Cognard, G. Theureau, A. G. Lyne, C. A. Jordan, and J. A. Zensus. Generic tests of the existence of the gravitational dipole radiation and the variation of the gravitational constant. *Mon. Not. R. Astron. Soc.*, 400:805–814, 2009.
- [133] D. C. Backer, S. R. Kulkarni, C. Heiles, M. M. Davis, and W. M. Goss. A millisecond pulsar. *Nature*, 300:615–618, 1982.
- [134] L. Shao, R. N. Caballero, M. Kramer, N. Wex, D. Champion, and A. Jessner. A new limit on local lorentz invariance violation of gravity from solitary pulsars. *Class. Quantum Grav.*, 30:165019, 2013.
- [135] N. Wex and M. Kramer. A characteristic observable signature of preferred-frame effects in relativistic binary pulsars. *Mon. Not. R. Astron. Soc.*, 380:455–465, 2007.
- [136] J. F. Bell and T. Damour. A new test of conservation laws and Lorentz invariance in relativistic gravity. *Class. Quantum Grav.*, 13:3121–3127, 1996.
- [137] L. Shao, N. Wex, and M. Kramer. New tests of local Lorentz invariance and local position invariance of gravity with pulsars. *ArXiv e-prints*, 1211.6558, 2012.

- [138] L. Shao and N. Wex. New limits on the violation of local position invariance of gravity. *Class. Quantum Grav.*, 30:165020, 2013.
- [139] J.-P. Uzan. Varying Constants, Gravitation and Cosmology. *Living Rev. Relativity*, 14, 2011. <http://www.livingreviews.org/lrr-2011-2>.
- [140] T. Damour, G. W. Gibbons, and J. H. Taylor. Limits on the variability of  $G$  using binary-pulsar data. *Phys. Rev. Lett.*, 61:1151–1154, 1988.
- [141] F. Hofmann, J. Müller, and L. Biskupek. Lunar laser ranging test of the Nordtvedt parameter and a possible variation in the gravitational constant. *Astron. Astrophys.*, 522:L5, 2010.
- [142] Planck Collaboration, P. A. R. Ade, N. Aghanim, C. Armitage-Caplan, M. Arnaud, M. Ashdown, F. Atrio-Barandela, J. Aumont, C. Baccigalupi, A. J. Banday, and et al. Planck 2013 results. I. Overview of products and scientific results. *ArXiv e-prints*, 1303.5062, 2013.
- [143] K. Nordtvedt.  $\dot{G}/G$  and a cosmological acceleration of gravitationally compact bodies. *Phys. Rev. Lett.*, 65:953–956, 1990.
- [144] J. M. Lattimer and M. Prakash. Neutron Star Structure and the Equation of State. *Astrophys. J.*, 550:426–442, 2001.
- [145] A. T. Deller, J. P. W. Verbiest, S. J. Tingay, and M. Bailes. Extremely High Precision VLBI Astrometry of PSR J0437–4715 and Implications for Theories of Gravity. *Astrophys. J.*, 685:L67–L70, 2008.
- [146] S. Weinreb, J. Bardin, H. Mani, and G. Jones. Matched wideband low-noise amplifiers for radio astronomy. *Review of Scientific Instruments*, 80:044702, 2009.
- [147] L. Blanchet and G. Schäfer. Higher order gravitational radiation losses in binary systems. *Mon. Not. R. Astron. Soc.*, 239:845–867, 1989.
- [148] L. Blanchet and G. Schäfer. Higher order gravitational radiation losses in binary systems: Erratum. *Mon. Not. R. Astron. Soc.*, 242:704, 1990.
- [149] R. Nan, D. Li, C. Jin, Q. Wang, L. Zhu, W. Zhu, H. Zhang, Y. Yue, and L. Qian. The Five-Hundred-Meter Aperture Spherical Radio Telescope (FAST) Project. *International Journal of Modern Physics D*, 20:989–1024, 2011.
- [150] A. R. Taylor. The Square Kilometre Array. *Proceedings of the International Astronomical Union*, 8:337–341, 2012.

- [151] R. Smits, M. Kramer, B. Stappers, D. R. Lorimer, J. Cordes, and A. Faulkner. Pulsar searches and timing with the Square Kilometre Array. *Astron. Astrophys.*, 493:1161–1170, 2009.
- [152] R. Smits, S. J. Tingay, N. Wex, M. Kramer, and B. Stappers. Prospects for accurate distance measurements of pulsars with the Square Kilometre Array: Enabling fundamental physics. *Astron. Astrophys.*, 528:A108, 2011.
- [153] M. A. C. Perryman, K. S. de Boer, G. Gilmore, E. Høg, M. G. Lattanzi, L. Lindegren, X. Luri, F. Mignard, O. Pace, and P. T. de Zeeuw. GAIA: Composition, formation and evolution of the Galaxy. *Astron. Astrophys.*, 369:339–363, 2001.
- [154] S. M. Ransom, J. M. Cordes, and S. S. Eikenberry. A New Search Technique for Short Orbital Period Binary Pulsars. *Astrophys. J.*, 589:911–920, 2003.
- [155] B. Allen, B. Knispel, J. M. Cordes, J. S. Deneva, J. W. T. Hessels, D. Anderson, C. Aulbert, O. Bock, A. Brazier, S. Chatterjee, P. B. Demorest, H. B. Eggenstein, H. Fehrmann, E. V. Gotthelf, D. Hammer, V. M. Kaspi, M. Kramer, A. G. Lyne, B. Machenschalk, M. A. McLaughlin, C. Messenger, H. J. Pletsch, S. M. Ransom, I. H. Stairs, B. W. Stappers, N. D. R. Bhat, S. Bogdanov, F. Camilo, D. J. Champion, F. Crawford, G. Desvignes, P. C. C. Freire, G. Heald, F. A. Jenet, P. Lazarus, K. J. Lee, J. van Leeuwen, R. Lynch, M. A. Papa, R. Prix, R. Rosen, P. Scholz, X. Siemens, K. Stovall, A. Venkataraman, and W. Zhu. The Einstein@Home Search for Radio Pulsars and PSR J2007+2722 Discovery. *Astrophys. J.*, 773:91, 2013.
- [156] N. Wex and S. M. Kopeikin. Frame Dragging and Other Precessional Effects in Black Hole Pulsar Binaries. *Astrophys. J.*, 514:388–401, 1999.
- [157] K. Liu. *Exploring Pulsar-Black Hole Binaries Using The Next Generation of Radio Telescopes*. PhD thesis, University of Manchester, UK, 2012.
- [158] N. Wex, K. Liu, R. P. Eatough, M. Kramer, J. M. Cordes, and T. J. W. Lazio. Prospects for probing strong gravity with a pulsar-black hole system. *Proceedings of the International Astronomical Union*, 8:171–176, 2012.
- [159] K. Liu, N. Wex, M. Kramer, J. M. Cordes, and T. J. W. Lazio. Prospects for Probing the Spacetime of Sgr A\* with Pulsars. *Astrophys. J.*, 747:1, 2012.
- [160] R. P. Eatough, H. Falcke, R. Karuppusamy, K. J. Lee, D. J. Champion, E. F. Keane, G. Desvignes, D. H. F. M. Schnitzeler, L. G. Spitler, M. Kramer, B. Klein, C. Bassa, G. C. Bower, A. Brunthaler, I. Cognard, A. T. Deller, P. B.

- Demorest, P. C. C. Freire, A. Kraus, A. G. Lyne, A. Noutsos, B. Stappers, and N. Wex. A strong magnetic field around the supermassive black hole at the centre of the Galaxy. *Nature*, 501: 391–394, 2013.
- [161] G. Hobbs, A. Archibald, Z. Arzoumanian, D. Backer, M. Bailes, N. D. R. Bhat, M. Burgay, S. Burke-Spolaor, D. Champion, I. Cognard, W. Coles, J. Cordes, P. Demorest, G. Desvignes, R. D. Ferdman, L. Finn, P. Freire, M. Gonzalez, J. Hessels, A. Hotan, G. Janssen, F. Jenet, A. Jessner, C. Jordan, V. Kaspi, M. Kramer, V. Kondratiev, J. Lazio, K. Lazaridis, K. J. Lee, Y. Levin, A. Lommen, D. Lorimer, R. Lynch, A. Lyne, R. Manchester, M. McLaughlin, D. Nice, S. Osłowski, M. Pilia, A. Possenti, M. Purver, S. Ransom, J. Reynolds, S. Sanidas, J. Sarkissian, A. Sesana, R. Shannon, X. Siemens, I. Stairs, B. Stappers, D. Stinebring, G. Theureau, R. van Haasteren, W. van Straten, J. P. W. Verbiest, D. R. B. Yardley, and X. P. You. The International Pulsar Timing Array project: using pulsars as a gravitational wave detector. *Class. Quantum Grav.*, 27:084013, 2010.
- [162] B. Bertotti, B. J. Carr, and M. J. Rees. Limits from the timing of pulsars on the cosmic gravitational wave background. *Mon. Not. R. Astron. Soc.*, 203:945–954, 1983.
- [163] S. M. Kopeikin. Binary pulsars as detectors of ultralow-frequency gravitational waves. *Phys. Rev. D*, 56:4455–4469, 1997.
- [164] F. B. Estabrook and H. D. Wahlquist. Response of Doppler spacecraft tracking to gravitational radiation. *General Relativity and Gravitation*, 6:439–447, 1975.
- [165] S. Detweiler. Pulsar timing measurements and the search for gravitational waves. *Astrophys. J.*, 234:1100–1104, 1979.
- [166] A. Sesana, A. Vecchio, and C. N. Colacino. The stochastic gravitational-wave background from massive black hole binary systems: implications for observations with Pulsar Timing Arrays. *Mon. Not. R. Astron. Soc.*, 390:192–209, 2008.
- [167] A. Sesana, A. Vecchio, and M. Volonteri. Gravitational waves from resolvable massive black hole binary systems and observations with Pulsar Timing Arrays. *Mon. Not. R. Astron. Soc.*, 394:2255–2265, 2009.
- [168] K. J. Lee, F. A. Jenet, and R. H. Price. Pulsar Timing as a Probe of Non-Einsteinian Polarizations of Gravitational Waves. *Astrophys. J.*, 685:1304–1319, 2008.

- [169] K. J. Lee, F. A. Jenet, R. H. Price, N. Wex, and M. Kramer. Detecting Massive Gravitons Using Pulsar Timing Arrays. *Astrophys. J.*, 722:1589–1597, 2010.
- [170] F. A. Jenet, A. Lommen, S. L. Larson, and L. Wen. Constraining the Properties of Supermassive Black Hole Systems Using Pulsar Timing: Application to 3C 66B. *Astrophys. J.*, 606:799–803, 2004.